# AN INVESTIGATION INTO HOW MIXOTROPHY AND DELETERIOUS CHEMICAL PRODUCTION GIVE HARMFUL ALGAE A COMPETITIVE ADVANTAGE IN SYSTEMS INFLUENCED BY ANTHROPOGENIC DISTURBANCE

A Dissertation

by

SIERRA ELENA CAGLE

Submitted to the Office of Graduate and Professional Studies of
Texas A&M University
in partial fulfillment of the requirements for the degree of

DOCTOR OF PHILOSOPHY

| | |
|---|---|
| Chair of Committee, | Daniel L. Roelke |
| Committee Members, | Anna R. Armitage |
| | Masami Fujiwara |
| | Kirk O. Winemiller |
| Head of Department, | Kirk O. Winemiller |

December 2019

Major Subject: Wildlife and Fisheries Sciences

# ABSTRACT

Harmful algae blooms (HABs)are an increasing problem world-wide. The increasing occurrence and magnitude of HABs has often been linked to anthropogenic disturbances, some of which include salinization, nutrient ratios skewed away from the Redfield ratio, and increased nutrient loading. The research presented here contributes to the impressive pre-existing collection of studies focusing on the HAB problem.

In Chapter 1, it is shown that co-occurring disturbances can have synergistic effects on a mixotrophic HAB species, *Prymnesium parvum*. It was found that increased salinity, community composition change via removal of large zooplankton, and elevated *P. parvum* propagule pressure interact to influence the abundance of *P. parvum* cells, and that the effect is dependent on system specific salinity history. When *P. parvum* was inoculated into a plankton community at low density it increased most if zooplankton were removed and salinity was elevated.

In Chapter 2, it was demonstrated that when the nitrogen to phosphorous ratio was skewed away from the Redfield ratio allelochemicals produced by *P. parvum* had acute mass mortality effects on multiple trophic levels. But, when nutrients were supplied at the Redfield ratio allelochemicals were ineffective and cell-to-organism contact was required for deleterious effects to occur. Importantly, only when the *P. parvum* population was at high densities did it appear to have negative effects on other organisms, suggesting that mass effects of allelochemicals may not contribute to bloom initiation.

In Chapter 3, it was demonstrated that flexible nutrition could lead to population persistence of an otherwise non-competitive theoretical phytoplankton species, but only when the species was highly inedible to zooplankton grazers. Additionally, it was shown that as nutrient loading was increased, system stability decreased via the initiation of zooplankton- phytoplankton boom-bust cycles. However, the presence of a mixotrophic population stabilized the system by reducing the number of cycles that occurred. Notably, when nutrient loading was elevated community dynamics became complex and the mixotroph population density was unpredictable from year to year, sometimes reaching high densities. This finding demonstrates how a bloom of a mixotroph can get started with enrichment when no role of toxins is considered.

# DEDICATION

To my family,

Without this—there is nought—

All other Riches be

As is the Twitter of a Bird—

Heard opposite the Sea—

I could not care—to gain

A lesser than the Whole—

For did not this include themself—

As Seams—include the Ball?

I wished a way might be

My Heart to subdivide—

'Twould magnify—the Gratitude—

And not reduce—the Gold—

Emily Dickenson

# ACKNOWLEDGEMENTS

I would like to thank my committee chair, Dr. Daniel Roelke, for his guidance, mentorship, and teaching over the past 5+ years. It has been so much fun and absolutely invaluable to me. I would also like to thank my committee members, Dr. Masami Fujiwara, Dr. Kirk Winemiller, and Dr. Anna Armitage, for their guidance and support throughout the course of this research. Each of these individuals provided me unique perspective and constructive critiques that I am so thankful for. Thanks to my friends and colleagues in the department, who I have also learned so much from and to those who have propped me up and just been so much fun to be around. Finally, thanks to the department faculty and staff for always being so helpful and all around awesome!

# CONTRIBUTORS AND FUNDING SOURCES

## Contributors

This work was supervised by a dissertation committee consisting of Professors Daniel Roelke, Kirk Winemiller, and Masami Fujiwara of the Department of Wildlife and Fisheries Science and Professor Anna Armitage of the Department of Marine Biology.

All work conducted for the dissertation was completed by the student independently.

## Funding Sources

Graduate study was supported in part by the Mills Scholarship from the Texas Water Resource Institute. Tuition support was also provided by the William Roach Scholarship and the J.H. Benedict, Sr. Memorial Graduate Student Scholarship.

TABLE OF CONTENTS

Page

LIST OF FIGURES

Page

LIST OF TABLES

Page

# CHAPTER I

## INTRODUCTION

Algae. They're everywhere. Often you don't see them, but they're around, growing, generating oxygen and holding up the aquatic food web. Other times, you do see them… in scums or slimes or floating mats. You smell them, or their effects, the rotting stench of dead fish. They ruin holiday plans by closing recreational areas and spur economic hardships.

In recent years the negative effects associated with algal overgrowth and blooms of toxic species have become familiar to the general public due to headline-making events. In 2014, a harmful alga bloom (HAB) of toxin producing cyanobacteria in Lake Erie impacted the drinking water of 500,000 people in the surrounding area. In 2016, Floridians began to suffer effects from a wide spread mélange of toxic algae including blooms of cyanobacteria and the red-tide species *Karenia brevis.* A recent report to Congress on freshwater HABs (produced by a non-partisan advisory firm and published August, 2018) stated "Scientific research indicates that in recent years, the frequency and geographic distribution of harmful algal blooms (HABs) have been increasing nationally and globally." Indeed, the scientific literature has been suggesting for several years now that a proliferation and range expansion of HABs is occurring, as well as an increase in the frequency and magnitude of bloom events (Anderson, 1989; Hallegraeff, 1995; Smayda, 1990, 2002). Much of the research focus aimed at understanding these species has been related to bloom initiation and forming mechanisms associated with deleterious chemical

production, a common characteristic of these species (Fistarol et al., 2003; Graneli et al., 2008; Jonsson et al., 2009; Legrand et al., 2003; Muhl et al., 2018). However, most HABs also share a less well known characteristic, the ability to obtain growth limiting elements in both dissolved and particulate forms, a trait known as mixotrophy (Glibert, 2015; Smayda, 2002). These shared characteristics are central to the species success because they allow them to make a living under variable environmental conditions, likely giving them an advantage in a rapidly changing world (Glibert, 2015; Smayda, 1997).

An important environmental factor that has been linked to proliferation of certain HAB species is nutrient abundance and stoichiometry (Anderson et al., 2002; Davidson et al., 2014; Fu et al., 2012; Hallegraeff, 1993; Heisler et al., 2008; Smayda, 1990). In aquatic ecosystems, historical nutrient regimes tend to be relatively stable, however human activity has greatly altered these regimes in many areas. In some cases, systems have undergone eutrophication where increased nutrient loads lead to alteration of biotic and abiotic system components, while in other areas systems have experienced oligotrificiation due to increased regulation of nutrient application on the surrounding landscape. Both manifestations have been associated with increased abundance of HABs (Glibert et al., 2010; Heisler et al., 2008; Shumway et al., 2018).

Further, both situations lead to changes in bulk nutrient concentrations in the aquatic environment and along with them the ratio of nutrients may also be influenced. For example, the phosphorous content of some fertilizers has become highly regulated but not the nitrogen content, which leads to a disparity in the ratio of nitrogen to

phosphorous entering aquatic ecosystems of watersheds in which application is heavy. This is concerning due to study findings that demonstrate stimulation of deleterious chemical production in some HAB species when nutrient ratios are skewed away from those of the Redfield ratio (C:N:P of 106:16:1). To illustrate, laboratory and mesocosm studies with golden algae, *Prymnesium parvum*, have shown that high or low N:P ratios relative to Redfield, increase deleterious chemical production (Errera et al., 2008; Granéli & Johansson, 2003b).

Additionally, it may be that increased frequency and magnitude of nutrient-regime-related disturbance leads to less stable plankton communities. Other system disturbances such as reduced freshwater inflow, shifting temperatures, increased ambient salinity levels, and increased prevalence of disease or parasites may also act to destabilize the plankton community, allowing more flexible HAB species to proliferate.

Such ecosystem disturbances are increasing in most areas, and are commonly compounded with various other anthropogenic disturbances to generating novel disturbances in some cases. The resulting loss of resistance/resilience in disturbed plankton communities likely occurs due to the adaptation of species to a historical fluctuation regime that has been altered (Reynolds, 2006; Roelke et al., 2010a; Sommer et al., 1986). This idea is similar to that of the seasonality hypothesis introduced by Janzen. In his 1967 paper, Janzen explains that "mountain passes are higher in the tropics" due to more stable temperature regimes at these latitudes and the local adaptation of species to this stability. Such adaptation makes even small differences in

temperature, as encountered on mountains due to elevation gradients, intolerable and therefore effective barriers.

It is easy to adapt Janzen's temperature related hypothesis to different environmental abiotic factors and recognize that the stability of a system in the face of change will be determined, in part, by how well the biotic community is pre-adapted to deal with fluctuations in the changing parameter. If the community is not well adapted to variation in the changing parameter, then the shifted regime may cause organismal stress, individual losses and even whole species population losses. In such cases open niche space may lead to increased invasibility of phytoplankton assemblages and/or opportunity for resident HAB populations to proliferate (Shea & Chesson, 2002).

In the following chapters I present studies that examine:

1. The relationship between co-occurring anthropogenic disturbances, a system's historical natural fluctuation regime, and population density of an invasive and toxic mixotroph in local communities of freshwater plankton.
2. How N:P ratios influence mixotrophy and deleterious chemical production in laboratory cultures of a mixotrophic alga species using multi-trophic level bioassays and live time series counts of mixed cultures.
3. The effects of mixotrophic phytoplankton on stability of a theoretical plankton system across a range of nutrient loading regimes and implications related to bloom initiation.

# CHAPTER II

# COMPOUNDING EFFECTS OF CO-OCCURRING DISTURBANCES ON POPULATIONS OF A HARMFUL BLOOM-FORMING MIXOTROPH PROTIST*

## Introduction

Freshwater systems throughout the world are changing, in part, due to anthropogenic activities. These activities lead to disturbances that include altered hydrology and salinization. Anthropogenic activities can also facilitate species invasions, leading to increased occurrence and range expansion of pests and disease, which in turn disrupt indigenous communities. In the extreme, this disruption can take the form of harmful algae blooms (HABs). Due to the increasing frequency and magnitude of such disturbances, it is likely that some will co-occur, possibly leading to compounded effects.

Naturally occurring environmental fluctuations, different from the anthropogenically-facilitated disturbances mentioned above, are important ecosystem shaping processes. Such environmental fluctuations include seasonal changes in temperature, light, mixing depth, nutrient availability and inflows. In aquatic systems these environmental fluctuations play a critical role in shaping communities, especially phytoplankton assemblages (Glasby & Underwood, 1996; Reynolds, 2006; Sommer et al., 1986). Because they vary in frequency and magnitude from system to system

*Reprinted with permission from "Compounding effects of co-occurring disturbances on populations of a harmful bloom-forming mixotroph protist" by Cagle, S. E., Roelke, D. L., & Muhl, R. M., 2019. *Hydrobiologia*, 831(1), 23-31, Copyright [2019] by Springer Nature.

(Shade et al., 2012), a specific system will likely have a characteristic environmental fluctuation regime to which organisms are adapted. Here I present a case study in which it is investigated how the effects of co-occurring disturbances might interact to influence the abundance of a harmful algal bloom-forming species, *Prymnesium parvum* (Carter, 1937). Specifically, the experimentally manipulated disturbances included increased salinity and community composition change via the removal of large zooplankton. The effects of the co-occurring disturbances were tested at two propagule levels, ambient and elevated *P. parvum* densities, treating elevated *P. parvum* density as a third disturbance. The role that historical exposure to salinity related fluctuations played in influencing the effect of these co-occurring disturbances was also examined.

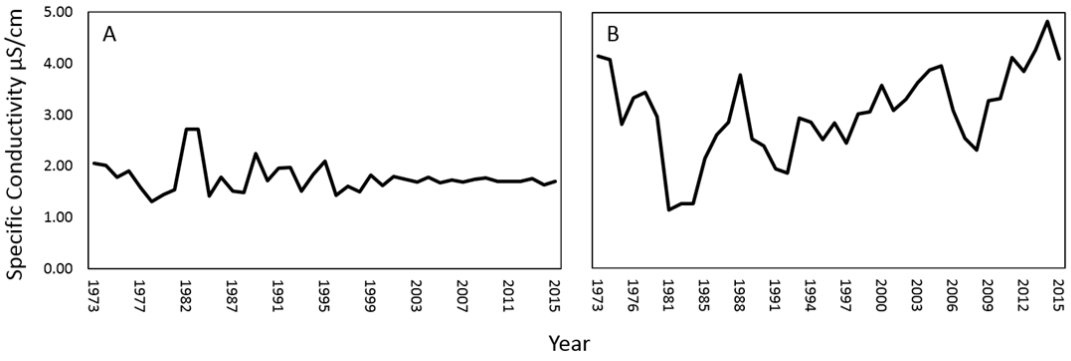


**Figure 2-1. Specific conductivity data for Lake Whitney (LW) and Lake Possum Kingdom (LPK) located in the Brazos River Basin of south-central USA. Data was obtained from a public database maintained by the Texas Commission for Environmental Quality (TCEQ) and averaged over a yearly period.**

To conduct the study I turned to freshwater systems of south-central USA, specifically those lakes located along the Brazos River Basin. In this region, salty inflows occur as a result of runoff flowing over a salt-rich, geologic formation in the upper reaches of the basin. This creates a salinity gradient along the river, where lakes positioned in the upstream portion of the basin experience higher salinity and salinity fluctuations compared to lakes downstream (Wurbs, 1991, 2002) (see Figure 2-1). Organisms residing in lakes positioned in the upstream portion of the basin may be adapted to these dynamic salinity conditions, and are thus more resistant and resilient to co-occurring disturbances involving, in part, salinity change. Indeed, findings from previous studies show that salinity thresholds below which *P. parvum* blooms do not occur are site specific, which suggests that adaptation of the local plankton community to salinity magnitude and variation plays a role in bloom incidence ((Roelke & Eldridge, 2010); Hambright et al., 2015).

Additionally, throughout this region extended periods of drought which may be influenced by anthropogenic caused climate change have exacerbated natural salinity magnitude and fluctuation. During these times, populations of the toxic and allelopathic *P. parvum* can reach bloom level densities. Such bloom events alter the naturally occurring zooplankton assemblages, typically killing off many larger-bodied taxa like copepods, cladocera and rotifers (Brooks et al., 2010); Roelke et al., 2012). At other times, however, *P. parvum* populations of the region may be low (even below detection limits using microscopy), causing consideration for the role propagule pressure may play in facilitating establishment and bloom formation of *P. parvum*.

Of the two reservoirs, Lakes Possum Kingdom and Whitney, it was hypothesized that the resident plankton of Lake Possum Kingdom (positioned higher in the watershed) would be more resistant to co-occurring disturbances involving salinity than the resident plankton of Lake Whitney (positioned lower in the watershed) because the natural salinity fluctuation regime is greater in Lake Possum Kingdom than it is in Lake Whitney. It was also hypothesized that compounding the disturbance by removing zooplankton and/or increasing *P. parvum* propagules would increase the ability of *P. parvum* to proliferate.

## Materials and Methods

### *Site Selection and Description*

The experimental design called for two bodies of water characterized by different historical salinity regimes, so as to assess the response to disturbance of plankton communities adapted to different environments. Because ion identity is known to influence *P. parvum* toxicity (Yariv & Hestrin, 1961), lake selection was focused on a single river basin where ion ratios were presumably similar throughout. The Brazos River Basin was selected because previous studies have demonstrated that saline inflows result in elevated salinity levels in lakes of this basin, the degree of which depends on the lake's position in the basin, where those lakes in the upper region typically experience higher salinity compared to those in the lower reaches (Wurbs, 1991, 2002). Specific conductivity data for Brazos River Basin lakes was obtained from a public database maintained by the Texas Commission for Environmental Quality (TCEQ). This data was reviewed and two lakes were chosen in which varying degrees of historical

salinity fluctuation had occurred, and for which it was known that *P. parvum* blooms could occur. Lake Possum Kingdom was chosen as the system representative of high magnitude salinity fluctuation (Figure 2-1), while Lake Whitney was representative of low fluctuation (Figure 2-1).

Lake Possum Kingdom is located (centered at 32.87° N, 98.50° W) further Northwest and upstream along the Brazos River than Lake Whitney (32.52° N, 97.43° W). In the region of Texas that the lakes are situated, the watershed receives an average of 90cm $year^{-1}$ rainfall. Lake Possum Kingdom has a capacity of $893x10^6$ $m^3$, a surface area of 80 $km^2$ and an average depth of ~11m. Lake Whitney has a capacity of $467x10^6$ $m^3$, a surface area of 95 $km^2$ and an average depth of ~5m. Bloom level *P. parvum* densities ($1x10^7$ cells $L^{-1}$) have been known to occur in each of these lakes, typically during the late fall through early spring. Additional description of these lakes can be found in Roelke et al. (2010a, 2010b).

***Experimental Design***

The Lake Whitney experiment was conducted during late October and the Lake Possum Kingdom experiment during early November, the time of year that *P. parvum* bloom initiation is common for Texas inland waterbodies (Roelke et al., 2010b). The structural design of the experimental unit was based on an established design used in similar experiments done by Roelke et al. (2010b) and is briefly described here. Within each site 20-L polycarbonate carboys were deployed, each of which became its own experimental unit. Water collected to initiate the experiment was taken from a depth of 0.5m, at a site location away from the shore. Each carboy was filled with 18L of water

from the experimental location, leaving air in the headspace to allow neutral buoyancy. After site water was added to the carboys, each received a specific treatment and was sealed. Additionally, carboys were covered with a neutral density screening to simulate light intensity equal to that at the depth from which the water was collected. This light intensity was determined based on Secchi disk depths typical of these bodies of water at this time of year. The carboys were then tethered to a platform, allowing free movement

**Table 2-1. Description of experimental treatments, where inclusion of a treatment for an experimental unit is denoted with an "X". Each treatment was conducted in triplicate and this design was replicated across two lake sites.**

| Treatment | *P. parvum* addition | Salt addition | Zooplankton removal |
|---|---|---|---|
| 1 | | | |
| 2 | | X | |
| 3 | | | X |
| 4 | | X | X |
| 5 | X | | |
| 6 | X | X | |
| 7 | X | | X |
| 8 | X | X | X |

with turbulence and mixing to occur for 7 days. A 7 day duration has been shown to allow a sufficient period of time for plankton response to occur, without encountering bottle effects (Errera et al., 2008; Roelke et al., 2010b).

The *in-situ* mesocosm experimental design consisted of 8 treatments (Table 2-1), done in triplicate, at two different sites, for a total of 48 experimental units. Experimental treatments included additions of the following: a salt solution, *P. parvum* culture, or a combination of these two things. Additionally, a control was provided, to which nothing was added. These 4 treatments were replicated with ambient lake waters containing two different natural size fractions, the first representative of the phytoplankton assemblage, where zooplankton larger than 61 μM were filtered out, and the second representative of the full plankton community (i.e. no zooplankton were removed). Because populations of large zooplankton tend to exhibit patchy distributions, in treatments containing the full plankton community, grazers larger than 152 μM were collected, simultaneous with water collection, combined, gently mixed, and then evenly distributed amongst these experimental units.

In treatments receiving a salt addition, the ambient salinity of each lake at the time of the experiment was increased by 1 practical salinity unit (psu). A salt solution reflective of the typical ion concentrations in the study lakes was made in the lab and used for experimental treatments (Baker et al., 2009). This solution was intended to represent brine discharge from local desalination facilities, which are located near both experiment sites and provide drinking water for the surrounding communities. Use of a representative solution rather than actual discharge waters was desirable because, in addition to reducing the extraneous variables in the experiment caused by salt ion variation in different discharges, use of a representative brine solution also decreased the possible effect of other unknown components of the discharge. Such components include

chemical additions used in the treatment process, and concentrated contaminants from the source water.

In treatments receiving a *P. parvum* culture addition, a culture aliquot containing a target population density of $0.5x10^6$ cells $L^{-1}$ ($1/20^{th}$ bloom density) was added to each unit. *P. parvum* culture obtained from the Roelke lab, isolated from the Colorado River (strain ZZ181, University of Texas, Austin, TX, USA), was used to inoculate experimental cultures. These cultures were maintained in batch using a modified f/2 media recipe (Guillard & Ryther, 1962), i.e., with phosphate reduced to $1/20^{th}$ of the Redfield ratio, and kept in an incubator at 15°C with a 12:12 (L:D) photoperiod and 150 $\mu E\ m^{-2}\ s^{-1}$ of irradiance from a fluorescent source. This photoperiod, irradiance and temperature are typical of Texas water bodies during the fall (Baker et al., 2009).

Cultures were grown at several salinity levels (media salinity raised using Instant Ocean), and those closest to the ambient salinity of the site at the time of experiment initiation were used as inoculum. For the Lake Whitney experiment, the culture used was grown at 0.75psu, while for the Lake Possum Kingdom experiment, the culture used was grown at 1.25psu. Prior to inoculation into experimental units, *P. parvum* cultures were screened for toxicity with an allelopathy bioassay.

The bioassay consisted of *Rhodomonas salina* (Hill & Wetherbee, 1989) as a biotarget for extracellular *P. parvum* allelochemicals. The *R. salina* culture was maintained in batch, using balanced f/2 media raised to 5psu using Instant Ocean, under a 12:12 light:dark cycle, at an irradiance of 11 uE $m^{-2}s^{-1}$, and a temperature of 20°C. Experiment samples were gravity filtered through GF/C glass fiber filters (47mm

diameter), in aliquots of 50mls, to obtain a cell-free filtrate while ensuring minimal cell breakage. The filtrates were stored in the dark and used for assay tests within 30 minutes of being processed. A 0.5 dilution series was set up, where 50% of each of 6 unit's volume was *R. salina* culture at a density of $1x10^4$ cells $ml^{-1}$ (Blossom et al., 2014a; Brooks et al., 2010), and the other 50% consisted of *P. parvum* cell-free filtrate diluted to various concentrations. Each culture was tested with triplicate assays. The test vials were incubated in the dark at a temperature of 25°C for 24 hours, after which time the contents of each vial were preserved using glutaraldehyde at a concentration of 5%v/v. Subsequent enumeration of *R. salina* cells was accomplished using a Sedgwick rafter counting cell, where predetermined transects were counted. All intact cells were counted (including rounded cells).

***Sampling and Analysis***

Response variables measured include *P. parvum* density and ambient toxicity, chlorophyll *a* as a proxy for total phytoplankton biomass, total zooplankton biovolume and biovolume of higher zooplankton taxonomic groups. However only results for *P. parvum* density and the related analysis methods are reported here. Data for all other response variables is reported in Appendix A.

Density of *P. parvum* was sampled at the time of experiment initiation, 3 days later at the midpoint, and finally on day 7. Sample density was quantified using the Utermöhl (1958) settling technique. Briefly, each 100 mL sample was collected and preserved with glutaraldehyde, 5% v/v. A 1ml subsample was later settled in a sedimentation chamber for 24 hours. *P. parvum* cells were counted in 20 randomly

selected fields of view using an inverted, phase contrast light microscope (400x, Leica Microsystems).

All data was square root transformed, improving normality of the residual error. Three-way ANOVAs were conducted using the transformed population density data from the final sampling to test for main effects, as well as interaction effects of the experimental variables. If a significant interaction effect on a response variable was determined, any significant main effects involved in the interaction were disregarded. Data from each lake was analyzed separately.

## Results

### *Abiotic Lake Conditions*

Abiotic conditions in Lakes Whitney and Possum Kingdom were similar in some aspects at the time of water collection for experiment initiation (Table 2-2). For example, temperature at 1m depth was 21°C and pH was 7.68 in Lake Whitney, while in Lake Possum Kingdom the temperature was 17.8°C and the pH was 7.70. In addition, both lakes typically have phosphorus levels in the eutrophic range (Patiño et al., 2014), so it is unlikely that nutrients were limiting in collected waters of either lake. In regards to salinity, the lakes differed. In Lake Whitney salinity was 0.73psu and in Lake Possum

Kingdom salinity was 1.71psu. Some of the treatments received addition of salts at the start of the experiment, for these treatments salinity was ~1.7psu for the Lake Whitney water (similar to the ambient salinity in Lake Possum Kingdom) and ~2.7psu for Lake Possum Kingdom water.

### *Ambient and Augmented* P. parvum *Population Response*

In Lake Whitney statistical results indicate a significant 3-way interaction between all experimental treatments (salt addition, *P. parvum* addition, zooplankton removal) (Table 2-3, $p$=0.0001). To understand this interaction, data were broken down across the *P. parvum* treatment, i.e., ambient vs. augmented *P. parvum* density, and the 2-way interaction between salt and zooplankton removal was examined. Here, it was found that when no *P. parvum* cells were added to a treatment there was no effect of increasing salinity, removing zooplankton, nor an interaction between these treatments. Differently, when the *P. parvum* population was augmented by adding culture a significant interaction between the salt and zooplankton treatments occurred (Table 2-3, $p$=0.0001), where only when salt was added and zooplankton removed was the *P. parvum* population significantly increased (Figure 2-2).

**Table 2-2. Abiotic conditions in Lake Whitney (LW) and Lake Possum Kingdom (LPK) at the time of experimental water collection. Measurements were taken away from the shoreline at a depth of 1m. *nutrient status as reported in Patiño et al. (2014).**

| Abiotic Parameter | Lake Whitney (LW) | Lake Possum Kingdom (LPK) |
|---|---|---|
| Temperature (˚C ) | 21 | 17.8 |
| pH | 7.68 | 7.7 |
| Secchi Depth (cm) | 147 | 165 |
| DO (% saturation) | 76.7 | 81.1 |
| Nutrient Status | eutrophic* | eutrophic* |
| Ambient Salinity (psu) | 0.73 | 1.73 |
| Manipulated Salinity (psu) | 1.71 | 2.71 |

**Table 2-3. Significance results from ANOVA analysis of square root transformed data collected during the final sampling period. Highest level interaction effects were first examined and if significant interpreted. If a response variable was not included in a significant interaction effect then its main effect was examined interpreted if significant. Data from each lake was analyzed separately.**

| Main and interaction effects of treatments on *P. parvum* cell density | P-values (significant at the α=0.05* or 0.01** level) | |
|---|---|---|
| | Lake Whitney | Lake Possum Kingdom |
| Salt * *P. parvum* * Zooplankton | 0.0001** | 0.146 |
| Salt * *P. parvum* | NA | 0.0005** |
| Salt * Zooplankton | NA | 0.146 |
| *P. parvum* * Zooplankton | NA | 0.09 |
| Zooplankton | NA | .006** |
| Signifigant 3-way interaction broken down | | |
| Ambient *P. parvum* --> Salt * Zooplankton | 0.499 | NA |
| Ambient *P. parvum* --> Salt | 0.067 | NA |
| Ambient *P. parvum* --> Zooplankton | 0.499 | NA |
| Augmented *P. parvum* --> Salt * Zooplankton | 0.0001 ** | NA |
| Simple main effect of P. parvum | $1.3x10^{-12}$ ** | $5.1x10^{-11}$ ** |

In Lake Possum Kingdom, no significant 3-way interaction effect was found, so all possible 2-way interactions were examined (Table 2-3). A significant 2-way interaction between salt and *P. parvum* additions occurred ($p$=0.0005) where, regardless of whether zooplankton were included in the treatment, the *P. parvum* density significantly increased (Figure 2-2). Because the zooplankton treatment did not interact with other treatments, its simple main effect (Table 2-3, p=0.006) was included in the results for interpretation. This result indicates that regardless of whether another

treatment was applied, zooplankton removal significantly influenced the *P. parvum* population (Figure 2-2).

Though it was recognized that effect of the *P. parvum* treatment significantly interacted with some or all of the other experimental treatments for each lake, analysis of the simple main effect of *P. parvum* addition was of central importance in exploring one of the hypotheses. Here it was found that *P. parvum* addition allowed for a significantly higher population density to persist at $T_{final}$ in each lake (Table 2-3, $p = 1.3 \times 10^{-12}$ for Lake Whitney and $p = 5.1 \times 10^{-11}$ for Lake Possum Kingdom).

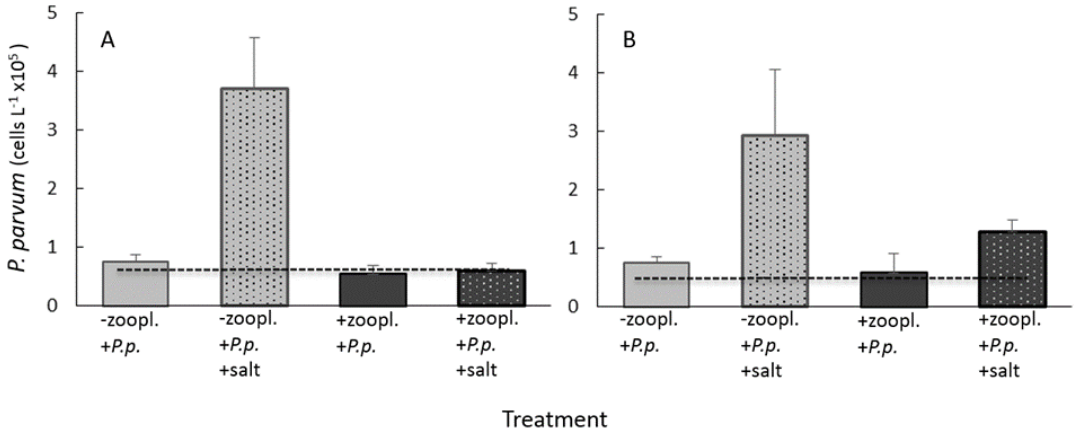


**Figure 2-2. The average initial (horizontal dashed lines) and final (vertical bars) *Prymnesium parvum* population densities for Lake Whitney and Lake Possum Kingdom experimental treatments (A, B). (mean + SD, n=3) Bar shading denotes salinity level, where light grey ~0.7psu, medium grey ~1.7psu, and dark grey ~2.7psu.**

## Discussion

Considering the effect of *P. parvum* propagule pressure in isolation, it was found that when the initial *P. parvum* density was increased to a level 1/20$^{th}$ that of bloom density for these lakes, the population persisted over the course of the experiment and remained significantly higher than in treatments with only the ambient *P. parvum* population. Furthermore, when no *P. parvum* propagules were introduced to the experimental units, the population density was low or below the detection threshold and remained so over the course of the experiment. These findings suggest that propagule pressure may be important for population establishment during the time of year that bloom initiation occurs in these lakes. If the propagules are able to persist under current conditions, as seen here, then bloom development may occur once conditions are conducive. In the case of the experimental systems, these conditions occurred in Lake Whitney when zooplankton were removed and salinity elevated to ~1.7psu, and in Lake Possum Kingdom when salinity was elevated to ~2.7psu. Indeed, other studies have shown that propagule pressure of *P. parvum* cells from upstream lakes play an important role in bloom initiation of these systems (Acosta et al., 2015; Errera et al., 2008) and that at times, blooms along the Brazos River Basin have occurred in a sequential manner, seemingly propagating downstream through the introduction of cells from one lake to the next (Roelke et al., 2016).

In treatments where *P. parvum* propagule pressure was increased, the populations either persisted or increased, and this outcome was dependent upon additional treatments applied, i.e., salt addition and/or zooplankton removal. For example, in treatments where

*P. parvum* was added and zooplankton removed, a similar response in *P. parvum* density for each lake was observed. That is, there was a significant increase in population density only when salt was added. Interestingly, though the response for these treatments in each lake mirrored one another, they differed when comparing treatments of similar salinity. Recall that the salt added treatment in Lake Whitney and the ambient salinity condition in Lake Possum Kingdom were ~1.7psu. Because an increase in the *P. parvum* population in Lake Whitney but not Lake Possum Kingdom at similar salinity was seen, while all other abiotic water parameters were also relatively similar, it is likely that differences in the indigenous phytoplankton assemblages of the two lakes were causative. Furthermore, these assemblage differences might be linked to the differing salinity histories of these lakes. Recall that in Lake Possum Kingdom both the historical salinity average and magnitude of fluctuations are greater than in Lake Whitney. Others have shown that small difference in salinity can lead to changes in assemblage composition (Flöder et al., 2010). It may be that the phytoplankton assemblage of Lake Possum Kingdom was comprised of species better able to tolerate relatively higher salinity and fluctuations of greater magnitude.

By comparing the salinity at which *P. parvum* was and was not able to increase in each lake, it can be suggested that the mechanism by which it increased was different in these systems. In Lake Possum Kingdom it is likely that the increased population of *P. parvum* occurred as a result of a higher specific growth rate due to elevated salinity (Baker et al., 2009) and likely an increase in toxicity/allelopathy that would have accompanied the higher population density. Differently, in Lake Whitney the increase in

*P. parvum* density that occurred when salt was added cannot be attributed to a change in growth rate alone since no *P. parvum* increase occurred at similar salinity in Lake Possum Kingdom. Instead, it may be that the phytoplankton assemblage of Lake Whitney was stressed, being less adapted to deal with salinity change, and experienced the loss of some cells due to lysis caused by osmotic effects. This would have opened niche space, providing newly available resources for the mixotrophic *P. parvum* in the form of particulate and dissolved organic matter released from dead cells (Skovgaard & Hansen, 2003; Tillmann, 2003).

In treatments where *P. parvum* was added and zooplankton were present, a different response across lakes was seen. For example, salt addition had no effect on *P. parvum* density in Lake Whitney. Contrasting this observation from the treatment where zooplankton were removed suggests that zooplankton from Lake Whitney completely suppressed the response of *P. parvum* to salt additions. It is likely that losses from grazing coupled with a low specific growth rate (Baker et al., 2007) may not have allowed the population to increase. As Roelke et al. (2016) discusses, preferential grazing of this size class of algae, without armor or other protective structures, and little to no toxicity, would expectantly be high. Differently, *P. parvum* increased when salt was added in Lake Possum Kingdom, even with grazing pressure. This increase, though, was significantly less. It may be that *P. parvum* cells were more toxic at this highest experimental salinity level (~2.7psu), that zooplankton were negatively affected by the high salinity, or a combination of these factors. Considering both lakes, these findings highlight the importance of grazers in suppression of this HAB species. Furthermore,

these findings suggest that interruption of these grazing processes (possibly through feeding of planktivorous fish, zooplankton pathogens or suppression of growth with arrival of cold fronts) may be important for *P. parvum* bloom formation, specifically at salinities just over the bloom threshold level.

Here it is shown that co-occurring disturbances can have synergistic or compounded effects on the harmful bloom-forming, mixotrophic protist, *P. parvum*. It was found that increased salinity, community composition change via the removal of large zooplankton, and elevated *P. parvum* propagule pressure can interact to influence the abundance of *P. parvum* cells. In Lake Whitney all three disturbances had to be applied for the *P. parvum* population to significantly increase, while in Lake Possum Kingdom zooplankton removal was not required for this to occur. Additionally, it is demonstrated that a community's historical exposure to a disturbance may influence effects when that disturbance co-occurs with another. As shown here, when salinity is similar between treatments, communities that have experienced a salinity regime of higher magnitude and greater fluctuation will be better able to suppress a *P. parvum* population increase. These findings highlight the important role of co-occurring disturbances in aquatic ecosystems, and the role historical exposure to disturbance may play in the formation of some HABs**.**

# CHAPTER III

# INVESTIGATION OF HOW N:P RATIOS INFLUENCE THE DELETERIOUS EFFECTS OF *PRYMNESIUM PARVUM,* LABORATORY EXPERIMENTS INVOLVING BIOASSAYS AND LIVE CELL COUNTS

## Introduction

Since the mid-1980s, the recognized range of a HAB forming, mixotrophic, haptophyte species, *Prymnesium parvum,* has expanded in North America. In the south central region of the U.S., where the range expansion to the Americas first occurred, a significant amount of work has focused on understanding bloom dynamics of this species, which appear complex and are influenced by a number of biotic and abiotic factors, including nutrient levels.

Laboratory and field studies have shown that nutrient stoichiometry influences deleterious effects of *P. parvum*, where nitrogen (N) to phosphorus (P) ratios shifted away from Redfield, increase toxicity or allelopathy (Errera et al., 2008; Granéli & Johansson, 2003b). Because deleterious effects of this species impact organisms of multiple trophic levels and the causative agent is unclear, effects to different trophic levels are differentiated. For purposes here, 'toxicity' refers to the negative effects of *P. parvum* or its exudates on species of higher trophic levels and 'allelopathy' as the negative effects of *P. parvum* or its exudates on species of the same trophic level. When a differentiation cannot be made the chemicals are termed "deleterious".

It is widely accepted that high or low N:P ratios increase the production of toxic/allelopathic chemicals in *P. parvum* (Johansson & Graneli, 1999; Roelke et al.,

2016). However, the active mechanism by which organisms experience the deleterious effects is not well understood, nor is the primary purpose for production of the chemicals. For example, there is conflicting evidence as to whether the alellopathic/toxic chemicals are produced and then exuded into the surrounding media or if they are retained inside the cell or on the cell surface, requiring direct cell-to-cell contact for negative effects to occur (Barreiro et al., 2005; Blossom et al., 2014b; Remmel & Hambright, 2012). And as previously stated, it is unknown whether the same chemicals produce toxic and allelopathic effects, though results from a study conducted by Blossom et al. (2014b) suggest that this is likely not the case (at least for juvenile fish). Furthermore, it has been assumed that for allelopathy to be sustained by natural selection an individual cell must benefit from the negative impact of the chemicals on other organisms. However, there may be some other selective mechanism at play of which the allelopathic effects are simply a byproduct.

Stemming from this earlier knowledge and the accompanying unknowns, in this research I ask: 1) Do the deleterious chemical(s) produced by *P. parvum* exist in the environment primarily as endochemicals only being released due to cell death/damage, or do they exist primarily as exochemicals which are exuded by the cell post-production, and does stoichiometry of the growth media influence this? 2) Do the chemicals produced affect species of different structural complexity and trophic levels (phytoplankton and zooplankton) in such a way that they experience correlated mortality? Bioassay tests comparing acute mortality between the cryptophyte *Rhodomonas salina* (a flagellated phytoplankter commonly used as a model for toxicity

assays, and co-occurring with *P. parvum* in natural environments) and the crustacean *Daphnia magna* (a large zooplankter commonly used as a model in toxicity assays, and co-occurring with *P. parvum* in natural environments) are performed to address these questions. To my knowledge, this is the first time such directly comparative experiments have been performed.

Additionally, observations and results from the first round of experiments, which were intended to probe the previous questions, indicated that stoichiometry of *P. parvum* growth media may influence the cell's behavior toward species that are simultaneously competitors and possible prey. This led me to further ask: 3) How is mortality of *R. salina* related to phagotrophic feeding by *P. parvum*?

Understanding the answers to these questions will provide further insight to aspects of *P. parvum* ecology concerning nutrient stoichiometry that may influence toxic/allelopathic potential of a population. Further, by better understanding where deleterious chemicals produced by *P. parvum* are located within the environment (primarily inside the cell or outside the cell) the underpinnings of how these chemicals contribute to bloom formation may be better understood and the evolutionary foundation for their selection made more clear.

## Methods

### *Experimental Design*

To explore the previously posed questions, two sets of experiments were conducted. The first consisted of a series of acute mortality bioassay tests using *R. salina* (target for allelopathic chemicals) and *D. magna* (target for toxic chemicals), Table 3-1.

The second set, repeated these experiments and added time series of counts on mixed live cultures, in order to compare *R. salina* mortality and *P. parvum* feeding behavior across treatments. Additionally, a third media treatment (imbalanced N-reduced) was added to the assay experiments in the second set of experiments however, these results are not

**Table 3-1. Treatment design for the bioassay tests. Imbalanced N-reduced treatment (7-9) result figures are reported in Appendix B.**

| Treatment | Redfield Ratio N:P Media | Imbalanced N:P ($1/20^{th}$ P) Media | Imbalanced N:P ($1/20^{th}$ N) Media | Whole Cell | Gravity Filtered | Vacuum Filtered |
|---|---|---|---|---|---|---|
| **1** | **X** | | | **X** | | |
| **2** | **X** | | | | **X** | |
| **3** | **X** | | | | | **X** |
| **4** | | **X** | | **X** | | |
| **5** | | **X** | | | **X** | |
| **6** | | **X** | | | | **X** |
| 7 | | | x | x | | |
| 8 | | | x | | x | |
| 9 | | | x | | | x |

included here but are shown in Appendix B. Also shown in Appendix B, rather than in this chapter's text, is the *D. magna* acute mortality bioassay from the first set of experiments. For details regarding each of the assay/test methods and culture conditions, see below sections.

Growth media treatments for the *P. parvum* cultures of both experiments 1 and 2 included balanced (N:P at the Redfield ratio) conditions, as well as imbalanced P-reduced conditions (N:P higher than Redfield ratio). Experimental cultures were used on day 17 after their initial inoculation, however cell densities and duration of time in the

stationary phase prior to experiment initiations differed between experiments 1 and 2 (Figure 3-1, Table 3-2). Additional treatments included differential culture processing to achieve 3 culture fractions (Table 3-1). The processes included gravity filtering and vacuum filtering (17kPa) to create *P. parvum* free filtrate (PFF). All filtering was done using GF/C filters (47mm filter diameter, 2μm pore diameter) with 50ml culture aliquots per filter. Additionally, a non-processed fraction treatment was used that included whole culture (i.e., *P. parvum* cells present).

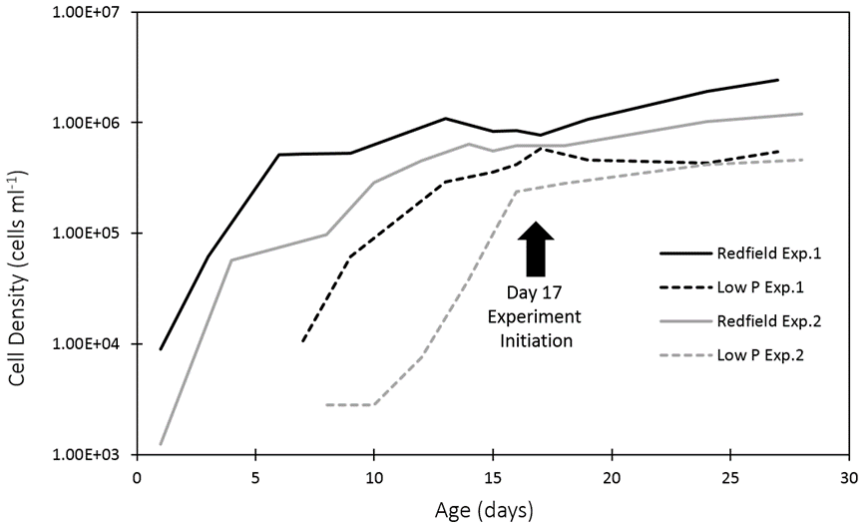


**Figure 3-1. Growth curves for experimental *Prymnesium parvum* cultures. Experiment 1 was run in June 2018, while the Experiment 2 was run in June 2019. All cultures were in stationary growth phase and 17 days of age at the time of experiment initiation.**

### P. parvum *Culture Conditions*

Cultures for experiment inoculation were obtained from the Roelke lab, Texas A&M University, which houses a *P. parvum* strain isolated from the Colorado River

(strain ZZ181, University of Texas, Austin, TX, USA). The stock cultures were maintained in batch using a f/2 media recipe (Guillard & Ryther, 1962) with salinity raised to 5 PSU (Instant Ocean). The experimental cultures were also maintained in batch using a f/2 media recipe and media with P-reduced to $1/20^{th}$ that of Redfield. These cultures were maintained at 5 PSU (Instant Ocean) and kept in an incubator at 15°C with a 12:12 light:dark photoperiod where the light condition was 150 μE $m^{-2}$ $s^{-1}$ from a cool-white fluorescent source.

**Table 3-2. Cell densities at time of experiment initiation for cultures grown in media with different N:P ratios. Experiment 1 was run in June 2018, while the Experiment 2 was run in June 2019. All cultures were in stationary growth phase and 17 days of age at the time of experiment initiation.**

| Media | Density Exp. 1 (cells $ml^{-1}$) | Density Exp. 2 (cells $ml^{-1}$) |
|---|---|---|
| Balanced N:P Media | 776,250 | 624,375 |
| Imbalanced P-reduced Media | 579,375 | 284,375 |

**R. salina *Acute Mortality Bioassay***

The bioassay consisted of *R. salina* (Hill & Wetherbee, 1989) as a biotarget for *P. parvum* allelochemicals. The *R. salina* prior to experiment initiation was maintained in batch culture; using balanced f/2 media; at 5 PSU (through addition of salts, Instant Ocean); under a 12:12 light:dark cycle where the light condition was 11 uE $m^{-2}$ $s^{-1}$; and a temperature of 20°C. A 0.5 dilution series was set up, where 50% of each of 6 unit's volume was *R. salina* culture at a density of $1x10^5$ cells $ml^{-1}$. The other 50% consisted of

*P. parvum* culture or PFF diluted to various concentrations. A control was created as part of each dilution curve which consisted of autoclaved reverse osmosis water with salinity raised to that of the culture conditions, 5ppt. Each of the 9 treatments was tested with triplicate assays, which gave a total of 18 dilution curves. The test vials were then incubated in the dark at a temperature of 25°C for 24 hours, after which time the contents of each vial was preserved using glutaraldehyde at a concentration of 5%v/v. Subsequent enumeration of *R. salina* cells was accomplished using a Hemocytomer counting chamber and counting all intact cells (including rounded cells) on the full gridded area on both sides of the chamber. This technique allowed for relatively rapid counting of many samples which was important due to increased clumping of preserved cells post preservation.

Data was analyzed using R software. The function "drm" was used to fit the data to a predicted regression and the "ED" was used to determine the LC50 for each individual treatment from the fitted curve. LC50's were used to compare the allelopathic effect of different treatments. Lower LC50 values indicated higher toxicity.

**D. magna *Acute Mortality Bioassay***

The bioassay consisted of *D. magna* as a biotarget for *P. parvum* toxins. The *D. magma* culture was maintained in hard water and fed with a mixture of *Selenastrum capriconatum* and wheatgrass powder. Freshly hatched *D. magna* were harvested and transferred to fresh media daily until the time of the test (within 7-10 days of hatching). Individuals were then gently pipetted into an experimental unit (4 individuals per unit) consisting of a well within a 6-well plate and 10mls of a specific culture treatment.

There was a total of 24 individuals tested for each of the 9 treatments. The assays were then incubated in the dark at 25 °C for 24 hours, after which time the status of each *D. magna* was recorded as dead or alive. The remaining live *D. magna* were euthanized.

The data was analyzed using logistic regression in R. Where necessary, data was corrected to compensate for imbalanced classification and separation issues, using R function "ROSE" or a one-step estimator (i.e. "maxit=1"), respectively. The full model included interaction terms, however there were no significant interactions between treatments, nor were there any significant predictors for the culture fraction treatments. Therefore, these terms were removed from the model. The model was re-fit using only the media type as predictor of mortality and p-values for comparisons within this factor are reported. P-values less than 0.05 indicated that a treatment effect was statistically significantly different from others.

***Time Series of Live Cell Counts***

For this test, two mixed cultures were created and subsequent time series of counts conducted. The mixed cultures consisted of 50 mls each of *R. salina* culture and one of the two *P. parvum* cultures grown under different nutrient conditions. Immediately after mixing the first count was conducted. Three individual counters each filled and counted cells in the 4-corner grids on both sides of a hemocytometer. Culture aliquots were each drawn from a different area of the bottom of the containing flask. Variables recorded included lysed *R. salina* cells, *P. parvum* attached to *R. salina* cells and actively feeding, and number of *P. parvum* attached to a single *R. salina*. The counts were repeated every five minutes for the first hour then at hours 1, 2, 9, and 24.

Data were analyzed using ANOVAs to determine whether differences between culture type responses were significant at each time point. P-values less than 0.05 indicated that there was a statistically significantly different between treatments at the given time point. The relationship between *R. salina* lysis and *P. parvum* phagotrophy was further analyzed using a regression plot of the two response variables for both culture types. In excel correlation coefficients ($R^2$) were calculated and the slopes of regression lines forced through the origin were used to compare the relationship between variables for each culture type. The intercept was set to the origin to facility biological interpretation of the fitted line. Differences between slope of the fitted line for both treatments was used to interpret the relationship between *R. salina* lysis and feeding *P. parvum*. A shallower slope would signify broadcast allopathy while a steeper slope would indicate contact interaction. The $R^2$ values for both treatment data sets were used to evaluate the dependency of *R. salina* lysis on *P. parvum* feeding.

## Results

### R. salina *Acute Mortality Bioassay*

Considering experiments 1 and 2, overarching trends in LC50 values were similar (Table 3-3). For both experiments LC50's were lower (indicating greater deleterious effect per unit) for treatments that used *P. parvum* culture grown in imbalanced P-reduced media (Figure 3-2, D-F, J-L), than for treatments that used *P. parvum* grown in balanced Redfield N:P media (Figure 3-2, A-C, G-I). In fact, the only time an LC50 could be determined for the Redfield treatments was during the 2$^{nd}$ experiment for the vacuum filtered culture fraction. For the low P culture treatments, the

lowest LC50 values occurred in the whole cell treatments. Differently, the low P treatments in experiment two were in general lower than those of the 1st experiment. In experiment 2, where the culture was at lower density and earlier in stationary phase there was little difference between the LC50 values of the vacuum and gravity filtered culture treatments, but for experiment 1 where the culture was denser and further into the stationary phase the LC50 for the vacuum filtered treatment was about half that of the gravity filtered treatment.

An important difference to highlight is that between the low P and Redfield treatments of the gravity filtered culture fraction in both experiments. Here results show that deleterious effects are almost non-existent in treatments using the balanced Redfield N:P media culture (Figure 3-2, A, G) but readily occur in the imbalanced P-reduced media treatments (Figure 3-2, D, J). The differences between the two treatments are especially exaggerated during experiment 2 where the *P. parvum* culture used was less dense and earlier in the stationary growth phase.

**D. magna *Acute Mortality Bioassay***

The histogram of *D. magna* mortality by treatment (Figure 3-3) clearly shows the significant difference between media type treatments that is reported in Table 3-4. Results from this test also show that while the low P treatments are significantly different from the control, where no mortality occurred, Redfield treatments are not. For this test, as with the *R. salina* assay, mortality is higher in the low P treatments than in the Redfield treatments, however here there are no differences between culture fractions.

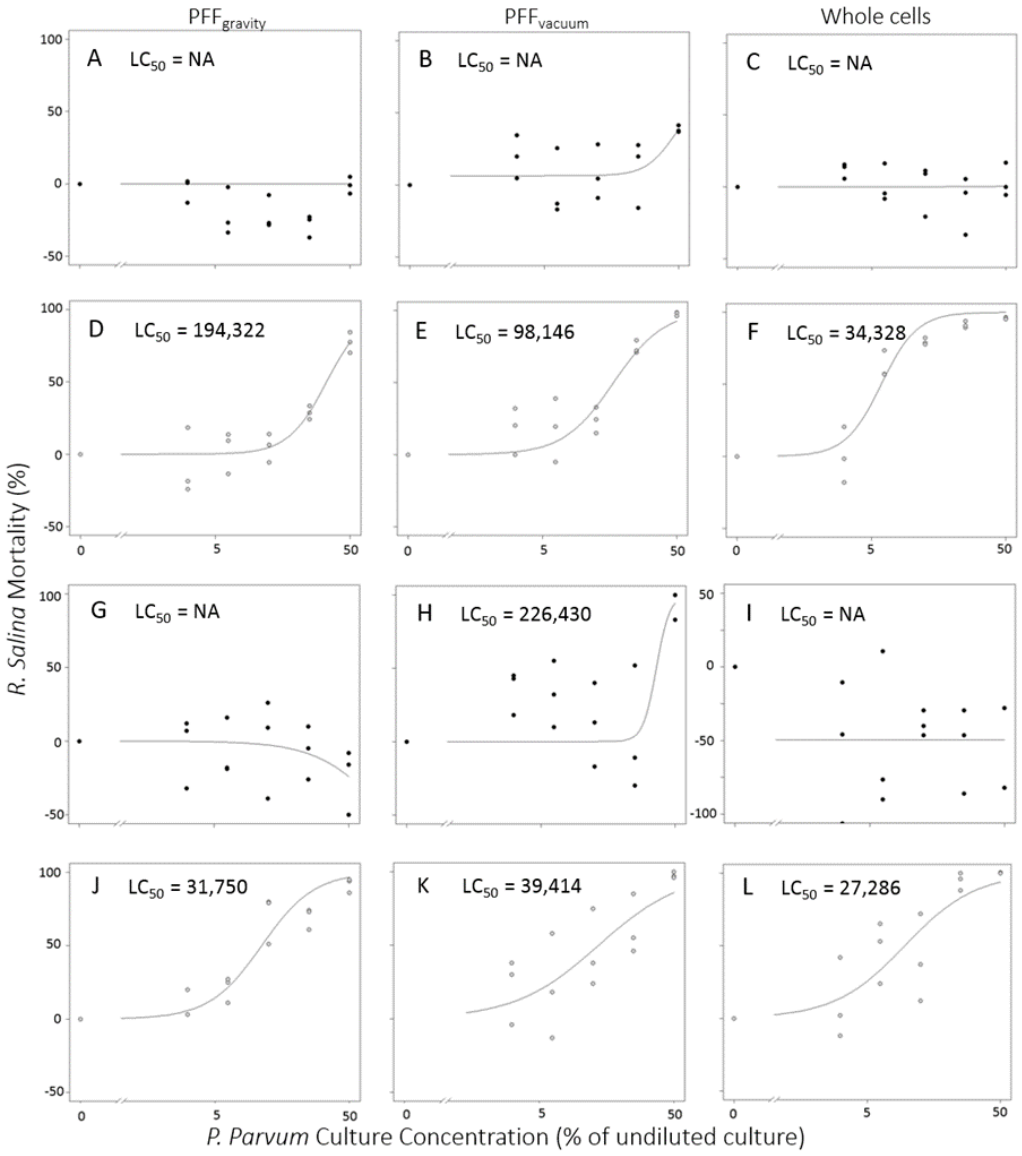


**Figure 3-2. Results for the *Rhodomonas salina* acute mortality assay. Here *R. salina* mortality as a percentage of the control density is shown on the y-axis and the *Prymnesium parvum* undiluted culture percentage is shown along the x-axis. A 6-point dilution series was used so that LC50's for the culture fractions could be determined, which are reported as cell densities (cells ml$^{-1}$). Black data points indicate tests using *P. parvum* cultures grown in balanced N:P media (A-C and G-H) and grey data points indicate tests using cultures grown in imbalanced P-reduced media (D-F and J-L). Figures A-F are from the 1$^{st}$ round of experiments, while figures G-L are from the 2$^{nd}$ set of experiments.**

**Table 3-3. $LC_{50}$ concentrations for the *Rhodomonas salina* acute mortality assay reported as % of undiluted *Prymnesium parvum* culture and as *P. parvum* cell density (cells $ml^{-1}$). If standard error for the estimation was greater than 25% the $LC_{50}$ was reported as NA.**

| Media | Density Exp. 1 (cells $ml^{-1}$) | Density Exp. 2 (cells $ml^{-1}$) |
|---|---|---|
| Balanced N:P Media | 776,250 | 624,375 |
| Imbalanced P-reduced Media | 579,375 | 284,375 |

***Time Series of Live Cell Counts***

The proportion of lysed *R. salina* cells post mixing of the cultures is significantly different between culture media types at almost every time point (Figure 3-4, A). Except at T0, the proportion of lysed *R. salina* cells is always higher in the low P treatment than in the Redfield treatment. The large difference between lysed *R. salina* cells occurs within 5 minutes of the cultures being mixed, which means that widespread cell lysis (~75-100%) occurs rapidly in the low P culture but not in the balanced culture where the highest lysed *R. salina* proportion (~25%) occurred during the 50-minute post mixing count.

*R. salina* phagocytosis by *P. parvum* was significantly different between *P. parvum* culture types at four time-points, ¾ of which occurred within the first 30 minutes of the test (Figure 3-4, B). During this early period *R. salina* phagocytosis was high in the low P culture, but near zero in the Redfield culture. After the 30-minute mark *R. salina* phagocytosis occurred by *P. parvum* cells grown in both media types.

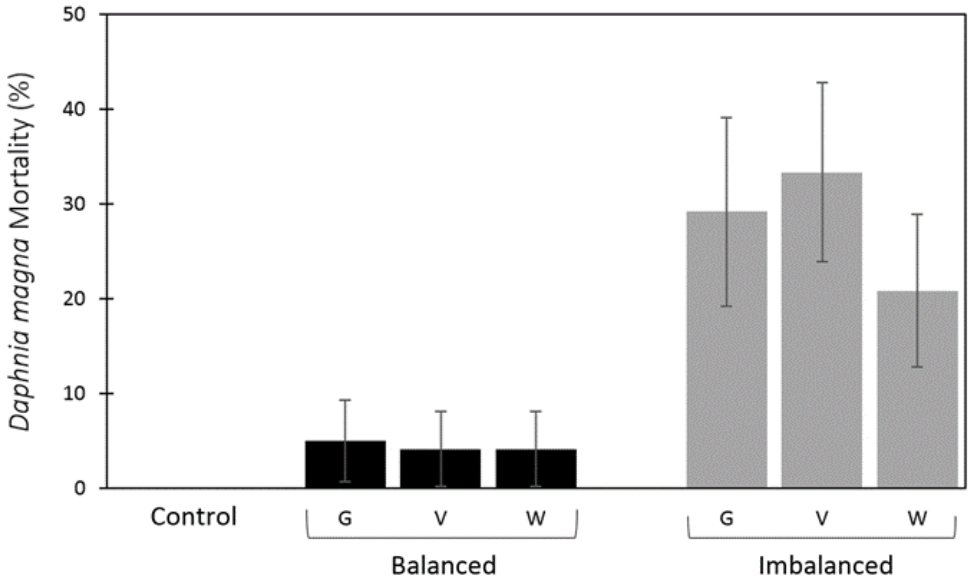


**Figure 3-3. *Daphnia magna* mortality reported as a percentage when exposed to various *Prymnesium parvum* culture fractions grown in media with different N:P ratios (balanced or imbalanced P-reduced). Error bars represent the standard deviation for the binomial distribution.**

**Table 3-4. Statistical analysis of *Daphnia magna* acute mortality assay results. A generalized linear model was fit to data using logistic regression and p-values are reported for comparisons between the levels (control, balanced, or imbalanced P-reduced) of the only significant predictor (*P. parvum* growth media).**

| Comparison | Std. Error | P-value |
|---|---|---|
| Control : Imbalanced P-reduced Media | 0.5483 | 0.009* |
| Control : Balanced N:P Media | 0.5483 | 0.695 |
| Balanced N:P Media : Imbalanced P-reduced Media | 0.4673 | $0.01 \times 10^{-5}$* |

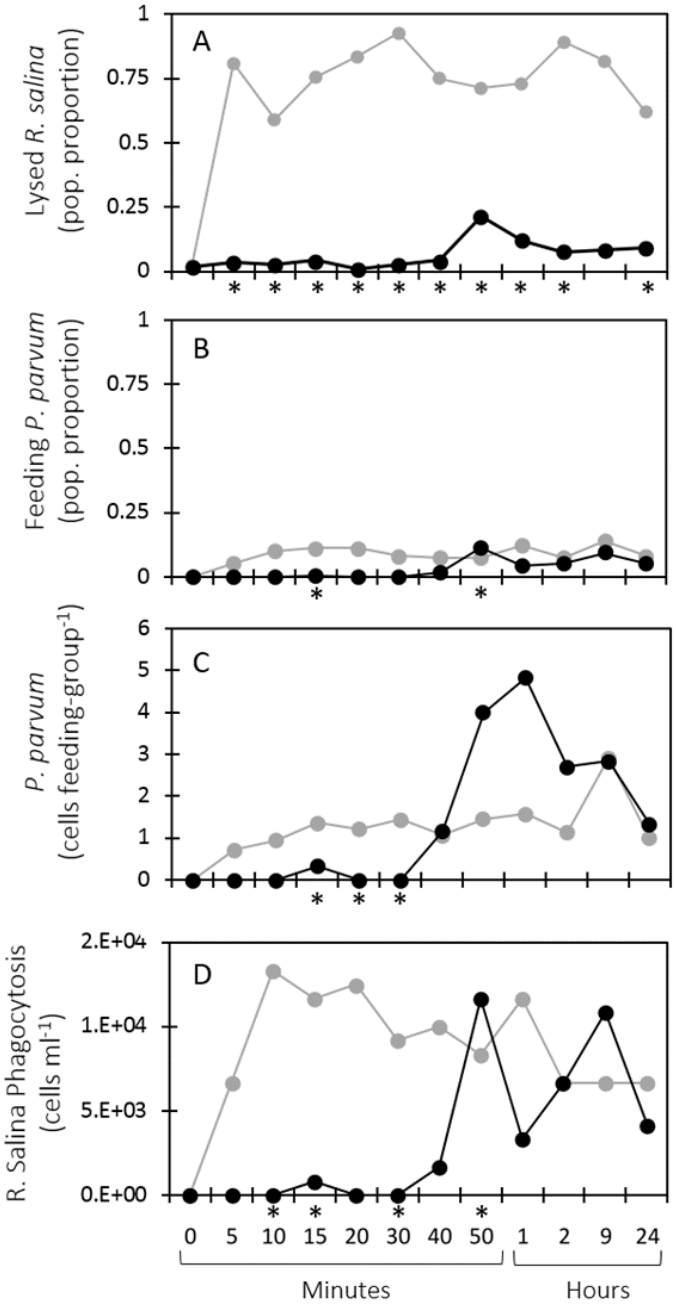


**Figure 3-4. Live count data from a mixed culture of *Rhodomonas salina* and *Prymnesium parvum* over a 24-hour period, post mixing of the two cultures. Each point is an average of three simultaneous counts. No error bars are shown, rather significant differences between responses at each time point are indicated by presence of an asterisk (*).**

To further explore the relationship between *R. salina* lysis and *P. parvum* phagotrophy a regression plot of these two response variables was created for both culture types (Figure 3-5). The slope of the fitted regression line for the Redfield culture treatment is 0.9301, while the slope for the low P culture treatment is 0.1287. A gentler slope can be interpreted to mean lysis of *R. salina* occurs at higher densities in relation to feeding *P. parvum* cells (i.e. a greater deleterious effect per feeding cell which is a signature of broadcast allelopathy), while a steeper slope should be interpreted as lower densities of *R. salina* cell lysis in relation to feeding *P. parvum* cells (a signature of contact interaction). $R^2$ values are 0.554 and 0.114 for the Redfield and low P culture treatments respectively. Here a low linear relationship can be interpreted as a lack of dependence between *R. salina* lysis and *P. parvum* feeding, while a stronger linear relationship indicates greater dependence of *R. salina* lysis on *P. parvum* feeding.

For both culture types similar population proportions engaged in phagotrophy over the 24-hour time period, and this proportion was low, less than 25% (Figure 3-4, C). At only two time-points significant differences were determined, and these differences were small.

The number of *P. parvum* cells per feeding group was significantly different between culture types at three consecutive time points (Figure 3-4, D, 15, 20, and 30 minute counts). During this period the low P culture averaged between one-to-two cells per feeding group, while the low p culture averaged less than one cell per feeding group. However, this pattern disappears near the end of the first hour. Though the trends in the data do not show significant differences past the 30-minute count due to high variability,

the average number of cells per feeding group in the low P treatment stays near constant for the duration of the 24- hour experiment, while in the Redfield treatment it increases after the 30-minute count.

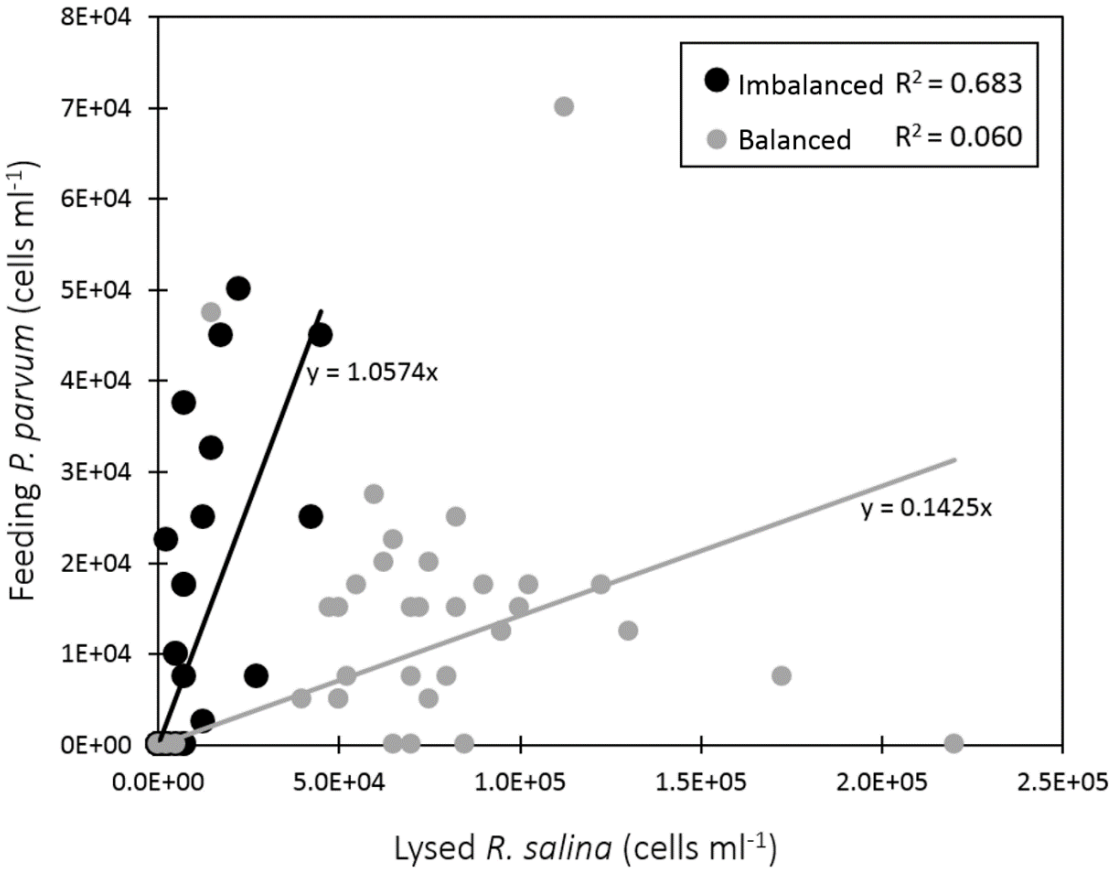


**Figure 3-5. Regression plot of lysed *Rhodomonas salina* cells versus feeding *Prymnesium parvum* during live counts from mixed cultures. Counting took place at variable intervals over a 24-hour period.**

**Discussion**

Results from the *R. salina* acute mortality assay demonstrate that there are strong differences in the deleterious effects of cultures grown in balanced Redfield N:P media compared to those of cultures grown in imbalanced P-reduced media. These results are in agreement with the accepted paradigm that nutrient ratios skewed away from the Redfield ratio increase the deleterious effect of *P. parvum* on intra-trophic species (Graneli and Johansson, 2003). But do differences between the nutrient ratios in these two media types lead to differences in where the deleterious chemicals are found in the environment, i.e., exuded into the water or associated with cell-to-cell contact? To answer this question, the effects of the different culture fractions must be considered.

Comparing the LC50 values between media type for any one of the different culture fractions in isolation leads to the paradigm described above. Differently, when the comparison is made across culture fractions you begin see a larger picture. For both media type treatments, vacuum filtering the *P. parvum* culture increases mortality of *R. salina* as compared to gravity filtration. This suggests that both media types lead to production of deleterious chemicals within the cell but only in the low P culture are those chemicals exuded into the environment in effective concentrations.

So then, is predation by *P. parvum* cells from the balanced Redfield N:P media type inhibited due to the lack of allelochemical production? The whole-culture treatments for the *R. salina* assay suggest that inhibition may have occurred since even at the highest densities of *P. parvum* cell presence there is no clear effect on *R. salina* mortality. However, it may be that *P. parvum* actually did induce *R. salina* mortality via

predation but at a low enough rate that at the end of the 24-hour assay there was little difference in cell density between assay dilutions and the control. If this did occur, then cell-to-cell interactions between predator and prey may be more important for mediation of chemically induced cell death in this balanced nutrient scenario. Evidence that this may in fact be the case is found by turning to the time series counts.

The time-series data, with cell density enumerations and observations of behavior, demonstrate that the balanced Redfield N:P media culture led to low density *R. salina* mortality and that this mortality was correlated with *P. parvum* phagocytosis. Additionally, the slope of the regression line generated by the data for this treatment was close to one (0.9301). This indicates that a near 1:1 ratio of *R. salina* lysis and *P. parvum* feeding occurred (i.e. most lysed *R. salina* counted were being fed on). If the deleterious chemicals produced and held within the cell are necessary for prey ingestion, then it is likely that cell-to-cell interactions are important for *P. parvum* grown under balanced Redfield N:P conditions. Alternatively, it may be that exochemicals at low concentration caused the lysis of these cells which were then located and fed on by *P. parvum*.

In the tests conducted here relatively low levels of mixotrophic/predatory response in cultures of both media types is reported. It may be that *P. parvum* populations take longer than 24 hours to generate a large scale mixotrophic response to available prey. Additionally, in the low P culture during the time series counts it was observed that many *P. parvum* cells had developed clearly visible feeding vacuoles at their posterior region (opposite the haptonema), yet were not feeding on the highly available lysed *R. salina* cells. It is speculated that this may have been due to difficulties

in sensing chemical gradients given off by their lysed prey in an environment where these cues were concentrated. If so, then there may be a "sweet spot" at which cell densities are able to maximize mixotrophy.

Further considering the regression results for the imbalanced P-reduced media treatments, the gentle slope of the fit regression line between *R. salina* lysis and *P. parvum* feeding (0.1287) suggests that deleterious chemicals were exuded into the media by the *P. parvum* cells. This suggestion is further supported by the low linear correlation for this treatment indicating that exuded chemicals do not influence mixotrophic behavior.

Turning to results for the *D. magna* acute mortality bioassay tests, it is shown that overall media type effects are consistent between trophic levels (i.e. the low P treatment increases deleterious effects in both *R. salina* and *D. magna*). However, no significant differences between the culture fraction used were recognized. Therefore, it is likely that either the same chemical has deleterious effects on both species or that these chemicals are produced in proportion to one another. Assuming the former is the case, *D. magna* appear to be less sensitive than *R. salina* to these chemicals. *P. parvum* cell densities in the *D. magna* treatments were double those used in the highest density dilution for the *R. salina* assay. At 50% culture density near 100% *R. salina* mortality occurred whereas at 100% culture density less than 50% D. magna mortality occurred. This relationship is not surprising given that *D. magna* are multicellular organisms with chitin exoskeletons that are likely to be susceptible to lysing chemicals.

These findings are useful for interpreting the conclusions of a study done by Remmel and Hambright (2012). In that study, LC50s obtained from live non-larval fish and *P. parvum* attachment rates onto already-dead *D. magna* were conflated to conclude that "contact micropredation rather than exotoxicity is the role of *Prymnesium* toxins".

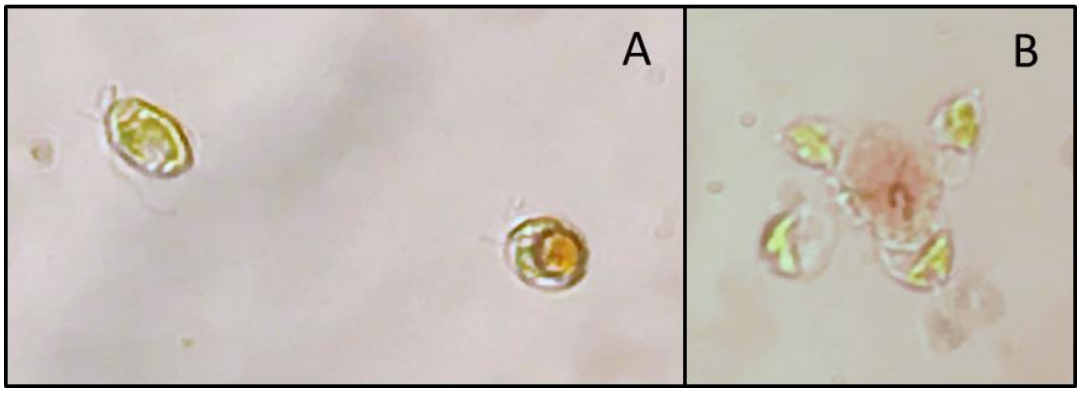


**Figure 3-6. (A) On the left is a normal shaped *Prymnesium parvum* cell. On the right is a *P. parvum* cell that has phagocytized some portion of a *Rhodomonas salina* which is now contained in a vacuole. (B) Four *P. parvum* cells surround a lysed *R. salina* cell, and can be observed approaching the lysed cell with food vacuole (haptonema is pointed away from the lysed cell).**

This conflation makes the presumption that micropredation is at play, although it was not directly observed. Other studies have also shown that *P. parvum* cells seem to readily attach to the surface of immobile objects (Johnsen & Lein, 1989) an observation that Remmel and Hambright (2012) also demonstrated. This is not proof that micropredation was the acting mechanism leading to *D. magna* mortality. Our cultures did not display high density attachment rates to *R. salina* cells nor was *D. magna* mortality increased by direct contact with live cells. Furthermore, observations reported

here show that cell attachment was mediated via the food vacuole at the posterior end of the cell (Figure 3-6) rather than the haptonema as reported by Remmel and Hambright (2012). These observations suggest that different *P. parvum* strains or even populations may exhibit different feeding strategies.

Over all, what do the differences between *P. parvum* populations growing in environments with different N:P ratios mean on a larger ecological scale? At low *P. parvum* densities, when bloom initiation occurs these differences may mean little. From the *R. salina* bioassay results, it is apparent that at low densities the effectiveness of *P. parvum* deleterious chemicals is greatly reduced (it should be noted that all LC50s reported are well above bloom density, typically understood to be ~10,000 cells $ml^{-1}$). Therefore, it is likely that other factors, such as flexibility in nutrition via mixotrophy, play an important role in allowing population increase to kick off and bloom initiation to occur.

However, when the growing population hits some critical density then widespread effects of deleterious chemical production may occur and reinforce the bloom trajectory. The cell density necessary to reach this level will likely depend on the nutrient stoichiometry (N:P ratio) of the environment as shown by this study's results. If the ambient N:P ratio is skewed then a lower density is required for large scale effects to occur. However, if the ambient N:P ratio is balanced the critical density will be much greater and perhaps less likely to become realized. If it is reached, effects may be different due to the primary location of produced chemicals residing within the cell.

From an evolutionary standpoint, these results coupled with those of Jonsson et al. (2009) suggest that some mechanism other than cellular benefit from allelopathic interactions may maintain deleterious chemical production in *P. parvum*. Here it is shown that micro-predation is not that mechanism, at least under imbalanced reduced-P media conditions.

# CHAPTER IV

# INTERACTIVE EFFECTS OF NUTRIENT LOADING AND MIXOTROPHS ON SEASONAL PLANKTON DYNAMICS

## Introduction

Mixotrophy is a common characteristic of many harmful algae bloom (HAB) species (Burkholder et al., 2008; Shumway et al., 2018). This characteristic encompasses a wide range of nutritional strategies in which an organism is able to combine components of heterotrophic nutrition with autotrophic nutrition (Stoecker, 1998; Stoecker et al., 2017). One strategy among mixotrophic phytoflagellates is to rely primarily on photo-autotrophy but supplement nutrient or carbon intake via phagotrophy. This flexibility in nutrient acquisition is thought to allow mixotrophs an advantage in a rapidly changing world (Glibert, 2015; Smayda, 1997).

Though mixotrophy has been identified as a common and important characteristic among many HABs, it has received little attention as a possible bloom initiating mechanism. This is largely due to the overshadowing HAB characteristic of deleterious chemical production, which has been considered of primary importance in bloom dynamics of these species. Much of the study devoted to this area of research has investigated allelopathic properties of the deleterious chemicals, and it cannot be denied that these chemicals play an important role in population dynamics of the producing species by deterring grazers and suppressing competitors (Granéli et al., 2008; Muhl et al., 2018; Shumway et al., 2018).

However, a study conducted by Jonsson et al. (2009) reported that there was insufficient evidence for allelopathy as a bloom initiating mechanism. This conclusion was largely based on findings showing that allelochemicals were ineffective when a population was at low density. But, for some slow growing species, it is difficult to explain their ability to achieve high density blooms without the competitive edge provided by allelochemicals. Perhaps at low density, mixotrophy provides a mechanism by which the population is jump-started, and able to grow to a level where other factors, such as allelochemicals can contribute to continuing bloom formation. Therefore, I ask: How do mixotrophic abilities contribute to the competitive ability of an otherwise non-competitive phytoplankton species? And, in absence of any deleterious chemicals can a slow growing mixotroph population persist and increase?

Though the deleterious chemical concentration may be too low to have a widespread effect when population density is low, it may still allow zooplankton predators to detect and avoid the less palatable meal. Therefore, understanding how mixotroph edibility to zooplankton influences population dynamics when allelochemicals do not have mass-effects, is merited. Thus another question is posed: Does mixotroph edibility to zooplankton influence the population's ability to persist and increase?

Further, it has been reported that in some cases the frequency and magnitude of HAB events is tied to eutrophication, but the mechanisms that moderate this relationship are not well understood (Glibert et al., 2010; Heisler et al., 2008). Systems that have undergone eutrophication, experience increased nutrient loads that lead to alteration of

biotic and abiotic system components. It has been suggested that the increased nutrient concentrations can directly stimulate HAB populations (Glibert et al., 2010). However, for mixotrophic HAB species, increased nutrients may also have indirect stimulatory effects. Therefore, understanding how nutrient loads influence aquatic food webs, especially with consideration to the mixotrophic component, is of great importance.

Like zooplankton, mixotrophic organisms are grazers and like phytoplankton they compete for inorganic resources and are grazed upon. Because their influence spans multiple trophic levels, it is likely that they have a strong effect on system dynamics, especially if abundant. It has been suggested that this influence may be stabilizing if the mixotrophs are bactiverous (Mitra et al., 2014). However, if the population is strongly reliant on phagotrophy of edible phytoplankton (small, immobile cells), it may be that some conditions induce the occurrence of destabilizing, predator-prey dynamics. Indeed, the paradigm known as the paradox of enrichment describes the situation in which nutrient enrichment causes destabilization of phytoplankton-zooplankon systems due to over-exploitation of resources, i.e. boom-bust cycles (Rosenzweig, 1971). Given that aquatic nutrient regimes are in a widespread state of flux, a final question is asked: How do mixotrophs influence system stability under a range of nutrient loads?

To investigate the posed questions a self-organizing numerical model was built that could reproduce well-known PEG successional dynamics (Sommer et al. 1986) in a multi-nutrient, multi-phytoplankton, single zooplankton system, influenced by multiple dynamic abiotic factors. To explore the impact of a mixotroph on the system, one phytoplankton species was parameterized in a way such that flexible nutrition could be

turned on or off (i.e. the population was either photo-autotrophic or photo-mixotrophic). Under a specific nutrient regime, influence of mixotrophic nutrition and edibility to the zooplankton population on species competition was explored. Such a model is the first of its kind. Further, system dynamics were investigated under different phosphorous (P) loading regimes, with and without the presence of a mixotroph, to determine its influence on system stability.

## Methods

### *Model Description and Parameterization*

The numerical model was based on a chemostat design and developed with the goal to reproduce seasonal succession dynamics that have been well studied and described (Sommer et al. 1986). PEG dynamics have been shown to occur in many temperate lake systems, as well as in some coastal systems. To achieve such a model, a dynamic phytoplankton assemblage and a dynamic grazer population were included and were influenced by seasonally dynamic abiotic factors including temperature, averaged mix-layer irradiance, and nutrient (nitrogen and phosphorous) concentrations. All model parameters are reported in Appendix C.

The phytoplankton assemblage included 100 species whose dynamics were driven by competition for nutrients, nutrient concentrations, temperature and light influenced growth rates, as well as grazing and dilution losses. These populations were parameterized to reflect an ecological tradeoff between each species maximum growth rate ($r_i$) and their edibility to the zooplankton population ($E_i$). An additional trade-off was also imposed for each species between its maximum growth rate ($r_i$) and half-

saturation coefficient ($kS_{i,j}$). These trade-offs were linear and organized the assemblage such that fast growing species were grazed at a higher rate and were less competitive than slow growing species at low nutrient concentrations. Temperature, light and dilution losses influenced all phytoplankton species in the same way.

The zooplankton population was parameterized based on data for the genus *Daphnia,* a common and important component of the plankton assemblage in many freshwater systems. This population's dynamics were driven by a phytoplankton species' edibility and abundance. Specific parameter designations are shown in Appendix C – Parameter Table.

Abiotic factors, which include averaged mix-layer irradiance, temperature, inflow rate, and nutrient concentrations were governed by parameter designations, latitudinal location designation, and/or biotic factors. The parameters were chosen to reflect those of the well-studied eutrophic temperate Lake Mendota, located in Wisconsin, USA and were held constant across all experimental simulations reported.

To give one of the phytoplankton populations (Species 1) mixotrophic nutritional abilities, three parameters were added: maximum phagotrophy rate ($f_{max}$), half-saturation for phagotrophy ($k_f$), and phagotrophy threshold ($f_{threshold}$). The maximum phagotrophy rate translates directly to the maximum mixotroph growth rate on phagotrophy. The maximum growth rate on inorganic nutrients ($u_{max}$), the half-saturation coefficient for inorganic nutrient uptake ($kSi,j$), and internal cell quotas ($\theta_{fix}$) remained as they had previously been assigned for Species 1, thereby preserving the ecological trade-offs previously described.

The mixotrophic phytoplankton species had the ability to take up inorganic nutrients (N and P) from the media or to obtain them by phagocytizing other highly edible phytoplankton. At any given time the mixotroph could utilize the nutrient acquisition method that was least limiting to their growth rate, assuming the current rate of growth could be sustained. Additionally, a tradeoff was imposed where the characteristic of flexible nutrition came at a cost to the maximum growth rate (the mixotroph had the lowest growth rate of any of the 100 phytoplankton species). Slow growth of many mixotrophic HAB species has been documented. Biological mechanisms that may lead to this tradeoff are several. For example, it may be that cell surface area is given to vacuole/phagocyte machinery and is not available for nutrient sequestration channels. It is also likely that it is energetically costly to maintain the machinery that facilitates mixotrophy.

Differential equations for the state variables (100 phytoplankton populations, one zooplankton population, and two nutrient concentrations) were generated and solved numerically using a differential equation solver (ode45) in MATLAB (The Math Works, Inc.). The solving function used a variable time-step with local error tolerance set to $10^{-6}$. Each of these modeled factors and their equations is described in detail below.

***Differential Equations***

The system is described by four differential equation forms that depict 100 autotrophic species (Eq. 1), a zooplankter (Eq. 2), a mixotroph (Eq. 3), and two inorganic nutrients (Eq. 4):

$$\frac{dA_i}{dt} = A_i\left(u_{A,i} - h\right) - Zg_i - \psi_1 M f_i \quad (1)$$

$$\frac{dZ}{dt} = Z(u_Z - m - h) + \psi_2 Z_{rest} \quad (2)$$

$$\frac{dM}{dt} = M(u_M - h) - Zg_M \quad (3)$$

$$\frac{dS_j}{dt} = h\left(S_{src,j} - S_j\right) - \sum_{i=0}^{n}\left(A_i u_{A,i}\theta_{fix,A|j}\right) + S_{Z,egest} \quad (4)$$

$$-Mu_{M,a}\theta_{fix,M|j}(\psi_1 - 1)$$

where state variables are $A_i$ the autotroph population density of species $i$ ($10^6$cells$_A$ L$^{-1}$), $Z$ the zooplankton population density (indv. L$^{-1}$), $M$ the mixotrophic species population density ($10^6$cells$_M$ L$^{-1}$), and $S_j$ the ambient concentration of nutrient $j$ (µM).

Additional parameters in Eq. 1 are $u_{A,i}$ the specific growth rate of species $i$ (d$^{-1}$, see Eq. 5 below), $h$ the hydraulic flushing coefficient (d$^{-1}$), $g_i$ the rate at which autotroph species $i$ is grazed ($10^6$cells$_A$ indv$^{-1}$ day$^{-1}$, see Eq. 20), $\psi_1$ the coefficient used to enable autotroph losses due to mixotrophy (unit-less, see Eq. 17), and $f_i$ the rate at which autotrophs are phagocytized by mixotrophs ($10^6$cells$_A$ $10^6$cells$_M^{-1}$ day$^{-}$1, see Eq. 28).

In Eq. 2, additional parameters are $\mu_Z$ the specific growth rate for the zooplankton population (d$^{-1}$, see Eq. 18), $m$ the grazer population specific mortality rate

($d^{-1}$), $\psi_2$ the coefficient enabling seasonal zooplankton hatching (unit-less, see Eq. 23), and $Z_{rest}$ the zooplankton population density added through hatching (indv. $L^{-1}$ $d^{-1}$).

In Eq. 3, additional parameters are $u_M$ the specific growth rate of mixotrophs ($d^{-1}$, see Eq. 24) and $g_M$ the rate at which mixotrophs are grazed by zooplankton ($10^6 cells_M$ $indv^{-1}$ $d^{-1}$, see Eq. 21).

Additional parameters in Eq. 4 are $S_{src,j}$ the concentration of nutrient j in a generic source (μM), $\theta_{fix,A|j}$ the fixed cellular content of nutrient *j* in autotrophs (μmole $10^6 cells_A^{-1}$), $S_{Z,egest}$ the concentration of nutrient produced by grazer egestion (μM $d^{-1}$, see Eq. 30-33), $\theta_{fix,M|j}$ the fixed cellular content of nutrient *j* in the mixotroph (μmole $10^6 cells_M^{-1}$), and $\psi_1 - 1$ (unit-less) a term enabling nutrient decreases resulting from uptake by mixotrophs while growing autotrophically (described more further below).

***Mathematical Equations and Operators***

*Autotroph Growth*

The autotroph specific growth rate, $u_{A,i}$, is a multiplicative function of the most limiting nutrient, light, and temperature. This relationship builds on the work of studies which have assumed the specific autotroph growth rate is determined by light and inorganic nutrient availabilities (Diehl, 2002; Fasham et al., 1990; Huisman & Weissing, 1995; Withrow et al., 2018), by also considering the effect of temperature. Indeed, studies have long discussed the importance of interactions between these three factors on autotroph growth (Eppley et al., 1969; Middlebrooks & Porcella, 1971). The most limiting nutrient has been determined by applying Liebig's Law of Minimum (De Baar, 1994) to growth rates estimated by independent Monod functions (Monod, 1949). Light

limitation on the growth rate is also determined through application of a saturating function (Diehl, 2002; Huisman and Weissing, 1995). Differently, the temperature based growth limitation is determined by the ratio of the growth rate given the temperature on a specific day and the growth rate at the optimal temperature for autotrophic growth. The equation for specific growth rate, $u_{A,i}$, takes the following form:

$$u_{A,i} = u_{max,i}\left(min\left[\frac{\mathrm{S}_j}{\mathrm{S}_j + k_{S,i|j}}, \frac{\mathrm{S}_{j+1}}{\mathrm{S}_{j+1} + k_{S,i|j+1}}\right]\right)\left(\frac{I_z}{I_z + k_I}\right)\left(\frac{u_{\mathrm{T}}}{u_{\mathrm{T},max}}\right) \quad (5)$$

where, $u_{max,i}$ is the maximum specific growth rate of species $i$ ($d^{-1}$), $kS_{i,j}$ is the half-saturation coefficient of species $i$ for nutrient $j$ limited growth (μM), 'min' is a function that selects the minimum growth rate at any given time based on nutrients, $I_z$ is the average irradiance autotrophs experience throughout the mixed layer calculated by integrating from the surface to the depth of the mixed layer $z$ and dividing by the mixed layer depth (quanta $cm^{-2}$ $s^{-1}$, see Eq. 7), $kI$ is the half-saturation coefficient for light limited growth (quanta $cm^{-2}$ $s^{-1}$), $u_T$ is the temperature based growth rate for a specific temperature of a given day ($d^{-1}$, see Eq. 14), and $u_{T,max}$ is the growth rate where $T_t = T_{opt}$ ($d^{-1}$).

The averaged mixed-layer irradiance, $I_z$, follows Lambert-Beer's Law and is calculated using the following equations:

$$I_z = \frac{\int_0^z I_o e^{-z\sigma_{total}}}{z} \quad (6)$$

If $t < \text{ϟ}_{set}$, or $t > \text{ϟ}_{end}$, then $z = z_{deep}$, otherwise $z = z_{shallow}$ (7)

$$\sigma_{total} = 1000c\sigma_c \sum_{i=1}^{n} A_i + M + \sigma_w \quad (8)$$

where, $I_o$ is the averaged mixed-layer irradiance integrated over the photosynthetically active radiation wavelength range (PAR) incident upon the water surface (quanta $cm^{-2}$ $s^{-1}$, see Eq. 9), *z* is the depth of the mixed layer (m) determined by Operator 7, $\sigma_{total}$ is the light extinction coefficient ($m^{-1}$, see Eq. 8), *c* is the chlorophyll concentration (mg Chl *a* $10^6 cells_A^{-1}$), $\sigma_c$ is the light extinction coefficient based on the total concentration of phytoplankton, both autotrophs and mixotrophs ($m^2$ mgChl$a^{-1}$), $\sigma_w$ is the light extinction coefficient based on pure water, tripton and cDOM ($m^{-1}$), $\text{ϟ}_{set}$ is the day of the year when the seasonal thermocline is set, $\text{ϟ}_{end}$ is the day of the year when breakdown of the seasonal thermocline occurs along with the onset of fall turnover, $z_{deep}$ is the depth of the mixed layer when the water column is fully mixed, and $z_{shallow}$ is the depth of the mixed layer during summer stratification. Dates for $\text{ϟ}_{set}, \text{ϟ}_{end}, and\ z$ were approximated based on the work of Magee et al. (2016).

The irradiance integrated over PAR and incident upon the water surface, $I_o$, is a function of time of year and latitude. It is calculated based on the work of Brock (1981). Equation notation of Brock (1981) is used where possible and equations take the form:

$$I_0 = I6(\Omega) \tag{9}$$

$$I6 = (24/\pi)(I0/R1^2)\begin{bmatrix} W1\,sin(L)\,sin(D1) \\ +\,sin(W1)\,cos(L)\,cos(D1) \end{bmatrix} \tag{10}$$

$$R1 = 1/\left\{1 + \left[0.033cos\left(\frac{360d}{365}\right)\right]\right\}^{1/2} \tag{11}$$

$$W1 = arccos\{-[tan(L)\,tan(D1)]\} \tag{12}$$

$$D1 = 23.45sin\left[\frac{360(284+d)}{365}\right]\left(\frac{\pi}{180}\right) \tag{13}$$

where, $I6$ is the total solar radiation at the top of the atmosphere (quanta $cm^{-2}$ $s^{-1}$, see Eq. 10) and Ω is used as an atmospheric correction (unit-less), *I0* is the solar constant, a value representing the energy received per unit time at the earth's mean distance from the sun, outside the atmosphere (quanta $cm^{-2}$ $s^{-1}$), $R1$ is the radius vector of the earth, used to modulate the solar constant with the Earth's eccentrical orbit (unit-less, see Eq. 11), $W1$ is the hour angle, the angle between the setting sun and south point which accounts for the daily rotation of the Earth around itself (°, see Eq. 12), $L$ is the latitude (radians), $D1$ is the declination of the Earth, the angular distance at solar noon between the Sun and the Equator, north-positive (°, see Eq. 13), and '$d$' is the Julian day of the

year. For the model simulations the latitude of Lake Mendota was used, 0.75 radians (43°N).

The temperature based growth rate for all phytoplankton, $u_T$, is calculated based on the Epply-Norberg model (Grimaud et al., 2017) and takes the form:

$$u_T = 1 - \left(\frac{T_d - T_{opt}}{w}\right)^2 \alpha e^{\beta T_d} \quad (14)$$

where $T_d$ is the water temperature of day $d$ (°C, see Eq. 15), $T_{opt}$ is the optimal growth temperature for all phytoplankton (°C), $w$ is the thermal niche width for all phytoplankton (°C), and $\alpha$ and $\beta$ are constants in the Epply function (Eppley, 1972).

The water temperature on a given day $T_d$, is based on a sinusoidal function (°C, see Eq. 15). The equation for this determination takes the form:

$$T_d = \frac{(T_{max} - T_{min})\left(\cos\left((2\pi d_t) + \pi\right)\right)}{2} + \frac{(T_{max} - T_{min})}{2} + T_{min} \quad (15)$$

where, $T_{max}$ is the maximum water temperature in summer, $T_{\min}$is the minimum water temperature in winter, and $d_t$ is the day of the year as a decimal between 0-1. Approximations for $T_{\min}$ and $T_{max}$are based on Lake Mendota (Snortheim et al., 2017), and an under-ice temp of 1.74°C is used (Magee et al., 2016).

Additionally, losses to the autotroph population from mixotrophs needed to be accounted for. These losses only occurred when mixotroph growth was supported by

phagotrophy but not by the ambient nutrient pool. Therefore, the following logic operator was applied:

$$\text{If, } u_{M,S} > u_{M,f}\text{, then, } \psi_1 = 0\text{, otherwise } \psi_1 = 1 \quad (16)$$

where, $\psi_1$ is a unit-less coefficient used to enable autotroph losses from mixotroph phagotrophy, $u_{M,S}$ is the specific autotrophic growth rate for the mixotroph population and is determined in the same way as that of the photoautotroph ($d^{-1}$, see Eq. 24). The parameter, $u_{M,f}$, is the specific phagotrophic growth rate for the mixotrophic population ($d^{-1}$, see Eq. 25).

*Zooplankton Growth*

The specific growth rate for the zooplankton population, $u_Z$ ($day^{-1}$), was determined by applying Liebig's Law of the Minimum to the total N and P ingested relative to the fixed N and P body composition (Roelke, 2000) of an individual zooplankton using:

$$u_Z = \min\left[\frac{S_{ingstd,Z|j}}{\theta_{fix,Z|j}}, \frac{S_{ingstd,Z|j+1}}{\theta_{fix,Z|j+1}}\right] \quad (17)$$

where $S_{ingstd,Z|j}$ is the rate of nutrient uptake through grazing by zooplankton (μmole $indv.^{-1}$ $d^{-1}$, see Eq. 18) and $\theta_{fix,Z|j}$ is the fixed body composition of nutrient *j* for an individual zooplankton (μmole $indv.^{-1}$).

Equations used to calculate the rate of nutrient uptake through grazing by zooplankton, $S_{ingstd,Z|j}$ take the form:

$$S_{ingstd,Z|j} = \sum_{i=1}^{n} (g_i \theta_{fix,A|j}) + g_M \theta_{fix,M|j} \quad (18)$$

$$g_i = \varepsilon_i g_{potential} \left( A_i \Big/ \left( \sum_{i=1}^{n} A_i + M \right) \right) \quad (19)$$

$$g_M = \varepsilon_M g_{potential} \left( M \Big/ \left( \sum_{i=1}^{n} A_i + M \right) \right) \quad (20)$$

$$g_{potential} = g_{max} \left[ \left( \sum_{i=1}^{n} A_i + M - g_{threshold} \right) \Big/ \left( k_g + \sum_{i=1}^{n} A_i + M \right) \right] \quad (21)$$

where $g_i$ and $g_M$ are the rates at which autotroph species *i* and mixotrophs are grazed ($10^6$cells indv$^{-1}$ day$^{-1}$, see Eq. 19 and 20), $\theta_{fix,A|j}$ and $\theta_{fix,M|j}$ are the fixed cellular content of nutrient *j* in all phytoplankton (μmole $10^6$cells$^{-1}$), $\varepsilon_i$ and $\varepsilon_M$ are the edibility of autotroph species *i* and mixotrophs (unit-less), $g_{potential}$ is the potential rate of zooplankton grazing based solely on the total density of all prey, i.e., all phytoplankton ($10^6$cells indv$^{-1}$ day$^{-1}$, see Eq. 21), $g_{max}$ is the maximum zooplankton grazing rate ($10^6$cells indv$^{-1}$ day$^{-1}$), $g_{threshold}$ is the threshold below which phytoplankton cannot be

grazed ($10^6$cells $L^{-1}$), and $k_g$ is the zooplankton half-saturation coefficient for grazing ($10^6$cells $L^{-1}$).

Additionally, zooplankton migration into the system from the benthos via hatching of resting-stage eggs, $Z_{rest}$, is accounted for and the logic operator used to enable this takes the following form:

$$\text{If, } T_d = T_{hatch} \text{and } d < \text{ϟ}_{set}\text{, then } \psi_2 = 1\text{, otherwise } \psi_2 = 0 \qquad (22)$$

where, $\psi_2$ is a coefficient used to turn seasonal zooplankton migration on or off. Here hatching of zooplankton resting-stage eggs is dependent on temperature and is modeled to replicate the hatching of eggs post ice-off, stimulated by temperatures typical of this time of year in temperate lakes (Cáceres, 1998; Cáceres & Schwalbach, 2001; Gyllström & Hansson, 2004).

*Mixotroph Growth*

The mixotroph specific growth rate, $u_M$, is determined using an equation similar to that of the autotrophs, where a multiplicative relationship exists between the most limiting nutrient, light, and temperature. Studies have shown that in some mixotrophic species, nutrients but not carbon from phagocytized particles are incorporated into the cell biomass (Brutemark & Granéli, 2011; Carpenter et al., 2018; Rahat & Jahn, 1965). These studies suggest that though the mixotrophic species can utilize nutrients from phagocytized particles for growth, it is still reliant on carbon fixation. Therefore, light as a factor in the multiplicative relationship is still necessary. Considering the nutrient

limited growth effects of the mixotroph, there are differences from that of the autotroph. Here nutrient limited growth can be determined by either the availability of ambient inorganic nutrients, or the availability of "pre-packaged nutrients" in the form of other readily edible algae. These two forms of nutrient limited growth are meant to reflect differences between flexible mixotroph nutrition, in which either uptake across the cell membrane or phagotrophy can be used by the cell. The equation for $u_{\mathrm{M}}$ takes the form:

$$u_{\mathrm{M}} = \left(max\left[u_{M,S}, u_{M,f}\right]\right)\left(\frac{I_z}{I_z + k_I}\right)\left(\frac{u_{\mathrm{T}}}{u_{\mathrm{T},max}}\right) \tag{23}$$

where $u_{M,S}$ is the specific autotrophic growth rate for the mixotroph population and is determined in the same way as that of the autotroph ($d^{-1}$, see Eq. 24). The parameter, $u_{M,f}$, is the specific phagotrophic growth rate for the mixotrophic population ($d^{-1}$, see Eq. 25), and is determined in a similar way as that of the zooplankton growth rate. Both $u_{M,S}$ and $u_{M,f}$ are instantaneous rates. All other terms are as previously described. Equations for $u_{M,S}$ and $u_{M,f}$ take the form:

$$u_{M,S} = u_{max,\mathrm{M}}\left(min\left[\frac{\mathrm{S}_j}{\mathrm{S}_j + k_{S,M|j}}, \frac{\mathrm{S}_{j+1}}{\mathrm{S}_{j+1} + k_{S,M|j+1}}\right]\right) \tag{24}$$

$$u_{M,f} = min\left[\frac{S_{ingstd,M|j}}{\theta_{fix,\mathrm{M}|j}}, \frac{S_{ingstd,M|j+1}}{\theta_{fix,\mathrm{M}|j+1}}\right] \tag{25}$$

where, $u_{max,\mathrm{M}}$ is the maximum specific growth rate for the mixotroph population based on growth in inorganic nutrient media ($d^{-1}$), $kS_{M|j}$ is the half-saturation coefficient of mixotrophs for inorganic nutrient *j* limited growth (μM), $S_{ingstd,M|j}$ is the potential rate of nutrient *j* uptake through phagotrophy by mixotrophs (μmole $10^6$ $cells_M^{-1}$ $d^{-1}$, see Eq. 26), $\theta_{fix,\mathrm{M}|j}$ is the fixed cellular content of nutrient j in mixotrophs (μmole $10^6$ $cells_M^{-1}$), and all other terms are as previously described.

The rate of nutrient uptake through phagotrophy by mixotrophs, $S_{ingstd,M|j}$, is calculated in the same way as that of the zooplankton, however mixotrophs are only able to phagocytize the most edible autotroph species ($\varepsilon_i > 0.5$). This limitation is imposed to account for studying findings suggesting that some mixotrophic species primarily prey upon small cells that are non-motile and/or lack grazer defenses (Granéli et al., 2012; Roelke et al., 2016). Equations used to calculate $S_{ingstd,M|j}$ take the form:

$$S_{ingstd,M|j} = \sum_{i=1}^{n} (f_i \theta_{fix,A|j}) \tag{26}$$

$$f_i = \varepsilon_i f_{potential} \left( A_i \Big/ \sum_{i=1}^{n} A_i \right) \tag{27}$$

$$f_{potential} = f_{max} \left[ \left( \sum_{i=1}^{n} A_i - f_{threshold} \right) \Big/ \left( k_{\mathrm{f}} + \sum_{i=1}^{n} A_i \right) \right] \tag{28}$$

where, $f_i$ is the rate of phagotrophy based on prey encounters and that prey's edibility ($10^6$cells$_A$ $10^6$cells$_M^{-1}$ d$^{-1}$see Eq. 27), $f_{potential}$ is the rate of phagotrophy based on total autotroph cell density (cells$_A$ cell$_M^{-1}$ d$^{-1}$, see Eq. 28), $f_{max}$ is the maximum rate of phagotrophy (cells$_A$ cells$_M^{-1}$ d$^{-1}$), $f_{threshold}$ is the phagotrophy threshold (cells$_A$ L$^{-1}$), $k_f$ is the half saturation coefficient for phagotrophy (cells$_A$ L$^{-1}$), and all other parameters are as previously described.

*Nutrient (N&P) Concentration*

The concentration of nitrogen (N) and phosphorous (P) produced via grazer egestion, $S_{Z,egest|j}$ and $S_{Z,egest|j+1}$, respectively, are determined as in Roelke (2000) (μM d$^{-1}$, see Eq. 29 & 31). These equations and the logic statements applied to their solutions take the form:

$$S_{Z,egest|j} = Z\left(g_i\theta_{fix,A|j} - g_i\theta_{fix,A|j+1}\left(\frac{\theta_{fix,Z|j}}{\theta_{fix,Z|j+1}}\right)\right) \quad (29)$$

$$\text{If, } S_{Z,egest|j} < 0, \text{ then, } S_{Z,egest|j} = 0 \quad (30)$$

$$S_{Z,egest|j+1} = Z\left(g_i\theta_{fix,A|j+1} - g_i\theta_{fix,A|j}\left(\frac{\theta_{fix,Z|j+1}}{\theta_{fix,Z|j}}\right)\right) \quad (31)$$

$$\text{If, } S_{Z,gest|j+1} < 0, \text{ then, } S_{Z,gest|j+1} = 0 \quad (32)$$

where all parameters are as previously defined. A mixotrophic egestion term was unnecessary because autotrophs and mixotrophs were identical stoichiometrically.

***Baseline (PEG) Model Analysis***

Prior to running experimental simulations with the added mixotrophic population, sensitivity analyses and baseline (PEG) model dynamics were generated. This strategy was employed to further understanding of model functioning before increasing complexity. For these simulations, initial conditions were set to 0.1 $x10^6$ cells $L^{-1}$ for all phytoplankton populations and 0.1 indv. $L^{-1}$ for the zooplankton population. The mixotrophic species maximum rate of phagotrophy ($f_{max}$) was set to zero, effectively making it an autotroph. Sensitivity analyses were conducted by +50% and -50% variation of parameter values. Results for the sensitivity analysis are reported in Appendix D.

***Experimental Simulations***

The first set of experimental simulations were generated by allowing Species 1 mixotrophic abilities ($f_{max}$ = 0.89) and varying its edibility between runs ($E$ = 0.1, 0.5, 0.7 and 0.9). Additionally, the P concentration was held at the same level (0.0694 uM) as was used to generate the baseline dynamics and run sensitivity analyses. Initial conditions for these simulations used year 50, day 50 densities from the baseline simulation for all autotrophic phytoplankton and the zooplankton population. At this time point population dynamics had reached a repeating yearly pattern, (i.e. stable non-equilibrium dynamics had been achieved) and populations were near their yearly

minimum. The mixotroph initial density was set to $0.001x10^6$ cells $L^{-1}$. Each of the three experimental simulations for this test was run for 50 years.

For the next set of tests, 2 model parameters were used as experimental variables: P concentration and mixotroph presence (again, mixotroph presence was manipulated via the $f_{max}$ parameter). Both mixotroph present and absent simulations involved shifting P in increments of 0.05 between simulations, increasing from 0.05 to 3 uM. To generate initial conditions for these tests all populations were set to $0.1x10^6$ cells $L^{-1}$ and the model was allowed to reach a stable state. This was done both with and without the mixotroph present at an intermediate nutrient concentration of 0.694 uM. The resulting year 50, day 50 densities were used for the subsequent tests where nutrient concentration was variable. The model code, programmed in Matlab, is provided in Appendix E.

**Results**

***Baseline (PEG) Model Dynamics***

The baseline simulations were used to understand how the system functioned when no mixotrophic population was included. The dynamics described below for the baseline model encompass a yearly cycle that repeated every 365 days once the system reached a stable non-equilibrium state.

Temperature varied from a low of 1.74°C, increasing up to a high of 24.8°C around day 180 (Figure 4-1, A). Averaged mixed-layer irradiance was primarily influenced by the onset and breakdown of system stratification which occurred on days 122 and 245, respectively (Figure 4-1, B). During the period of system stratification, the mixing depth decreased from 25m to 8m, allowing cells to experience higher depth

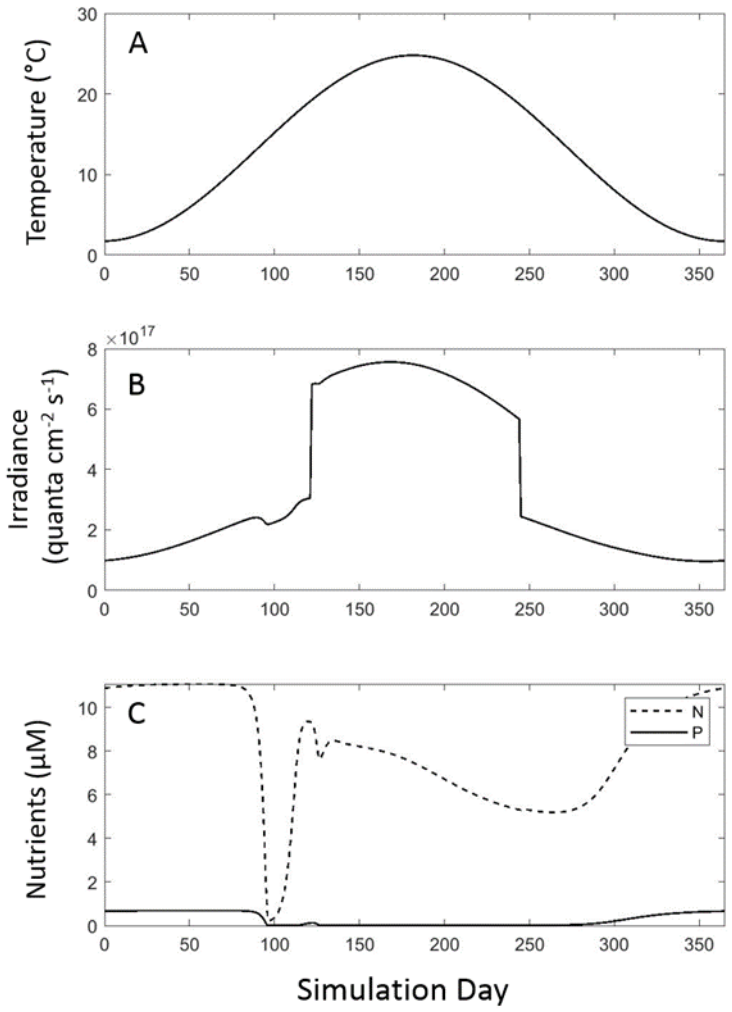


**Figure 4-1. Simulated abiotic system parameters when the biotic populations are at equilibrium. Temperature (A) is a function of Julian day of year. Irradiance (B) is integrated over depth and is a function of Julian day of year, mixing depth, and chlorophyll *a* concentration. Nutrient concentrations (C) are a function of inflow, dilution, and phytoplankton uptake.**

averaged irradiance. Phytoplankton biomass also had an effect on water column irradiance, however it was small in relation to that of stratification status. Dissolved nutrient concentrations in the system were primarily influenced by phytoplankton growth, as is evidenced by the inverse trend in nutrient concentration and phytoplankton

abundance (Figure 4-1, C). N concentrations were not depressed to the same extent as P due to grazer-driven nutrient cycling, resulting from a mismatch between the N & P internal cell quotas of the grazed phytoplankton and those of the grazer.

Abundance of specific components of the plankton varied over the simulated period of 50 years as the model self-organized and phytoplankton species unable to

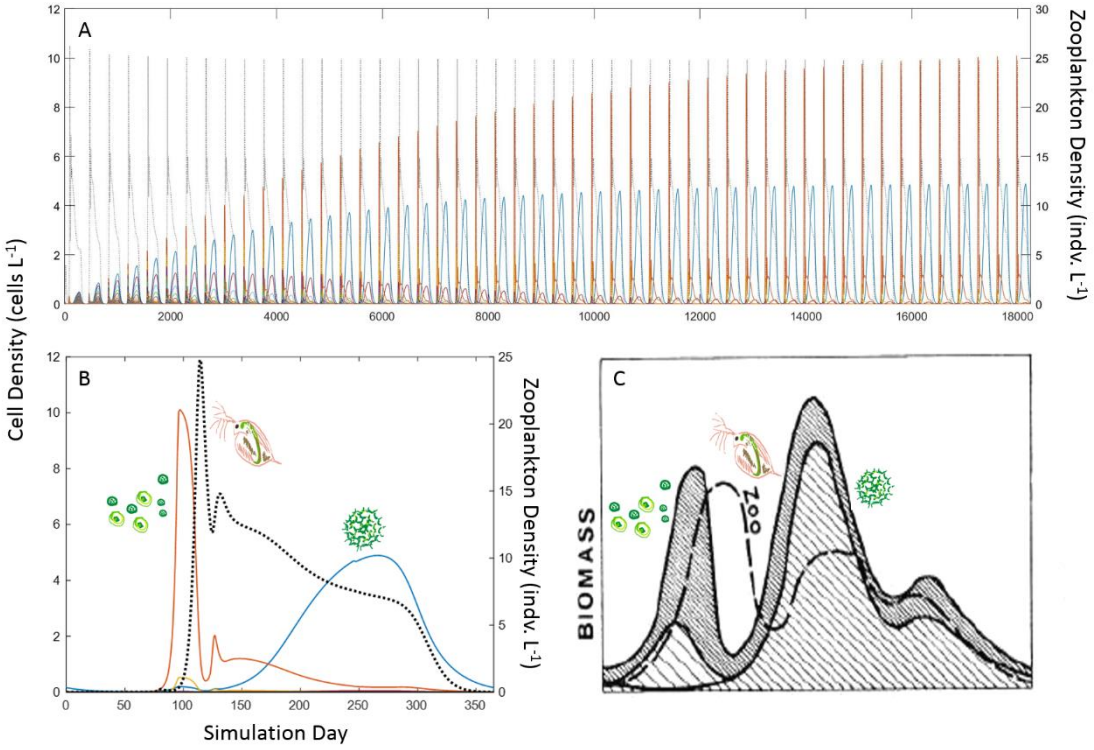


**Figure 4-2. (A) Population dynamics over the full 50-year simulation period when no mixotroph was included and P was at 0.694 µM. Autotrophic phytoplankton populations are indicated with colored lines, and the zooplankton population by the dashed black line. (B) Stable non-equilibrium dynamics of the surviving plankton community over the 50$^{th}$ simulated year. (C) Seasonal succession dynamics of the Plankton Ecology Group (PEG) conceptual model, shown to illustrate similarities between model results. Reprinted with permission from Sommer (1986).**

compete under the imposed conditions effectively went extinct (Figure 4-2, A). At the stable non-equilibrium state (simulated year 50), abundance was influenced by a

**Table 4-1 . Equilibrium density of the mixotroph population under simulations with variably defined mixotroph edibility and nutritional strategy.**

| Simulation | Edibility (0.1-1, unit-less) | Nutrition Strategy | Equilibrium Density (cells $L^{-1}$) |
|---|---|---|---|
| Baseline | 0.1 | Autotrophic | $< 1.0 \times 10^{-320}$ |
| 1 | 0.1 | Mixotrophic | 714,300 |
| 2 | 0.5 | Mixotrophic | 195,400 |
| 3 | 0.7 | Mixotrophic | $< 1.0 \times 10^{-186}$ |

combination of factors that varied seasonally in their magnitude of strength (Figure 4-2, B) which were consistent with the PEG model (Figure 4-2, C). Early on, low temperatures and irradiance suppressed the growth of phytoplankton. When these factors began to increase, high ambient nutrient concentrations allowed explosive growth of r-selected species (fast growing and highly edible). This early biomass peaked around day 100 and these populations effectively sequestered system nutrients. Growth of this highly edible assemblage stimulated zooplankton growth. Due to their high grazing rate, the zooplankton exploited and subsequently suppress the spring assemblage, ushering in a clear water phase.

During this transitional period, P remained low in the system, causing the fast growing species to lose their competitive edge. They were then overtaken by the slower

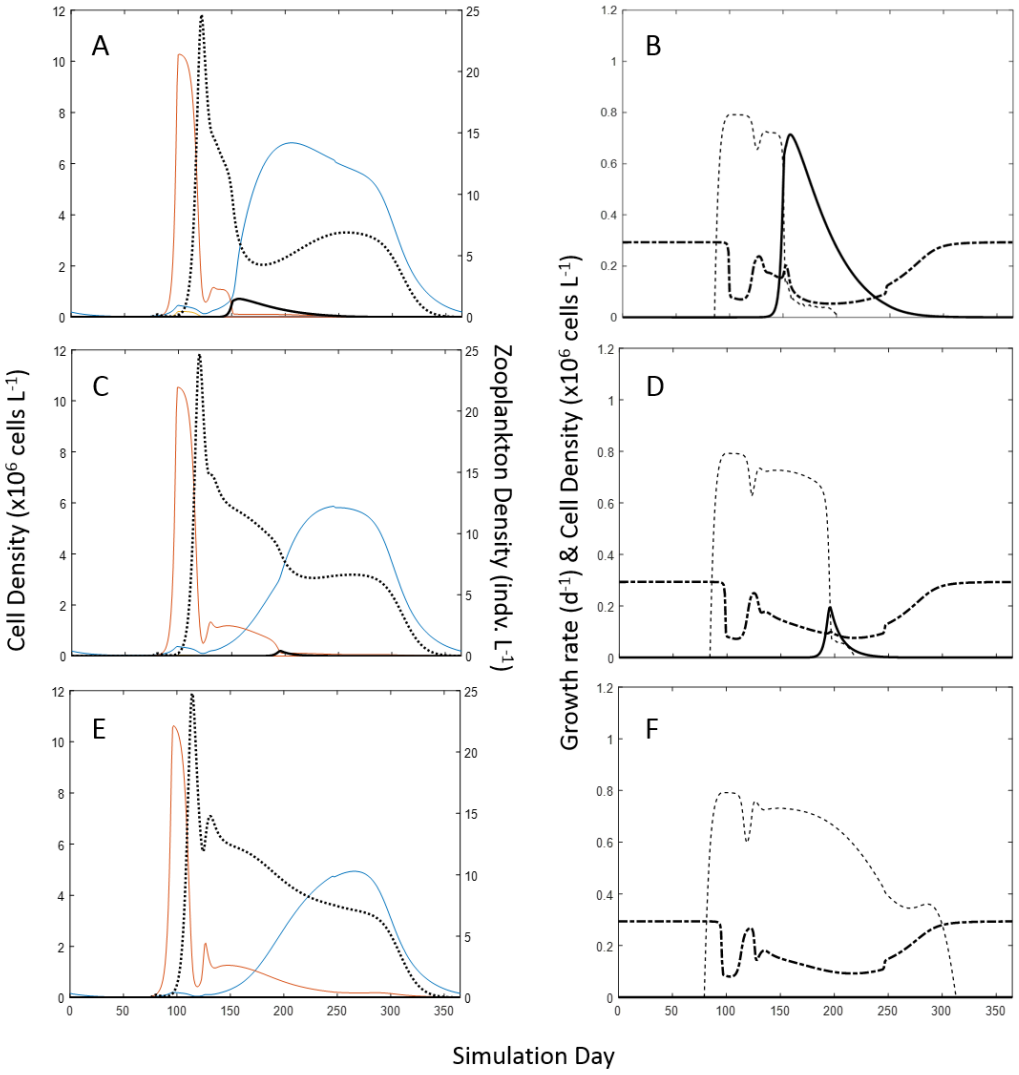


**Figure 4-3. (A, C, E) Equilibrium dynamics of the surviving plankton community with the inclusion of a mixotrophic population. Autotrophic phytoplankton populations are indicated with colored lines, the mixotrophic population by the solid black line, and the zooplankton population by the dashed black line. In all simulations a mixotrophic population was introduced at low density to an equilibrium plankton population. (B, D, F) Growth rates and equilibrium dynamics for the mixotroph population over one simulated year. The mixotroph population cell density is plotted as a solid black line, the growth rate based on inorganic nutrients is plotted as "--." and the growth rate based on phagotrophy is plotted as "-". Mixotroph edibility was varied between simulations (A, B) 0.1 (C, D) 0.5 (E, F) 0.7.**

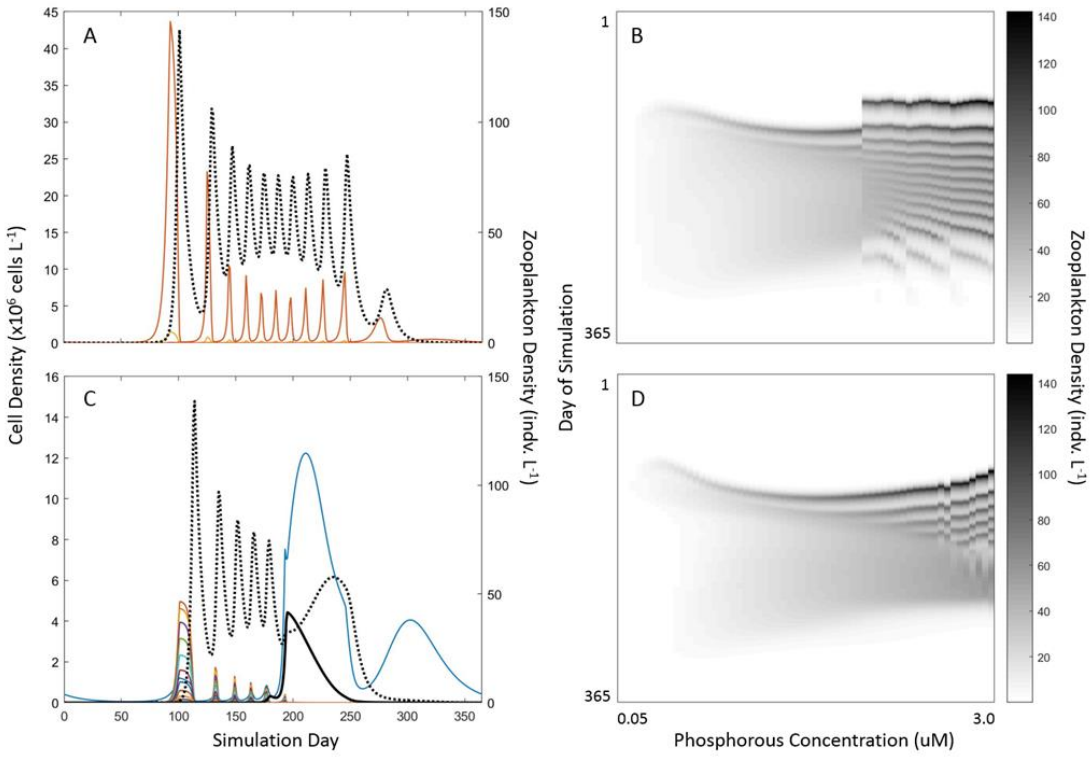


**Figure 4-4 . (A, C) Representative dynamics for the 50th simulated year at high phosphorous loading concentration, 2.95 µM. Autotrophic phytoplankton populations are indicated with colored lines, the mixotrophic population by a solid black line, and the zooplankton population by a dashed black line. (B, D) Zooplankton density as a function of a given simulation's phosphorous (P) loading concentration and day of the 50th simulated year. These images demonstrate the presence of boom-bust cycles at elevated P concentrations. (A, B) No-mixotroph simulations. (C, D) Mixotroph present simulations.**

and less edible K-selected species, which was able to more effectively sequester low-concentration nutrients. This population dominated the biomass throughout the rest of the year and because it was less edible, the zooplankton population declined from its early spring maximum. As the year ended all populations dropped to a seasonal low due to decreasing temperature and irradiance. Importantly, these dynamics are also described

as important characteristics and driving mechanisms of the PEG model, and similarities between the two models are shown (Figure 4-2, B & C).

Phytoplankton Species 1, which was identical to the mixotroph but lacking flexible nutrition, did not persist in the baseline simulation (Table 4-1). Its extinction was due assigned parameterization for the lowest maximum growth rate (0.3) amongst the phytoplankton assemblage. In spite of low edibility (0.1) and high half-saturation coefficient, the species could not overcome dilution effects.

***Variable Edibility Simulations***

When phytoplankton Species 1 was reparametrized so that it could function as a mixotroph with flexible nutrition, it was able to persist (Figure 4-3., A). The mixotroph population density achieved a yearly maximum density of about $7x10^5$ cells $L^{-1}$ (Table 4-1, Sim. 1) once the model reached a stable non-equilibrium state. This increased population density was due to an elevated specific growth rate resulting from phagotrophy prior to the yearly population maximum (Figure 4-3, B). However, when edibility was increased to 0.5 the mixotroph population density was cut down by more than 2/3 to about 1.9 $x10^5$ cells $L^{-1}$ (Figure 4-3, C & D). Further increasing edibility to 0.7 dropped the stable state density to a level effectively extinct from the system (Figure 4-3, E & F). Figures 4-3 (B, D, F) demonstrate that the phagotrophic growth rate remained near its maximum of 0.8 $d^{-1}$ but that increased grazing pressure led to decreased population growth.

Additional simulations were run to investigate the effect of the initial mixotroph density on its population dynamics. These results are not reported here because they did

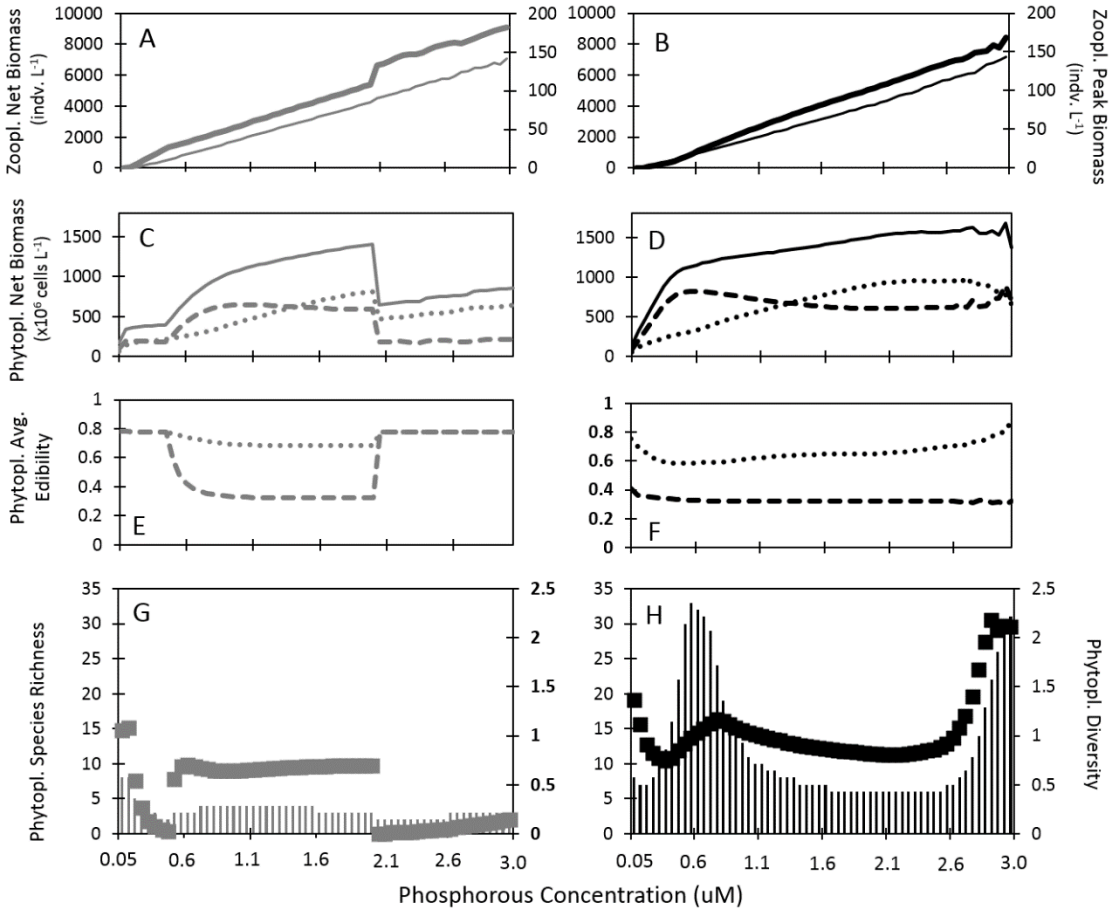


**Figure 4-5. System response variables for simulations run across a phosphorous loading range. (A, C, E, G) No-mixotroph simulations. (B, F, F, H) Mixotroph present simulations. (A, B) Zooplankton net biomass (bold line) and zooplankton yearly peak density (thin line). (C, D) Phytoplankton net biomass for the entire year (solid line), the 1st half of the year (dotted-line), and the 2nd half of the year (dashed-line). (E, F) Density weighted phytoplankton edibility average for the 1st half of the year (dotted-line), and the 2nd half of the year (dashed-line). (E, F) Yearly averaged phytoplankton species richness (bars) and Shannon diversity (squares).**

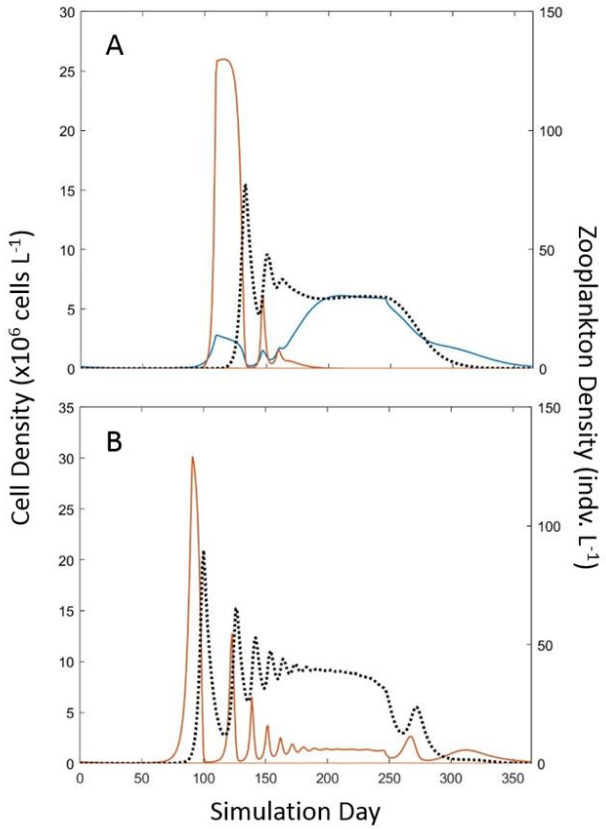


**Figure 4-6. Dynamics of the surviving plankton community over the 50th simulated year. Autotrophic phytoplankton populations are indicated with colored lines, the mixotrophic population by a solid black line, and the zooplankton population by a dashed black line. (A) 1.9 µM phosphorous loading concentration (B) 2.1 µM phosphorous loading concentration.**

not affect stable non-equilibrium state population density. However, it should be noted that the initial conditions do influence the number of yearly cycles required to reach the stable non-equilibrium state.

***Variable Nutrient Concentration and Mixotroph Presence Simulations***

Cyclic predator-prey dynamics increasingly dominated yearly succession as nutrient concentrations were increased (Figures 4-4, A & C). Over the range of P-

loading explored here this phenomenon is demonstrated by zooplankton density-maps, in which the dark banding pattern represents oscillating high-low zooplankton population density (Figures 4-4, B & D). Inclusion of a mixotroph in the system did not completely suppress the occurrence of cycles, however it did dampen the oscillations, reducing the maximum number of cycles from ~11 to ~6 (e.g., Figure 4-4, A & C). Regardless of the number of oscillations that occurred the zooplankton population showed a pattern of increasing yearly net biomass and peak density as nutrient concentrations increased (Figure 4-5, A & B).

Examining phytoplankton response variables across the range of nutrients tested, revealed that mixotroph presence had a large effect on community and assemblage response to nutrient enrichment. For example, when the mixotroph was not present in the simulation, zooplankton yearly net biomass abruptly increased from ~5,400 indv. $L^{-1}$ to ~6,600 indv. $L^{-1}$ (Figure 4-4, A&B) and phytoplankton yearly net biomass dropped sharply from ~1400x$10^6$ cells $L^{-1}$ to ~600x$10^6$ cells $L^{-1}$ (Figure 4-5, C & D) as the P concentration approached 2.0 μM. This change was due to a loss of phytoplankton diversity, wherein less edible, k-selected species were lost from the fall assemblage (Figures 4-5, E&F and 4-6 A & B).

By comparing phytoplankton net biomass with and without the mixotroph, it appears that the mixotroph presence had a stabilizing effect as P increased (Figure 4-5, C & D). No major shifts in biomass occurred, rather a steady and modest increase took place as nutrients increased, peaking near 1,500x$10^6$ cells $L^{-1}$. Further, the fall and spring

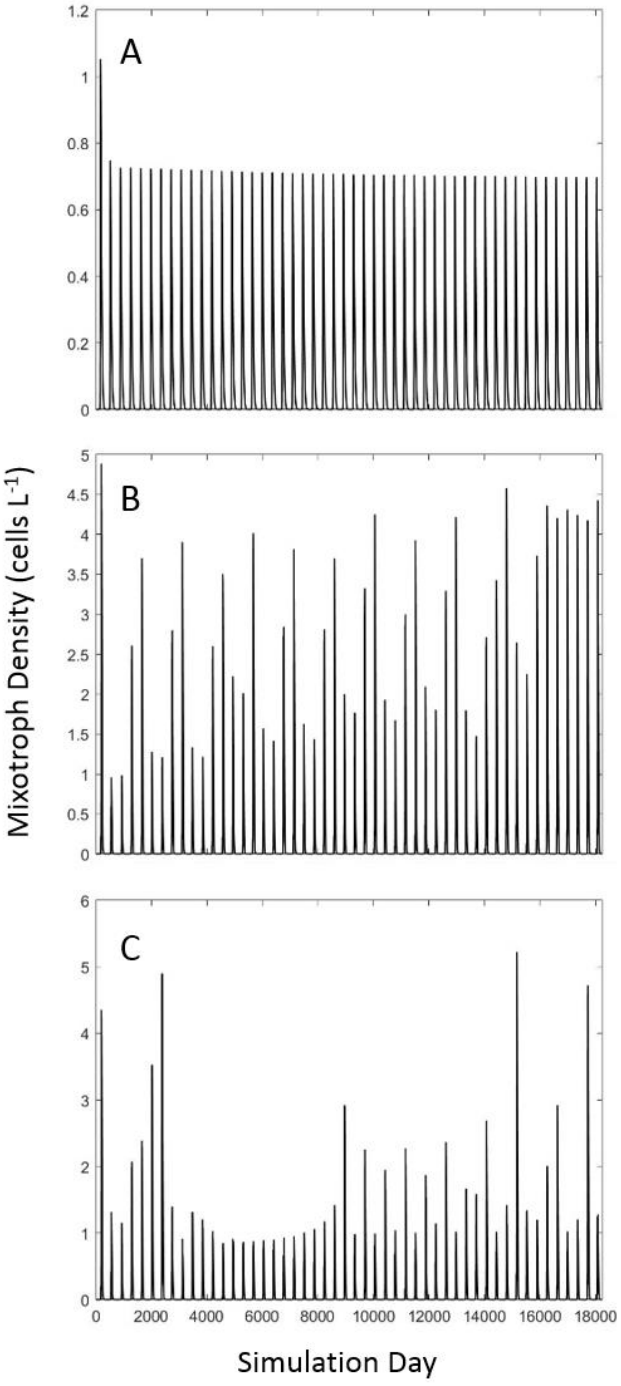


**Figure 4-7 . Representative mixotroph population dynamics over the full 50 year simulation period at various phosphorous loading concentrations of (A) 0.6 µM, (B) 2.95 µM, and (C) 3.0 µM.**

assemblage edibility characteristics remained intact over the simulated parameter range (Figure 4-5, E & F). Yearly averages of diversity and species richness were both elevated in all simulations that included the mixotroph (Figure 4-5, H). These parameters peaked over the same range of nutrient parameter space under which the mixotroph population was also highest.

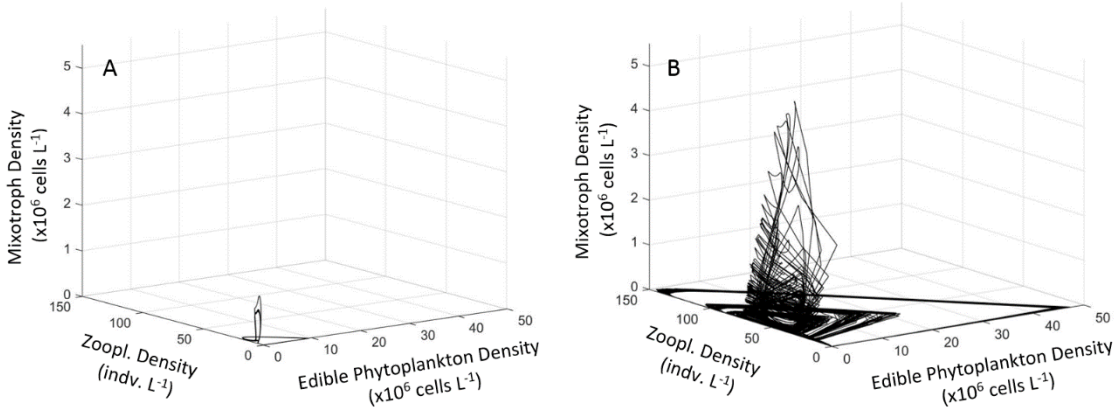


**Figure 4-8. Dynamics of the surviving plankton community over the 50th simulated year. Autotrophic phytoplankton populations are indicated with colored lines, the mixotrophic population by a solid black line, and the zooplankton population by a dashed black line. (A) 1.9 µM phosphorous loading concentration (B) 2.1 µM phosphorous loading concentration.**

Though the zooplankton and autotrophic phytoplankton populations cycled at high nutrient loading concentrations, the mixotroph population experienced a unimodal population trajectory (Figure 4-7). This population achieved a once yearly maximum that, though variable, was present across all nutrient levels (data not shown). At the high end of the nutrient loading range, the yearly maximum became unstable in some simulations, no longer reaching a repetitive yearly maximum density (Figure 4-7, B &

C). Under the unstable conditions, the population density varied from year to year, sometimes achieving relatively high densities >$4.0x10^6$ cells $L^{-1}$. The juxtaposition between system dynamics under high and low nutrient loading scenarios is shown in Figure 4-8, where it can be seen that the boom-bust cycles driven by edible phytoplankton-zooplankton interaction cause destabilization of the mixotroph population.

**Discussion**

Generating seasonal plankton succession dynamics in the theoretical system that were similar to those of the conceptual PEG model was an important step in the model building process. By doing this, a system was generated wherein the driving processes could be carefully explored and based on well described ecological phenomenon. Numerically reproducing PEG-like dynamics in a self-organizing model, as was done here, sheds light on the mechanisms structuring natural aquatic ecosystems and reinforces the significance of key biotic and abiotic system components.

Once the mixotroph population was included as part of the model its ability to persist amongst the phytoplankton assemblage depended on its mixotrophic abilities and its edibility to zooplankton. A modest maximum phagotrophy rate was chosen for the theoretical mixotroph, which translated to a relatively low maximum phagotrophic growth rate (0.8 $d^{-1}$). However, this growth rate was higher than the species maximum growth rate on inorganic nutrients. And, at some time points during the year (under stable non-equilibrium dynamics) the specific phagotrophic growth rate was higher than the specific autotrophic growth rate. During these times, nutrients were limiting not only

for the mixotroph population but for all simulated phytoplankton populations. Therefore, the ability to grow phagotrophically allowed the mixotroph population to increase when fast growing phytoplankton species were unable to. When the mixotrophic species flexible nutrition abilities were removed, leaving it a slow growing but barely edible phytoplankton species, it was unable to compete and persist in the system. These results demonstrate that a non-competitive species population can increase with the aid of flexible nutrition.

However, it is also shown that as the mixotrophic species edibility was increased, grazing pressure eventually overcame any competitive edge that it may have had. And so, the important role that grazers and biologically produced grazing deterrents may play in the dynamics of a mixotrophic population, as shown by other studies, is emphasized here too (Granéli & Johansson, 2003a; Uye, 1986; Watras et al., 1985).

Additionally, it was found that a persistent mixotroph population had a major impact on system stability under increased nutrient loading regimes. When no mixotroph was included in a simulation and nutrient loading was high cyclic predator-prey oscillations occurred, a result that is consistent with the Paradox of Enrichment (Rosenzweig, 1971). However, when the mixotroph was included in simulations the oscillations were suppressed, though not completely. In this theoretical system, the stabilizing effects arose out of the non-exploitative nature of the slow growing mixotroph's predatory interactions. Unlike the zooplankton population, the mixotroph was not able to respond as quickly to highly abundant resources, and therefore did not bring about "boom-bust" cycles. Rather, the mixotroph moderated the over-exploitative

nature of the zooplankton-phytoplankton relationship that occurred when nutrient loading was elevated, decreasing the number of cycles that occurred each year. These findings agree with literature suggesting that increased food-web complexity may lead to increased system stability (Rall et al., 2008; Haydon, 2000; Persson et al., 2001; Polis & Strong, 1996).

Furthermore, investigation of additional response variables demonstrated the stabilizing effect of a mixotroph as the nutrient loading regime was shifted across simulations. In no-mixotroph simulations, a shift occurred in all response variables as nutrient loading approached 2.0 μM. This shift was caused by a loss of the slow growing species from the model and lead to the increasing occurrence of boom-bust cycles. However, in simulations with a mixotroph present no major shifts in the system occurred and, diversity and richness remained stable and even increased at the highest nutrient loading levels.

Though the mixotroph had a stabilizing effect on zooplankton- autotroph system dynamics, reducing the number of yearly boom-bust cycles that occurred, at high nutrient levels mixotroph year-to-year dynamics became unpredictable, no longer reaching a stable non-equilibrium. And, at times the mixotroph population reached high densities ($>4.5x10^6$ cells –L). It is likely that these chaotic dynamics arose out of multi-trophic level, multi-predator interactions where, as nutrient loading increased and zooplankton-phytoplankton fluctuations occurred over greater magnitude and smaller periodicity, mixotroph population dynamics were subject to matches or mismatches with their cycling prey. This led either to high mixotroph growth or lack thereof.

These results demonstrate how bloom initiation of a mixotroph can occur with enrichment when no role of allelochemicals/toxins are considered. In a situation such as this, if the dominant system mixotroph is an HAB, unpredictable dynamics and occurrence of high density populations is an undesirable system state. Further, if the HAB produces deleterious chemicals and is able to reach a threshold at which the chemicals can produce mass effects, the bloom trajectory may be reinforced. This is a furthering of knowledge from Jonsson et al. (2009) who showed that broadcast release of deleterious chemicals was not an effective bloom initiating mechanism. Additionally, these results may shed light on why it is difficult to predict the occurrence of mixotrophic HABs based solely on environmental variables, when the year to year max density of the mixotroph is chaotic with enrichment.

# CHAPTER V

# CONCLUSIONS

Detangling the several mechanisms that may contribute to bloom formation of a specific species is no small task. This is due to the fact that the species of interest are embedded in a complex ecosystem matrix with which they interact. As Glibert and Burkholder (2018) stated,

> "The success of HAB lies at the intersection of the physiological adaptations of the harmful algal species and/or strain (population), the environmental conditions, interaction with co-occurring organisms (both biogeochemically and trophodynamically), and physical dynamics that alter abiotic conditions and/or aggregate or disperse cells (or can alter abiotic conditions in a favorable or unfavorable manner), in turn promoting or inhibiting their growth."

In this body of research, I have endeavored to contribute to the impressive pre-existing collection of studies focusing on the HAB problem. I have considered both species specific and general mechanisms for population success, and I have also investigated multi-trophic level species interactions and abiotic system components that may influence HAB population dynamics. Further, each study took into account some aspect of human induced aquatic system disturbance from increased salinity, to eutrophication, to nutrient ratios skewed away from the Redfield ratio.

In Chapter 1, results suggested that co-occurring disturbances can have synergistic or compounded effects on the harmful bloom-forming, mixotrophic protist, *P. parvum*. It was found that increased salinity, community composition change via the removal of large zooplankton, and elevated *P. parvum* propagule pressure can interact to influence the abundance of *P. parvum* cells, and that the effect is dependent on system

specific disturbance history. When *P. parvum* was inoculated into a plankton community at low density it increased most if zooplankton were removed and salinity was elevated.

In Chapter 2, it was demonstrated that when the nitrogen to phosphorous ratio was skewed away from the Redfield ratio allelochemicals produced by *P. parvum* had acute mass mortality effects on multiple trophic levels. But, when nutrients were supplied at the Redfield ratio allelochemicals were ineffective and cell-to-organism contact was required for deleterious effects to occur. Importantly, only when the *P. parvum* population was at high densities did it appear to have negative effects on other organisms, suggesting that mass effects of allelochemicals may not contribute to bloom initiation.

In Chapter 3, it was demonstrated that flexible nutrition could lead to population persistence of an otherwise non-competitive theoretical phytoplankton species, but only when the species was highly inedible to zooplankton grazers. Additionally, it was shown that as nutrient loading was increased, system stability decreased via the initiation of zooplankton- phytoplankton boom-bust cycles. However, the presence of a mixotrophic population stabilized the system by reducing the number of cycles that occurred. Notably, when nutrient loading was elevated community dynamics became complex and the mixotroph population density was unpredictable from year to year, sometimes reaching high densities. This finding demonstrates how a bloom of a mixotroph can get started with enrichment when no role of toxins is considered.

REFERENCES

Acosta, F., Zamor, R. M., Najar, F. Z., Roe, B. A., & Hambright, K. D., 2015. Dynamics of an experimental microbial invasion. Proceedings of the National Academy of Sciences 112: 11594-11599.

Anderson, D. M., 1989. Toxic algal blooms and red tides: a global perspective. In, P. Okaichi, M. Anderson, T. Nemoto (Eds.), *Red tides: Biology, environmental science and toxicology* (pp. 11-16). New York: Elsevier Science.

Anderson, D. M., Glibert, P. M., & Burkholder, J. M., 2002. Harmful algal blooms and eutrophication: nutrient sources, composition, and consequences. Estuaries 25: 704-726.

Baker, J. W., Grover, J. P., Brooks, B. W., Ureña- Boeck, F., Roelke, D. L., Errera, R., & Kiesling, R. L., 2007. Growth and toxicity of Prymnesium parvum (Haptophyta) as a function of salinity, light, and temperature. Journal of Phycology 43: 219-227.

Baker, J. W., Grover, J. P., Ramachandrannair, R., Black, C., Valenti, T. W., Brooks, B. W., & Roelke, D. L., 2009. Growth at the edge of the niche: an experimental study of the harmful alga Prymnesium parvum. Limnology and Oceanography 54: 1679-1687.

Barreiro, A., Guisande, C., Maneiro, I., Lien, T. P., Legrand, C., Tamminen, T., Lehtinen, S., Uronen, P., & Granéli, E., 2005. Relative importance of the different negative effects of the toxic haptophyte Prymnesium parvum on

Rhodomonas salina and Brachionus plicatilis. Aquatic Microbial Ecology 38: 259-267.

Blossom, H. E., Andersen, N. G., Rasmussen, S. A., & Hansen, P. J., 2014a. Stability of the intra-and extracellular toxins of Prymnesium parvum using a microalgal bioassay. Harmful Algae 32: 11-21.

Blossom, H. E., Rasmussen, S. A., Andersen, N. G., Larsen, T. O., Nielsen, K. F., & Hansen, P. J., 2014b. Prymnesium parvum revisited: relationship between allelopathy, ichthyotoxicity, and chemical profiles in 5 strains. Aquatic Toxicology 157: 159-166.

Brock, T. D., 1981. Calculating solar radiation for ecological studies. Ecological Modelling 14: 1-19.

Brooks, B. W., James, S. V., Valenti Jr, T. W., Urena- Boeck, F., Serrano, C., Berninger, J. P., Schwierzke, L., Mydlarz, L. D., Grover, J. P., & Roelke, D. L., 2010. Comparative toxicity of Prymnesium parvum in inland waters. JAWRA Journal of the American Water Resources Association 46: 45-62.

Brutemark, A., & Granéli, E., 2011. Role of mixotrophy and light for growth and survival of the toxic haptophyte Prymnesium parvum. Harmful Algae 10: 388-394.

Burkholder, J. M., Glibert, P. M., & Skelton, H. M., 2008. Mixotrophy, a major mode of nutrition for harmful algal species in eutrophic waters. Harmful Algae 8: 77-93.

Cáceres, C. E., 1998. Interspecific variation in the abundance, production, and emergence of Daphnia diapausing eggs. Ecology 79: 1699-1710.

Cáceres, C. E., & Schwalbach, M. S., 2001. How well do laboratory experiments explain field patterns of zooplankton emergence? Freshwater Biology 46: 1179-1189.

Carpenter, K. J., Bose, M., Polerecky, L., Lie, A. A., Heidelberg, K. B., & Caron, D. A., 2018. Single-cell view of carbon and nitrogen acquisition in the mixotrophic alga Prymnesium parvum (Haptophyta) inferred from stable isotope tracers and NanoSIMS. Frontiers in Marine Science 5: 157.

Carter, N., 1937. New or interesting algae from brackish water. Arch. Protistenk. 90: 1-68.

Davidson, K., Gowen, R. J., Harrison, P. J., Fleming, L. E., Hoagland, P., & Moschonas, G., 2014. Anthropogenic nutrients and harmful algae in coastal waters. Journal of Environmental Management 146: 206-216.

De Baar, H., 1994. von Liebig's law of the minimum and plankton ecology (1899–1991). Progress in Oceanography 33: 347-386.

DeMott, W. R., Zhang, Q. X., & Carmichael, W. W., 1991. Effects of toxic cyanobacteria and purified toxins on the survival and feeding of a copepod and three species of Daphnia. Limnology and Oceanography 36: 1346-1357.

Diehl, S., 2002. Phytoplankton, light, and nutrients in a gradient of mixing depths: theory. Ecology 83: 386-398.

Ebert, D., Lipsitch, M., & Mangin, K. L., 2000. The effect of parasites on host population density and extinction: experimental epidemiology with Daphnia and six microparasites. The American Naturalist 156: 459-477.

Eppley, R. W., 1972. Temperature and phytoplankton growth in the sea. Fisheries Bulletin 70: 1063-1085.

Eppley, R. W., Rogers, J. N., & McCarthy, J. J., 1969. Half-saturation constants for uptake of nitrate and ammonium by marine phytoplankton 1. Limnology and Oceanography 14: 912-920.

Errera, R. M., Roelke, D. L., Kiesling, R. L., Brooks, B. W., Grover, J. P., Schwierzke, L., Ureña-Boeck, F., Baker, J. W., & Pinckney, J. L., 2008. Effect of imbalanced nutrients and immigration on Prymnesium parvum community dominance and toxicity: results from in-lake microcosm experiments. Aquatic Microbial Ecology 52: 33-44.

Fasham, M., Ducklow, H., & McKelvie, S., 1990. A nitrogen-based model of plankton dynamics in the oceanic mixed layer. Journal of Marine Research 48: 591-639.

Fistarol, G. O., Legrand, C., & Granéli, E., 2003. Allelopathic effect of Prymnesium parvum on a natural plankton community. Marine Ecology Progress Series 255: 115-125.

Flöder, S., Jaschinski, S., Wells, G., & Burns, C. W., 2010. Dominance and compensatory growth in phytoplankton communities under salinity stress. Journal of Experimental Marine Biology and Ecology 395: 223-231.

Fu, F. X., Tatters, A. O., & Hutchins, D. A., 2012. Global change and the future of harmful algal blooms in the ocean. Marine Ecology Progress Series 470: 207-233.

Glasby, T. M., & Underwood, A., 1996. Sampling to differentiate between pulse and press perturbations. Environmental Monitoring and Assessment 42: 241-252.

Glibert, P. M., Berdalet, E., Burford, M. A., Pitcher, G. C., & Zhou, M. (Eds.) (2018). *Global ecology and oceanography of harmful algal blooms*. New York: Springer.

Glibert, P. M., 2015. More than propagule pressure: successful invading algae have physiological adaptations suitable to anthropogenically changing nutrient environments. Aquatic Ecosystem Health & Management 18: 334-341.

Glibert, P. M., Allen, J. I., Bouwman, A., Brown, C. W., Flynn, K. J., Lewitus, A. J., & Madden, C. J., 2010. Modeling of HABs and eutrophication: status, advances, challenges. Journal of Marine Systems 83: 262-275.

Granéli, E., Edvardsen, B., Roelke, D. L., & Hagström, J. A., 2012. The ecophysiology and bloom dynamics of Prymnesium spp. Harmful Algae 14: 260-270.

Granéli, E., & Johansson, N., 2003a. Effects of the toxic haptophyte Prymnesium parvum on the survival and feeding of a ciliate: the influence of different nutrient conditions. Marine Ecology Progress Series 254: 49-56.

Granéli, E., & Johansson, N., 2003b. Increase in the production of allelopathic substances by Prymnesium parvum cells grown under N-or P-deficient conditions. Harmful Algae 2: 135-145.

Granéli, E., Salomon, P. S., & Fistarol, G. O. (2008). The role of allelopathy for harmful algae bloom formation. In, V. Evangelista, L. Barsanti, A. M. Frassanito, V.

Passarelli, & P. Gualtieri (Eds.), *Algal Toxins: Nature, Occurrence, Effect and Detection* (pp. 159-+). Dordrecht: Springer.

Grimaud, G. M., Mairet, F., Sciandra, A., & Bernard, O., 2017. Modeling the temperature effect on the specific growth rate of phytoplankton: a review. Reviews in Environmental Science and Bio/Technology 16: 625-645.

Guillard, R. R., & Ryther, J. H., 1962. Studies of marine planktonic diatoms: I. Cyclotella nana Hustedt, and Detonula confervacea (Cleve) Gran. Canadian Journal of Microbiology 8: 229-&.

Guisande, C., Frangópulos, M., Maneiro, I., Vergara, A. R., & Riveiro, I., 2002. Ecological advantages of toxin production by the dinoflagellate Alexandrium minutum under phosphorus limitation. Marine Ecology Progress Series 225: 169-176.

Gyllström, M., & Hansson, L.-A., 2004. Dormancy in freshwater zooplankton: induction, termination and the importance of benthic-pelagic coupling. Aquatic Sciences 66: 274-295.

Hallegraeff, G. M. (1995). Harmful algal blooms: a global overview. In, G. M. Hallegraeff, D. M. Anderson, and A. Cembella (Eds.), *Manual on Harmful Marine Microalgae* (pp. 1–22). Paris: UNESCO.

Hallegraeff, G. M., 1993. A review of harmful algal blooms and their apparent global increase. Phycologia 32: 79-99.

Haydon, D. T., 2000. Maximally stable model ecosystems can be highly connected. Ecology 81: 2631-2636.

Heisler, J., Glibert, P. M., Burkholder, J. M., Anderson, D. M., Cochlan, W., Dennison, W. C., Dortch, Q., Gobler, C. J., Heil, C. A., Humphries, E., Lewitus, A., Magnien, R., Marshall, H. G., Sellner, K., Stockwell, D. A., Stoecker, D. K., & Suddleson, M., 2008. Eutrophication and harmful algal blooms: A scientific consensus. Harmful Algae 8: 3-13.

Hill, D. R. A., & Wetherbee, R., 1989. A Reappraisal of the Genus Rhodomonas (Cryptophyceae). Phycologia 28: 143-158.

Huisman, J., & Weissing, F. J., 1995. Competition for nutrients and light in a mixed water column: a theoretical analysis. The American Naturalist 146: 536-564.

Huisman, J., & Weissing, F. J., 2001. Fundamental unpredictability in multispecies competition. The American Naturalist 157: 488-494.

Ives, J. D., 1987. Possible mechanisms underlying copepod grazing responses to levels of toxicity in red tide dinoflagellates. Journal of Experimental Marine Biology and Ecology 112: 131-144.

Johansson, N., & Graneli, E., 1999. Influence of different nutrient conditions on cell density, chemical composition and toxicity of Prymnesium parvum (Haptophyta) in semi-continuous cultures. Journal of Experimental Marine Biology and Ecology 239: 243-258.

Johnsen, T. M., & Lein, T. E., 1989. Prymnesium parvum Carter (Prymnesiophyceae) in association with macro algae in Ryfylke, southwestern Norway. Sarsia 74: 277-281.

Jonsson, P. R., Pavia, H., & Toth, G., 2009. Formation of harmful algal blooms cannot be explained by allelopathic interactions. Proceedings of the National Academy of Sciences 106: 11177-11182.

Legrand, C., Rengefors, K., Fistarol, G. O., & Graneli, E., 2003. Allelopathy in phytoplankton-biochemical, ecological and evolutionary aspects. Phycologia 42: 406-419.

Magee, M. R., Wu, C. H., Robertson, D. M., Lathrop, R. C., & Hamilton, D. P., 2016. Trends and abrupt changes in 104 years of ice cover and water temperature in a dimictic lake in response to air temperature, wind speed, and water clarity drivers. Hydrology and Earth System Sciences, 20: 1681–1702.

Middlebrooks, E. J., & Porcella, D. B., 1971. Rational multivariate algal growth kinetics. Journal of the Sanitary Engineering Division 97: 135-140.

Mitra, A., Flynn, K. J., Burkholder, J. M., Berge, T., Calbet, A., Raven, J. A., Granéli, E., Glibert, P. M., Hansen, P. J., & Stoecker, D. K., 2014. The role of mixotrophic protists in the biological carbon pump. Biogeosciences 11: 995-1005.

Muhl, R. M., Roelke, D. L., Zohary, T., Moustaka- Gouni, M., Sommer, U., Borics, G., Gaedke, U., Withrow, F. G., & Bhattacharyya, J., 2018. Resisting annihilation: relationships between functional trait dissimilarity, assemblage competitive power and allelopathy. Ecology Letters 21: 1390-1400.

Patiño, R., Dawson, D., & VanLandeghem, M. M., 2014. Retrospective analysis of associations between water quality and toxic blooms of golden alga (Prymnesium

parvum) in Texas reservoirs: Implications for understanding dispersal mechanisms and impacts of climate change. Harmful Algae 33: 1-11.

Persson, A., Hansson, L.-A., Brönmark, C., Lundberg, P., Pettersson, L. B., Greenberg, L., Nilsson, P. A., Nyström, P., Romare, P., & Tranvik, L., 2001. Effects of enrichment on simple aquatic food webs. The American Naturalist 157: 654-669.

Polis, G. A., & Strong, D. R., 1996. Food web complexity and community dynamics. The American Naturalist 147: 813-846.

Rahat, M., & Jahn, T. L., 1965. Growth of Prymnesium parvum in the dark; note on ichthyotoxin formation. The Journal of Protozoology 12: 246-250.

Rall, B.C., Guill, C., & Brose, U., 2008. Foodweb connectance and predator interference dampen the paradox of enrichment. Oikos 117: 202-213.

Remmel, E. J., & Hambright, K. D., 2012. Toxin- assisted micropredation: experimental evidence shows that contact micropredation rather than exotoxicity is the role of Prymnesium toxins. Ecology Letters 15: 126-132.

Reynolds, C. S. (2006). *The ecology of phytoplankton.* Cambridge: Cambridge University Press.

Roelke, D., 2000. Copepod food-quality threshold as a mechanism influencing phytoplankton succession and accumulation of biomass, and secondary productivity: a modeling study with management implications. Ecological Modelling 134: 245-274.

Roelke, D. L., 2018. Grazers, pathogens and shelf-shading enhance phytoplankton species richness more and reduce productivity less when environments are less dynamic: a theoretical study. Estuarine, Coastal and Shelf Science 211: 152-165.

Roelke, D. L., Barkoh, A., Brooks, B. W., Grover, J. P., Hambright, K. D., LaClaire, J. W., Moeller, P. D., & Patino, R., 2016. A chronicle of a killer alga in the west: Ecology, assessment, and management of Prymnesium parvum blooms. Hydrobiologia 764: 29-50.

Roelke, D. L., & Eldridge, P. M., 2010. Losers in the 'Rock-Paper-Scissors' game: The role of non-hierarchical competition and chaos as biodiversity sustaining agents in aquatic systems. Ecological Modelling 221: 1017-1027.

Roelke, D. L., Grover, J. P., Brooks, B. W., Glass, J., Buzan, D., Southard, G. M., Fries, L., Gable, G. M., Schwierzke-Wade, L., & Byrd, M., 2010a. A decade of fish-killing Prymnesium parvum blooms in Texas: roles of inflow and salinity. Journal of Plankton Research 33: 243-253.

Roelke, D. L., Schwierzke, L., Brooks, B. W., Grover, J. P., Errera, R. M., Valenti, T. W., & Pinckney, J. L., 2010b. Factors Influencing Prymnesium parvum Population Dynamics During Bloom Initiation: Results from In- lake Mesocosm Experiments. JAWRA Journal of the American Water Resources Association 46: 76-91.

Rosenzweig, M. L., 1971. Paradox of enrichment: destabilization of exploitation ecosystems in ecological time. Science 171: 385-387.

Shade, A., Peter, H., Allison, S. D., Baho, D. L., Berga, M., Bürgmann, H., Huber, D. H., Langenheder, S., Lennon, J. T., & Martiny, J. B., 2012. Fundamentals of microbial community resistance and resilience. Frontiers in microbiology 3:417.

Shea, K., & Chesson, P., 2002. Community ecology theory as a framework for biological invasions. Trends in Ecology & Evolution 17: 170-176.

Shumway, S. E., Burkholder, J. M., & Morton, S. L. (Eds.) (2018). *Harmful algal blooms: A compendium desk reference.* Hoboken: John Wiley & Sons.

Skovgaard, A., & Hansen, P. J., 2003. Food uptake in the harmful alga Prymnesium parvum mediated by excreted toxins. Limnology and Oceanography 48: 1161-1166.

Smayda, T. J. (1990). Novel and nuisance phytoplankton blooms in the sea: evidence for a global epidemic. In, E. Granéli, B. Sundström, L. Edler and D.M. Anderson (Eds.), *Toxic Marine Phytoplankton* (pp 29-40). New York: Elsevier.

Smayda, T. J., 1997. Harmful algal blooms: their ecophysiology and general relevance to phytoplankton blooms in the sea. Limnology and Oceanography 42: 1137-1153.

Smayda, T. J., 2002. Adaptive ecology, growth strategies and the global bloom expansion of dinoflagellates. Journal of Oceanography 58: 281-294.

Snortheim, C. A., Hanson, P. C., McMahon, K. D., Read, J. S., Carey, C. C., & Dugan, H. A., 2017. Meteorological drivers of hypolimnetic anoxia in a eutrophic, north temperate lake. Ecological Modelling 343: 39-53.

Sommer, U., Gliwicz, Z. M., Lampert, W., & Duncan, A., 1986. The PEG-model of seasonal succession of planktonic events in fresh waters. Arch. Hydrobiol 106: 433-471.

Stoecker, D. K., 1998. Conceptual models of mixotrophy in planktonic protists and some ecological and evolutionary implications. European Journal of Protistology 34: 281-290.

Stoecker, D. K., Hansen, P. J., Caron, D. A., & Mitra, A., 2017. Mixotrophy in the marine plankton. Annual Review of Marine Science 9: 311-335.

Tillmann, U., 2003. Kill and eat your predator: a winning strategy of the planktonic flagellate Prymnesium parvum. Aquatic Microbial Ecology 32: 73-84.

True, A., Webster, D., Weissburg, M., & Yen, J., 2018. Copepod avoidance of thin chemical layers of harmful algal compounds. Limnology and Oceanography 63: 1041-1055.

Utermöhl, H., 1958. Zur Vervollkommnung der quantitativen Phytoplankton-Methodik: Mit 1 Tabelle und 15 abbildungen im Text und auf 1 Tafel. Internationale Vereinigung für Theoretische und Angewandte Limnologie: Mitteilungen 9: 1-38.

Uye, S., 1986. Impact of copepod grazing on the red-tide flagellate Chattonella antiqua. Marine Biology 92: 35-43.

Watras, C. J., Garcon, V. C., Olson, R. J., Chisholm, S. W., & Anderson, D. M., 1985. The effect of zooplankton grazing on estuarine blooms of the toxic dinoflagellate Gonyaulax tamarensis. Journal of Plankton Research 7: 891-908.

Withrow, F. G., Roelke, D. L., Muhl, R. M., & Bhattacharyya, J., 2018. Water column processes differentially influence richness and diversity of neutral, lumpy and intransitive phytoplankton assemblages. Ecological Modelling 370: 22-32.

Wolfe, G. V., 2000. The chemical defense ecology of marine unicellular plankton: constraints, mechanisms, and impacts. The Biological Bulletin 198: 225-244.

Wurbs, R. A. (1991). Natural salt pollution in the Brazos River Basin. Paper presented at the Hydraulic Engineering.

Wurbs, R. A. (1991). Natural salt pollution in the Brazos River Basin. In, R. M. Shane (Ed.), *Hydraulic Engineering* (pp. 1014-1019). New York: American Society of Civil Engineers.

Wurbs, R. A., 2002. Natural salt pollution control in the southwest. Journal (American Water Works Association) 94: 58-67.

Yariv, J., & Hestrin, S., 1961. Toxicity of the extracellular phase of Prymnesium parvum cultures. Microbiology 24: 165-175.

# APPENDIX A

## ADDITIONAL METHODS AND RESULTS NOT INCLUDED IN CHAPTER 2

### Methods

Response variables reported in this appendix include *P. parvum* ambient toxicity, chlorophyll *a* as a proxy for total phytoplankton biomass, total zooplankton biovolume and biovolume of higher zooplankton taxonomic groups. Chlorophyll *a* was sampled at the time of experiment initiation, 3 days later at the midpoint, and finally on day 7. Zooplankton and toxicity samples were taken from each unit only at the conclusion of the experiment.

Because there are no standards for prymnesins, direct chemical analysis of toxin production was not possible, therefore a bioassay was used to determine ambient toxicity. For assay tests, samples taken at the conclusion of the experiment were stored in dark Nalgene bottles with close to no head space and kept on ice during transport to prevent deterioration of ambient toxins. Assay tests were initiated within 24hrs of sample collection.

The bioassay consisted of R*hodomanas salina* as a biotarget for extracellular *P. parvum* allelochemicals. The *R. Salina* culture was maintained in batch, using balanced f/2 media raised to 5psu using Instant Ocean, under a 12:12 light:dark cycle, at an irradiance of 11 uE $m^{-2}s^{-1}$, and a temperature of 20 $^{o}$C. Experiment samples were gravity filtered through GF/C glass fiber filters (47mm diameter), in aliquots of 50mls, to obtain a cell-free filtrate while ensuring minimal cell breakage. The filtrates were stored in the dark and used for assay tests within 30 minutes of being processed. A 0.5 dilution series

was set up, where 50% of each of 6 unit's volume was *R. salina* culture at a density of $1x10^4$ cells ml-1 (Brooks et al., 2010; Blossom et al., 2014), and the other 50% consisted of *P. parvum* cell-free filtrate diluted to various concentrations. Each culture was tested with triplicate assays. The test vials were incubated in the dark at a temperature of 25°C for 24 hours, after which time the contents of each vial were preserved using glutaraldehyde at a concentration of 5%v/v. Subsequent enumeration of *R. salina* cells was accomplished using a Sedgwick rafter counting cell, where predetermined transects were counted. All intact cells were counted (including rounded cells).

Total phytoplankton biomass was estimated using the chlorophyll *a* concentration in each sample, following standard fluorometric procedures (Federation & Association, 2005). Two 50 mL samples were taken from each well-mixed unit and filtered through 47 mm GF/F glass fiber filters under low vacuum (kPa<17). The filters were immediately frozen until time of analysis, when pigments were extracted with 90% acetone, centrifuged, and analyzed with a Turner designs 10-AU fluorometer.

To characterize the zooplankton community present in each unit at the conclusion of the experiment, a 17L sample was concentrated down to 100ml, after being filtered through the cod end of a Schindler trap (61 um mesh size). These samples were preserved using buffered formalin, 5% v/v. Slides were prepared using the Utermöhl (1958) settling technique, with a 3-5ml sample volume. Zooplankton were counted until 200 organisms had been observed or 100% of the slide had been enumerated. Zooplankton dimensions were measured and best fit to geometric shapes, which were used to determine biovolume (Likens & Wetzel, 1991). Biovolume of higher

zooplankton taxonomic groups was estimated by categorizing observed zooplankton into the following groups: adult copepod adults, copepod nauplii, rotifers, and cladocerans.

***Analysis***

For all response variables 2- or 3-way ANOVAs, depending on the number of experimental variables included in the specific analysis, were conducted to test for main effects, as well as interaction effects of the experimental variables. If a significant interaction effect on a response variable was determined, any significant main effects were disregarded. Data from each lake was analyzed separately.

For Chl *a* response variable, the proportional changes were calculated as, $(Y_{final} - Y_{initial})/Y_{initial}$, and used for statistical tests. Initial analyses included examination of *P. parvum* cell density data where only treatments containing the ambient lake assemblages (i.e. no *P. parvum* was added) were included. Subsequent analyses, which are reported here include only treatments where *P. parvum* culture had been added.

Toxicity was mostly low in experiment samples, therefore EC50 values could not be calculated from dilution series data and an alternative method was needed to generate values indicative of toxicity. Here, bioassay data used for ANOVA analysis was generated in a multi-step process. Because of variation in *R. salina* cell density among dilution series controls, each sample from the dilution series was standardized by calculating its percentage of the control from a specific assay test ($Y_{sample}/Y_{control}*100$). A line was then fit to each set of dilution series points, and the slope of this line was calculated. This slope was used as an indicator of toxicity in a sample, where the more

negative the slope, the more toxic the sample, and a positive slope was considered indicative of a stimulatory effect of sample filtrate.

Analyses for total zooplankton biovolume, and biovolume of higher zooplankton taxonomic groups were conducted using $Y_{final}$ data only. This was necessary due to the questionable integrity of a sample taken at experiment initiation, leading to concern about our ability to accurately characterize the initial zooplankton assemblage.

Multivariate statistical analyses were also conducted using Principle Component Analysis (PCA) in R (version 3.3.2). The objective of this analysis was to better understand the relationship between response variables, specifically those for which there was high variation within treatment samples (biovolume of higher zooplankton taxonomic groups). Data used in this analysis included *P. parvum* density, chlorophyll *a*, total zooplankton biovolume and biovolume of higher zooplankton taxonomic groups. The "prcomp" function in R, with the "center" and "scale" arguments set as "TRUE", was used to conduct the PCA. The resulting PCs were ranked and examined using scree curves, which revealed that 56.4% of the variation within the data was represented on principle components 1 and 2.

## Results

### *Toxicity of* P. parvum

Samples taken from experimental units at the conclusion of the study showed mostly little to no ambient toxicity (Figure AA-1). Using our assay analysis methodology, a highly toxic sample where all target algal cells lysed upon exposure to the highest filtrate concentration, resulted in a slope of -2. The most negative slope

among our sample data, which indicated the highest toxicity level, came from a Lake Whitney (LW) treatment where the average slope was -0.72. For purposes here, this was considered a moderate level of toxicity. It should be pointed out though, that variation within this treatment's replicates, as well as that of other treatments from both lakes, was high (Figure AA-1). Moderate ambient toxicity was not common amongst treatments results, with most other treatment averages indicating low to no toxicity and some demonstrating a stimulatory effect on the target algae (Figure AA-1).

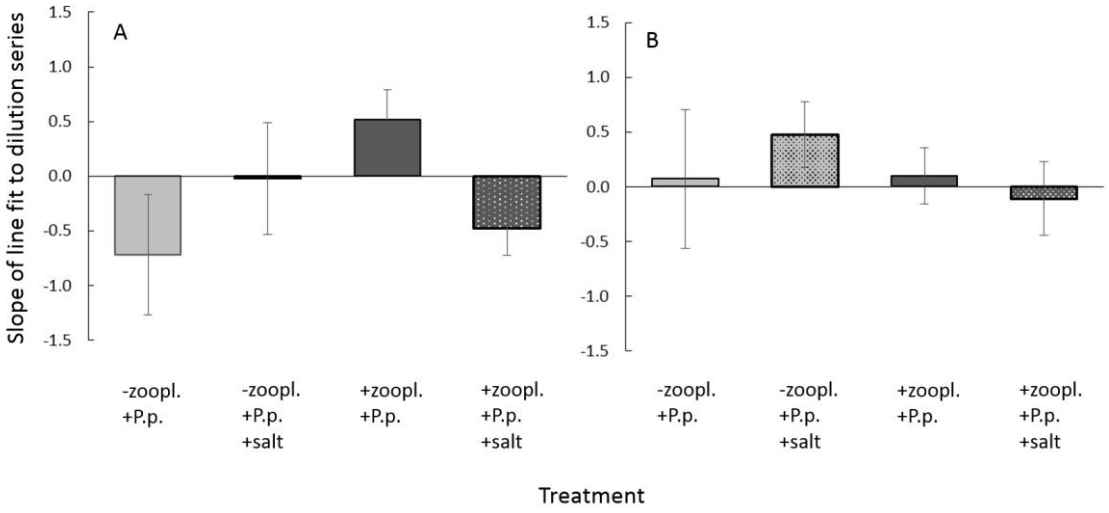


**Figure AA-1. Toxicity estimated from the average calculated slope of a line fit to 0.5 dilution series data for Lake Whitney (A) and Lake Possum Kingdom (B) experimental treatments. Dilution series data consisted of *R. salina*, the biotarget for extracellular *Prymnesium parvum* toxins, cell density in each of 6 units. (mean + SD, n=3)**

***Lake Whitney***

Looking at the chl *a* data, it was found that there was no significant effect or interaction effects of any treatment (Figure AA-2, A). Similar to our results for chl *a* in LW units, it was found that there was no significant difference between treatments for total zooplankton biovolume (Figure AA-3, A). Breaking the biovolume down into higher taxonomic groups, which includes copepod adults, copepod nauplii, cladocera, and rotifers, yielded no change in statistical results (Figure AA-4, A, C, E, and G). Though no effect of any treatment was observed for these groups, there are differences in trends among them. For copepod adults, all units with experimental manipulations had higher

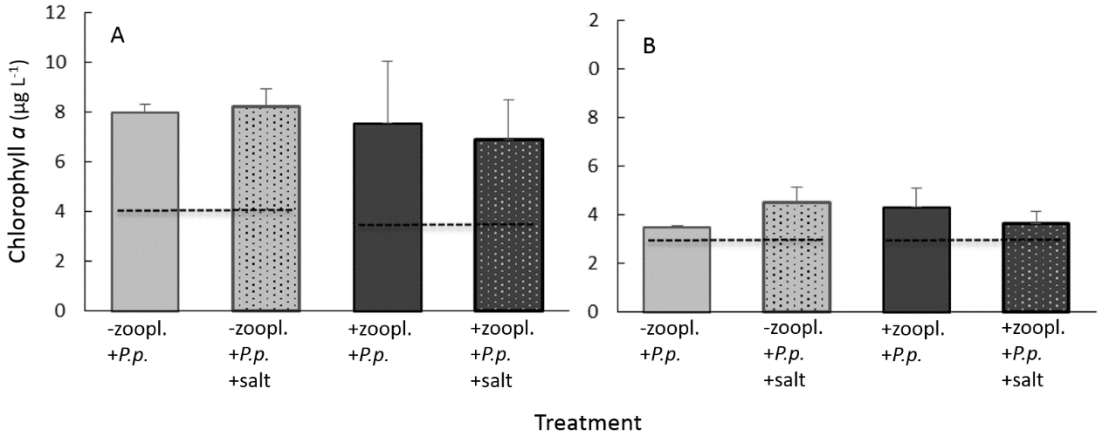


**Figure AA-2. The average initial (horizontal dashed lines) and final (vertical bars) Chlorophyll *a* concentrations for Lake Whitney (A) and Lake Possum Kingdom (B) experimental treatments, respectively. (mean + SD, n=3)**

biomass than the control (0.95 $mm^3 L^{-1} x10^8$), and the highest biomass (5.92 $mm^3 L^{-1} x10^8$) was seen in the salt only addition treatment. For copepod nauplii, the salt addition treatment and the *P. parvum* addition treatment had similar biomass (3.14 $mm^3 L^{-1} x10^7$ and 3.36 $mm^3 L^{-1}$ x

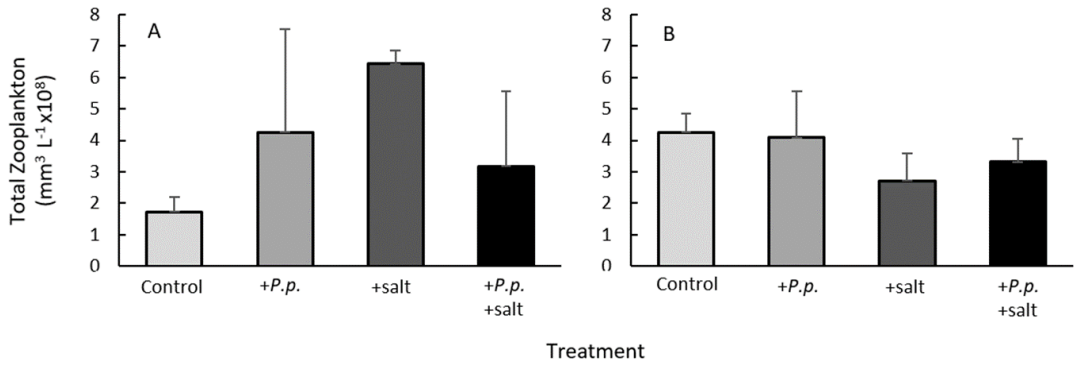


**Figure AA-3. The average final total zooplankton biovolumes for Lake Whitney (A) and Lake Possum Kingdom (B) experimental treatments. (mean + SD, n=3)**

$10^7$, respectively), which was higher than that of the control and combination treatments (1.36 $mm^3 L^{-1} x10^7$ and 1.60 $mm^3 L^{-1} x10^7$, respectively). Differently, both the rotifer and cladocera groups had the highest biomass in the control treatment (3.56 $mm^3 L^{-1} x10^6$ and 0.60 $mm^3 L^{-1} x10^8$, respectively), when compared to other treatments. Additionally, these groups showed similar trends in biomass of the other treatments, where the *P. parvum* addition treatment had the next highest biomass, after the control,

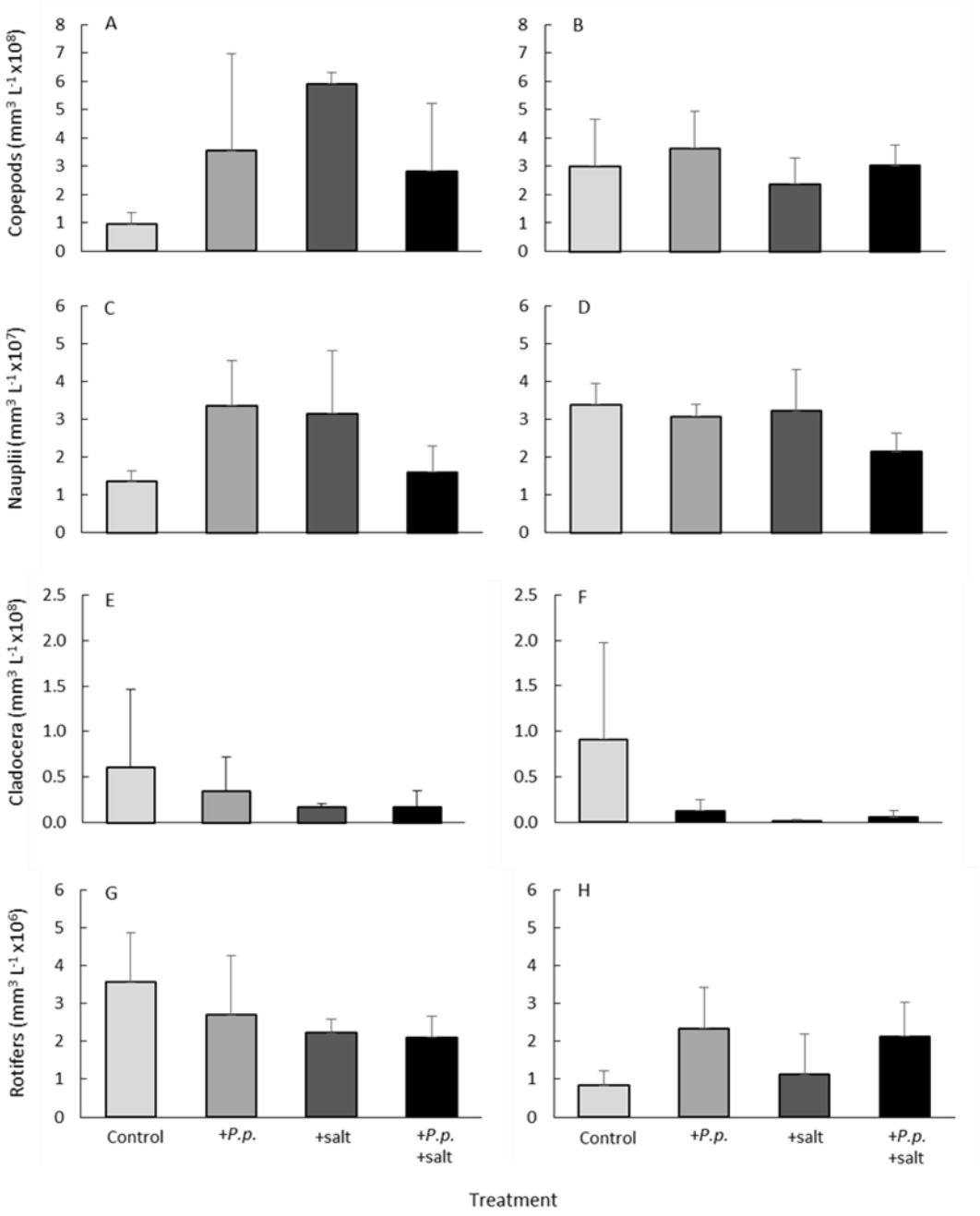


**Figure AA-4. The average final Copepod (A, B), Copepod Nauplii (C, D), Cladocera (E, F) and Rotifer (G, H) biovolumes for Lake Whitney and Lake Possum Kingdom experimental treatments, respectively. (mean + SD, n=3)**

and the salt addition and the combination treatments had the lowest biomass levels (2.22 $mm^3 L^{-1} x10^6$, 0.17 $mm^3 L^{-1} x10^8$ and 2.10, 0.17, respectively). Also of note is the high level of variation in replicates of certain treatments for total biomass and some higher taxa groups. This variation is also seen in the PCA analysis where samples from the same treatment are spread widely across PC1 (Figure AA-5). However, control treatments grouped together with strong positive weights along PC1, indicating a relatively low biomass of total zooplankton and copepod adults, which made up the bulk of total zooplankton biomass.

***Lake Possum Kingdom***

Looking at the chl *a* data for the LPK system (Figure AA-2, B), it was found that a significant interaction between the salt and size fraction treatments ($p$=0.038). Here, if zooplankton were removed, adding salt increased chl *a*, but if zooplankton were included, adding salt decreased chl *a*.

Analogous to the LW results, there was no significant difference between treatments for total zooplankton biovolume and, here too high levels of variation within replicates was observed for some groups (Figure AA-3, B). Differently, in the LPK system a significant effect of P. parvum treatment on copepod nauplii and rotifer biomass was found (p=0.035 and 0.039, respectively), though this effect was different for these groups (Figure AA-4, D and H). When P. parvum was added there was a decrease in biovolume of copepod nauplii but an increase in that of rotifers. These relationships were also observed in the PCA analysis. Here it was seen that the rotifer and P. parvum

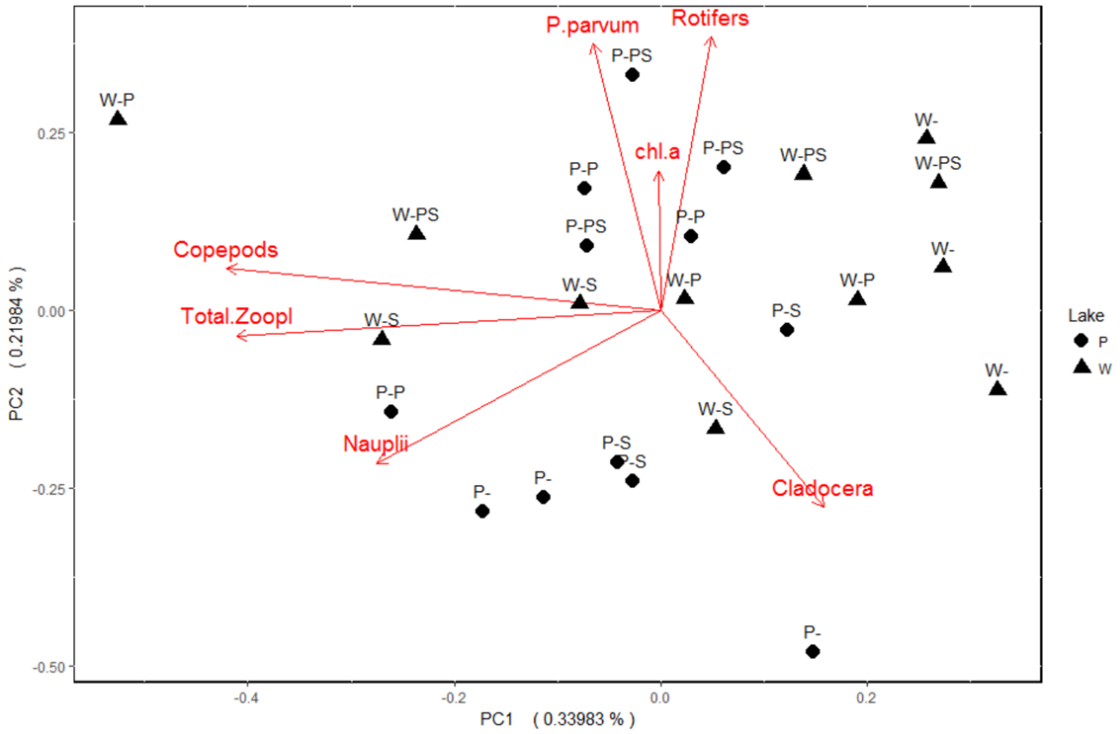


**Figure AA-5. Principle Component Analysis using data which included only samples from both lakes for treatments where the full community was present (i.e. zooplankton was added to all treatments) for *P. parvum* density, chlorophyll *a*, total zooplankton biovolume and biovolume of higher zooplankton taxonomic groups. Princiiple Components 1-3 represent 73% of the total variation within the data set. PC1 and PC2 represent 0.33983% and 0.21984% of the variation amongst the data. Loadings are represented by red arrows and data points by circles. Circles denote Lake Possum Kingdom samples, while triangles denote Lake Whitney samples. The key to sample identification is as follows: W-, Lake Whitney; P-, Lake Possum Kingdom; S, salt addition; P, *P. parvum* addition. from the *P. parvum* loading, and samples with low *P. parvum* populations tended to group with**

loadings grouped together with large positive weightings along PC2, as did samples with larger *P. parvum* populations in LP. Additionally, the copepod nauplii loading separated this loading. Though there was no significant effect of any treatment on the copepod adults and cladocera groups, trends varied (Figure AA-4,B and F). Here both copepod adults and nauplii had similar biomass levels across all treatments. For copepod adults, biomass ranged from 2.37-3.64 $mm^3$ $L^{-1}$ $x10^8$ for the salt addition treatment and the *P. parvum* addition treatment, respectively. For copepod nauplii, biomass ranged from 2.14-3.39 $mm^3$ $L^{-1}$ $x10^7$ for the combination treatment and the control treatment, respectively. Cladocera had the highest biomass in the control treatment (0.91 $mm^3$ $L^{-1}$ $x10^8$), with relatively low biomass in all other treatments, the lowest of which was in the salt addition treatment (0.02 $mm^3$ $L^{-1}$ $x10^8$).

**Table AA-1. Significance results from ANOVA analysis of square root transformed data collected during the final sampling period. Highest level interaction effects were first examined and if significant interpreted. If a response variable was not included in a significant interaction effect then its main effect was examined interpreted if significant. Data from each lake was analyzed separately.**

| Response Variable | Significant main effect(s) or interaction effect of treatments | |
|---|---|---|
| | Lake Whitney ($T_f$) | Lake Possum Kingdom ($T_f$) |
| chl *a* | - | Size Fraction & Salt int. (.04) |
| *P. parvum* cell density | Size Fraction & Salt int. (.001) | Size Fraction (.03), Salt (.003) |
| Total Zooplankton Biovolume | - | - |
| Adult Copepod Biomass | - | - |
| Copepod Nauplii Biomass | - | Salt* (.04) |
| Rotifer Biomass | - | Salt* (.04) |
| Cladocera Biomass | - | - |

APPENDIX B

ADDITIONAL RESULTS NOT INCLUDED IN CHAPTER 3

**Experiment 1**

The *Daphnia magna* acute mortality bioassay conducted during the first set of experiments (Figure AB-1) was not reported as results were similar to those for the second set of experiments. Methods used to conduct this test can be found in Chapter 3.

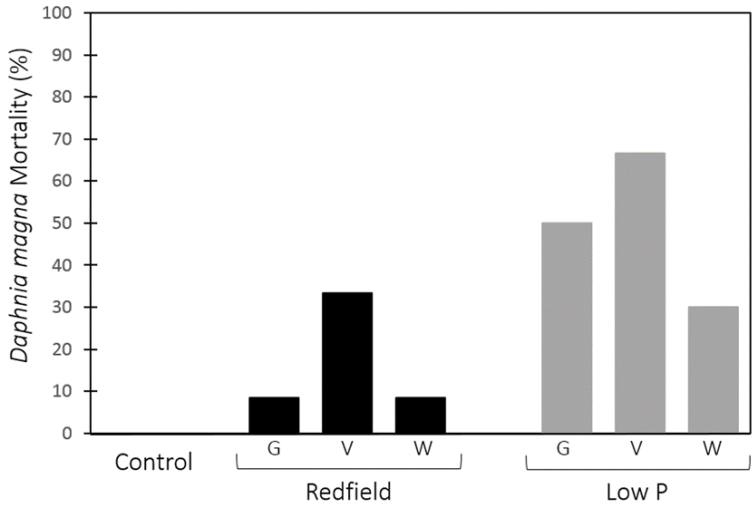


**Figure AB-1. Experiment 1, *Daphnia magna* mortality reported as a percentage when exposed to various *Prymnesium parvum* culture fractions grown in media with different N:P ratios.**

**Experiment 2**

The second set of experiments included a *P. parvum* culture grown using unbalanced low-nitrogen (N) media as an additional treatment added to the bioassay tests. These results were not included in Chapter 3, but are reported here in Appendix B, and include growth curve and final cell density of the experimental culture (Figures AB-

2, Table AB-1), *D. magna* acute mortality (Figure AB-3), and *R. salina* acute mortality (Figure AB-4, Table AB-2). To create this treatment, N was reduced to 1/20$^{th}$ its concentration in the balanced Redfield treatment (made using f/2 media recipe: Guillard & Ryther, 1962). All other methods pertaining to these results can be found in Chapter 3.

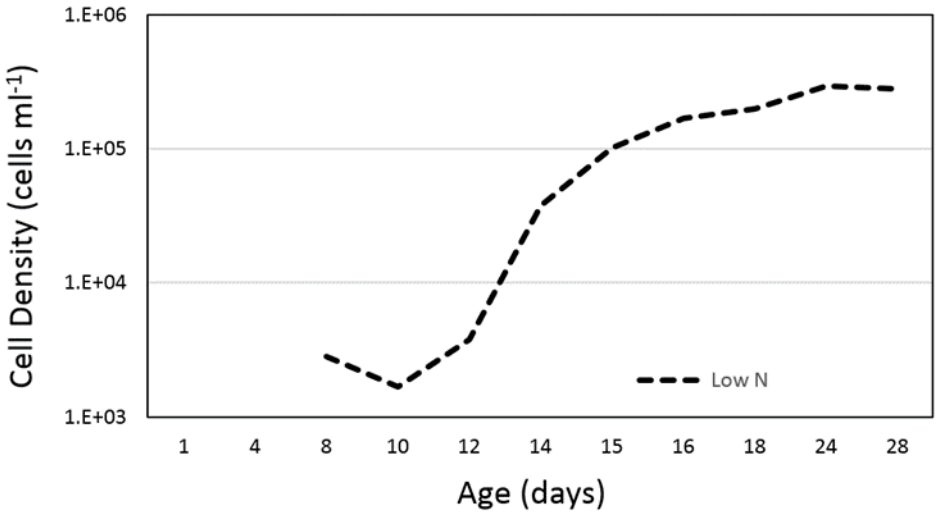


**Figure AB-2. Experiment 2, Growth curves for experimental *Prymnesium parvum* cultures. Experiment 1 was run in June 2018, while the Experiment 2 was run in June 2019. All cultures were in stationary growth phase and 17 days of age at the time of experiment initiation.**

**Table AB-1. Cell densities for *Prymnesium parvum* cultures grown in low N:P media at time of experiment initiation. R3 experiment was run in June 2018, while the R4 experiment was run in June 2019. All cultures are in stationary growth phase.**

| Media | Density Exp. 1 (cells ml-1) | Density Exp. 2 (cells ml-1) |
|---|---|---|
| Low N Media | NA | 198,750 |

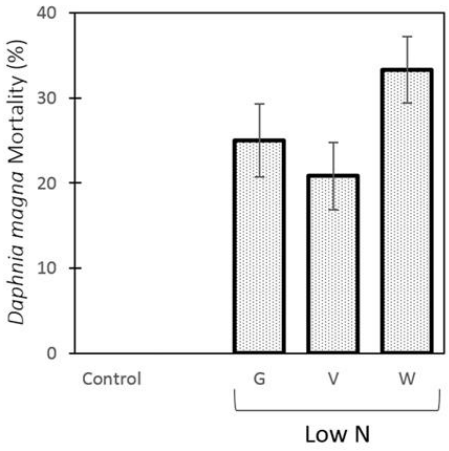


**Figure AB-3. Experiment 2, *Daphnia magna* mortality reported as a percentage when exposed to various *Prymnesium parvum* culture fractions grown in media with a low N:P ratio.**

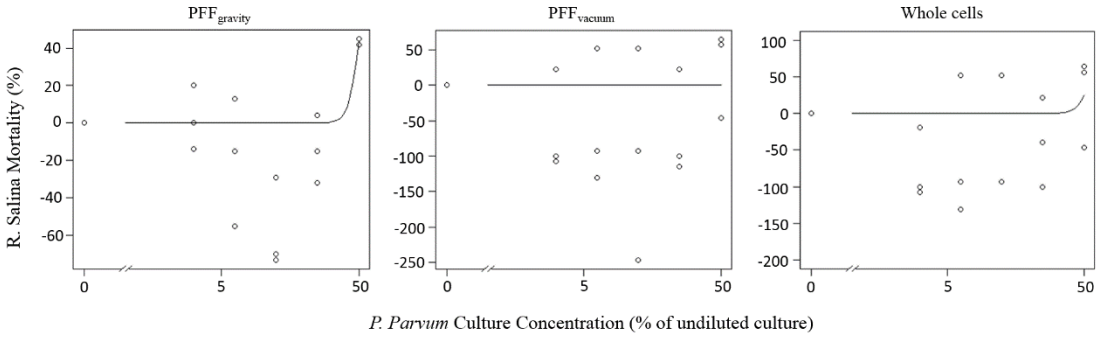


**Figure AB-4. Results for the *Rhodomonas salina* acute mortality assay for low N. treatments. Here *R. salina* mortality as a percentage of the control density is shown on the y-axis and the *Prymnesium parvum* undiluted culture percentage is shown along the x-axis. A 6-point dilution series was used so that LC50's for the culture fractions could be determined, which are reported as cell densities (cells ml$^{-1}$). These tests were conducted during the 2$^{nd}$ round of *P. parvum* laboratory experiments.**

**Table AB-2. $LC_{50}$ concentrations for the *Rhodomonas salina* acute mortality assay reported as % of undiluted *Prymnesium parvum* culture and as *P. parvum* cell density (cells ml$^{-1}$).**

| | Treatment | $LC_{50}$ (Std. Dev.) % of culture | $LC_{50}$ Cell Density (cells ml$^{-1}$) |
|---|---|---|---|
| Low N | $PFF_{gravity}$ | 102.22 (10.23) | 101,581 |
| | $PFF_{vacuum}$ | NA | NA |
| | Whole Cell | NA | NA |

APPENDIX C

PARAMETER TABLE FOR CHAPTER 4

**Table AC-1.**

| State Variables | Description | | Units | |
|---|---|---|---|---|
| $A_i$ | Autotroph population density of species *i* | | $10^6$cells$_A$ L$^{-1}$ | |
| $S_j$ | Ambient concentration of nutrient *j* | | µM = umol L$^{-1}$ | |
| $M$ | Mixotroph population density | | $10^6$cells$_M$ L$^{-1}$ | |
| $Z$ | Zooplankton population density | | indv L$^{-1}$ | |
| **Parameters** | **Description** | **Value/Eq. /Operator** | **Units** | **Reference** |
| $c$ | Chlorophyll concentration | 0.000125* | mgChl*a* $10^6$cells$_A$$^{-1}$ | Taylor et al., 1997; Mullin et al., 1966; Withrow et al., 2018 |
| $D1$ | Declination of the Earth | Eq. 13 | degrees (°) | Cooper, 1969; Brock, 1981 |
| $d$ | Julian Day of year | 1-365 | Julian Day | |
| $d_t$ | Julian Day of year as a decimal | 0-1 | Unit-less | |
| $f_i$ | Rate at which autotrophs are phagocytized by mixotrophs | Eq. 27 | $10^6$cells$_A$ $10^6$cells$_M$$^{-1}$ day$^{-1}$ | |
| $f_{potential}$ | Rate of phagotrophy based on total autotroph cell density | Eq. 28 | cells$_A$ cell$_M$$^{-1}$ d$^{-1}$ | |
| $f_{max}$ | Maximum rate of phagotrophy | 0.8 | cells$_A$ cell$_M$$^{-1}$ d$^{-1}$ | Legrand et al. 2001 |
| $f_{threshold}$ | Phagotrophy threshold | 0.1 | cells$_A$ L$^{-1}$ | |
| $g_{max}$ | Zooplankton maximum grazing rate | 0.192 | $10^6$cells indv$^{-1}$ day$^{-1}$ | DeMott, 1982 |
| $g_{potential}$ | Potential rate of zooplankton grazing | Eq. 21 | $10^6$cells indv$^{-1}$ day$^{-1}$ | |

**Table AC-1. Continued**

| Parameters | Description | Value/Eq. /Operator | Units | Reference |
|---|---|---|---|---|
| $g_i$ | Rate at which phytoplankton species $i$ is grazed | Eq. 19 | $10^6$cells$_A$ indv$^{-1}$ day$^{-1}$ | |
| $g_M$ | Rate at which mixotrophs are grazed by zooplankton | Eq. 20 | $10^6$cells$_M$ indv$^{-1}$ d$^{-1}$ | |
| $g_{threshold}$ | Threshold below which phytoplankton cannot be grazed | 0.1 | $10^6$cells L$^{-1}$ | Roelke, 2000 |
| $h$ | Hydraulic flushing coefficient | 0.05 | d$^{-1}$ | |
| $I_o$ | Irradiance integrated over the photosynthetically active radiation wavelength range (PAR) incident upon the water surface | Eq. 9 | quanta cm$^{-2}$ s$^{-1}$ | Brock, 1981 |
| I0 | Solar constant | 4.0883x10$^{17}$ | quanta cm$^{-2}$ s$^{-1}$ | Duffie and Beckman, 1980; Brock, 1981 |
| I6 | Total solar radiation at the top of the atmosphere | Eq. 10 | quanta cm$^{-2}$ s$^{-1}$ | Liu and Jordan, 1960; Duffie and Beckman, 1980; Brock, 1981 |
| $I_z$ | Average irradiance autotrophs experience throughout the mixed layer | Eq. 6 | quanta cm$^{-2}$ s$^{-1}$ | |
| $k_f$ | Half-saturation coefficient of phagotrophy | 0.01 | cells$_A$ L$^{-1}$ | |
| $k_g$ | Zooplankton half-saturation coefficient for grazing | 3.79 | $10^6$cells L$^{-1}$ | Roelke, 2000 |
| $kS_{i,j}$ | Half-saturation coefficient of autotroph species $i$ for nutrient $j$ limited growth | Species specific, N=0.25-1 P=0.0156-0.0625 | µM | Reynolds, 2006 |
| $kS_{M\|i,j}$ | Half-saturation coefficient of mixotrophs for nutrient $j$ limited growth | N=0.01 P=0.009 | µM | Baker, 2009 |

**Table AC-1. Continued**

| Parameters | Description | Value/Eq. /Operator | Units | Reference |
|---|---|---|---|---|
| $k_I$ | Half-saturation coefficient for light limited growth | $2.27e^{17}$ | quanta $cm^{-2}$ $s^{-1}$ | Converted from Diehl et al. Ecology |
| $L$ | Latitude | 0.75 | radians | (43°N) Brock, 1985 |
| $m$ | Grazer population specific mortality rate | 0.1 | $d^{-1}$ | Roelke et al., 2000 |
| r | Max. phytoplankton growth rate | | | |
| R1 | Radius vector of the Earth | Eq. 11 | Unit-less | Nicholls and Child, 1979; Brock, 1981 |
| $S_{ingstd,M\|j}$ | potential rate of nutrient $j$ uptake through phagotrophy by mixotrophs | Eq. 26 | µmole $10^6$cells$_M^{-1}$ $d^{-1}$ | |
| $S_{ingstd,Z\|j}$ | Rate of nutrient $j$ uptake through grazing by zooplankton | Eq. 18 | µmole $ind^{-1}$ $d^{-1}$ | |
| $S_{src,j}$ | Concentration of nutrient $j$ in a generic source | N=11.104 P=0.694 | µM | |
| $S_{Z,egest\|j}$ | Concentration of nutrient $j$ produced by grazer egestion | Eq. 29-32 | µM | Roelke et al., 2000, |
| $T_d$ | Water temperature of day $d$ | Eq. 15 | °C | |
| $T_{opt}$ | Optimal growth temperature for all phytoplankton | $T_{max}$ | °C | Set to mirror the maximum water temperature |
| $T_{max}$ | Maximum water temperature | 24.8 | °C | Magee et al., 2016 |
| $T_{\min}$ | Minimum water temperature | 1.74 | °C | Magee et al., 2016 |
| $u_M$ | Specific growth rate of mixotrophs | Eq. 23 | $d^{-1}$ | |
| $u_{M,S}$ | Specific autotrophic growth rate for the mixotroph population | Eq. 24 | $d^{-1}$ | |
| $u_{M,f}$ | Specific phagotrophic growth rate of the mixotrophic population | Eq. 25 | $d^{-1}$ | |

**Table AC-1. Continued**

| Parameters | Description | Value/Eq. /Operator | Units | Reference |
|---|---|---|---|---|
| $u_{A,i}$ | Specific growth rate of phytoplankton species $i$ | Eq. 5 | $d^{-1}$ | |
| $u_{max,i}$ | Maximum specific growth rate of species $i$ for autotrophs | Species specific, 0.3-3 | $d^{-1}$ | Reynolds, 2006 |
| $u_{max,M}$ | Maximum specific growth rate for the mixotroph population (based on growth in inorganic nutrient media) | 0.94 | $d^{-1}$ | Baker et al., 2007, 2009 |
| $u_{T,max}$ | Temperature based growth rate for phytoplankton where $T_t = T_{opt}$ | 2.87 | $d^{-1}$ | |
| $u_Z$ | Specific growth rate for the zooplankton population | Eq. 17 | $d^{-1}$ | Roelke, 2000 |
| $u_T$ | Temperature based growth rate for a specific temperature of a given day | Eq. 14 | $d^{-1}$ | Grimaud et al., 2017; Norberg, 2004 |
| $Wl$ | Hour angle | Eq. 12 | degrees (°) | Milankovitch, 1930; Brock, 1981 |
| $w$ | Thermal niche width for all phytoplankton | 25 | °C | Set to mirror the water temperature range |
| $z$ | Depth of the mixed layer | 8- 25, Operator 7 | m | Magee et al., 2017 |
| $z_{deep}$ | Depth of the mixed layer when the water column is fully mixed | 25 | m | Magee et al., 2017 |
| $z_{shallow}$ | Depth of the mixed layer during summer stratification | 8 | m | Magee et al., 2017 |
| $Z_{rest}$ | Zooplankton population density added through hatching | 0.0675 | indv $L^{-1}$ $d^{-1}$ | Caceres, 1998 |
| $\alpha$ | Parameter of the Eppley function | 0.59 | Unit-less | Norberg, 2004 |
| $\beta$ | Parameter of the Eppley function | 0.0633 | Unit-less | Norberg, 2004 |

**Table AC-1. Continued**

| Parameters | Description | Value/Eq. /Operator | Units | Reference |
|---|---|---|---|---|
| $\varepsilon_i$ | Edibility of autotroph species $i$ | Species specific, 0-0.125, 0.375-1 | Unit-less | |
| $\varepsilon_M$ | Edibility of mixotroph | Variable | Unit-less | |
| $\pi$ | Coefficient | 3.14 | Unit-less | |
| $\Omega$ | Atmospheric correction | 3/8 | Unit-less | Evans and Parslow, 1985 |
| $\sigma_c$ | Light extinction coefficient based on the total concentration of phytoplankton | 0.024 | $m^2$ mgChl$a^{-1}$ | |
| $\sigma_{total}$ | Light extinction coefficient | Eq. 8 | $m^{-1}$ | Riley, 1946 |
| $\sigma_w$ | Light extinction coefficient based on pure water, tripton and cDOM | 0.146 | $m^{-1}$ | |
| $\theta_{fix,A\|j}$ | Fixed cellular content of nutrient $j$ in autotrophs | N=0.25-1 P=0.0156-0.0625 | µmole $10^6$cells$_A^{-1}$ | Huisman et al., 2001; Roelke and Spathari, 2015 |
| $\theta_{fix,M\|j}$ | Fixed cellular content of nutrient $j$ in mixotrophs | N=0.01 P=0.009 | µmole $10^6$cells$_M^{-1}$ | |
| $\theta_{fix,Z\|j}$ | Fixed body composition of nutrient $j$ for an individual zooplankton | N=0.0349 P=0.0155 | µmole $indv^{-1}$ | |
| $\mathfrak{t}_{end}$ | Breakdown of the seasonal thermocline/ onset of fall turnover | 275 | Julian Day | Magee et al., 2016 |
| $\mathfrak{t}_{set}$ | Seasonal thermocline is set | 153 | Julian Day | Snortheim et al., 2017 |
| $\psi_1$ | Coefficient used to enable autotroph losses due to mixotrophy | 1 or 0, Operator 16 | Unit-less | |
| $\psi_2$ | Coefficient used to enable seasonal zooplankton hatching | 1 or 0, Operator 22 | Unit-less | |

APPENDIX D

SENSITIVITY ANALYSIS FOR CHAPTER 4

## Methods

Model simulations (with no mixotrophic population included) were run so as to gauge sensitivity of model responses to changes in a given parameter. Each of the tested parameters was shifted by +50% or -50% from the previously defined values, listed in Table V-5. In some cases a 50% increase or 50% decrease was not meaningful, so the parameter change was different than specified. These cases included the minimum of the edibility ($\varepsilon$) range which was tested only at +50% (0.5) and the breakdown of the seasonal thermocline ($\mathfrak{h}_{end}$), for which the +50% test value was set to day 365.

Responses of interest included: day of peak autotroph biomass, autotroph peak density (x106 cells L-1), phytoplankton edibility as a weighted average (0-1), phytoplankton richness at peak biomass, phytoplankton evenness at peak biomass, Shannon diversity at peak biomass, nutrient concentration (P) at peak biomass (uM), peak zooplankton density (indv L-1), and day of peak zooplankton density. All phytoplankton related response variables were measured for both the spring (days 1-182) and fall (day 183-365) assemblages.

Tested biological parameters included: per cell Chl *a* content ($c$), minimum of the edibility ($\varepsilon$) range, zooplankton maximum grazing rate ($g_{max}$), grazing threshold ($g_{threshold}$), seasonal zooplankton migration ($\psi_2$), zooplankton half-saturation coefficient for grazing ($k_g$), fixed cellular content of nutrient $j$ in phytoplankton ($\theta_{fix,A|j}$), grazer population specific mortality rate ($m$), phytoplankton initial cell density ($A$),

zooplankton initial cell density ($Z$), half-saturation coefficient for light limited growth ($k_I$).

Tested abiotic parameters included: concentration of resource $j$ in a generic source ($S_{src,j}$), hydraulic flushing coefficient ($h$), maximum water temperature ($T_{max}$), minimum water temperature ($T_{min}$), seasonal thermocline set day ($\text{Ϟ}_{set}$), breakdown of the seasonal thermocline day ($\text{Ϟ}_{end}$), depth of the mixed layer when the water column is mixed ($z_{deep}$), depth of the mixed layer during summer stratification ($z_{shallow}$), light extinction coefficient based on pure water, tripton and cDOM ($\sigma_w$).

**Results and Discussion**

Results were reported (Table V-5) for simulations where a shifted parameter caused a 50% difference in response value from that generated using the original value. Figures for parameters that had a widespread effect on the response variable were also generated for equilibrium seasonal dynamics of the biotic model components.

Parameters for which multiple response variables were highly influenced include the minimum of the edibility range, maximum zooplankton grazing rate, and hydraulic flushing coefficient. First, considering the minimum of the edibility range, a +50% shift in the original parameter value had a positive effect on fall phytoplankton edibility (157.84%) and a negative effect on fall phytoplankton richness (-50%). This outcome is logical given that the baseline fall assemblage was composed of less edible species and by increasing the edibility minimum, those species were either lost or less abundant in the modeled assemblage (Figure V-9, B). Additionally, increasing this parameter led to an 82.96% increase in the nutrient concentration (uM-P) occurring at peak

**Table AD-1. Sensitivity of given response variables to shifted parameters. Changes in response variables that were greater than or equal to 50% were reported.**

| Parameter | Shift (-50% or +50%) | Spring (S) or Fall (F) Assemblage | % Change in Response |
|---|---|---|---|
| Response: phytoplankton edibility (weighted average) | | | |
| Minimum of the edibility range | + | F | 157.84 |
| Maximum zooplankton grazing rate | - | F | 110.41 |
| Zooplankton specific mortality rate | + | F | 96.35 |
| Hydraulic flushing coefficient | + | F | 97.08 |
| Response: phytoplankton richness at peak biomass | | | |
| Minimum of the edibility range | + | F | -50.00 |
| Maximum zooplankton grazing rate | - | S | 575.00 |
| | - | F | 575.00 |
| Hydraulic flushing coefficient | - | S | 100.00 |
| | + | S | -50.00 |
| | - | F | 100.00 |
| | + | F | -50.00 |
| Response: phytoplankton evenness at peak biomass | | | |
| Maximum zooplankton grazing rate | - | S | 176.95 |
| | - | F | 70.70 |
| Hydraulic flushing coefficient | - | S | 103.71 |
| | + | F | -65.23 |
| Response: phytoplankton Shannon diversity at peak biomass | | | |
| Maximum zooplankton grazing rate | - | S | 558.43 |
| | - | F | 305.82 |
| Hydraulic flushing coefficient | - | S | 205.57 |
| | + | S | -71.80 |
| | + | F | -82.61 |
| Response: nutrient concentration (µM-P) at peak biomass | | | |
| Minimum of the edibility range | + | S | 86.92 |
| | + | F | 512.66 |
| Half-saturation for zooplankton grazing | - | F | -55.50 |
| | + | F | 70.45 |
| Half-saturation for light-limited growth | + | S | 58.78 |
| | - | F | -59.82 |
| | + | F | 56.94 |
| Hydraulic flushing coefficient | + | S | 759.25 |
| | - | F | -56.32 |
| Seasonal thermocline set | - | F | -50.38 |
| Response: peak zooplankton density | | | |
| Maximum zooplankton grazing rate | - | NA | -52.80 |

phytoplankton biomass in the spring and a 512.66% increase in that occurring during the fall peak (Figure V-9, A). Again, this was likely related to the loss of less-edible species (with low half-saturation for nutrient limited growth values) from the fall assemblage and the inability of the less rich assemblage to sequester nutrients to the same extent.

The maximum zooplankton grazing rate also had a widespread effect on model responses, influencing almost all reported response variables. A decrease in this parameter lead to a 110.41% increase in phytoplankton edibility of the fall assemblage.

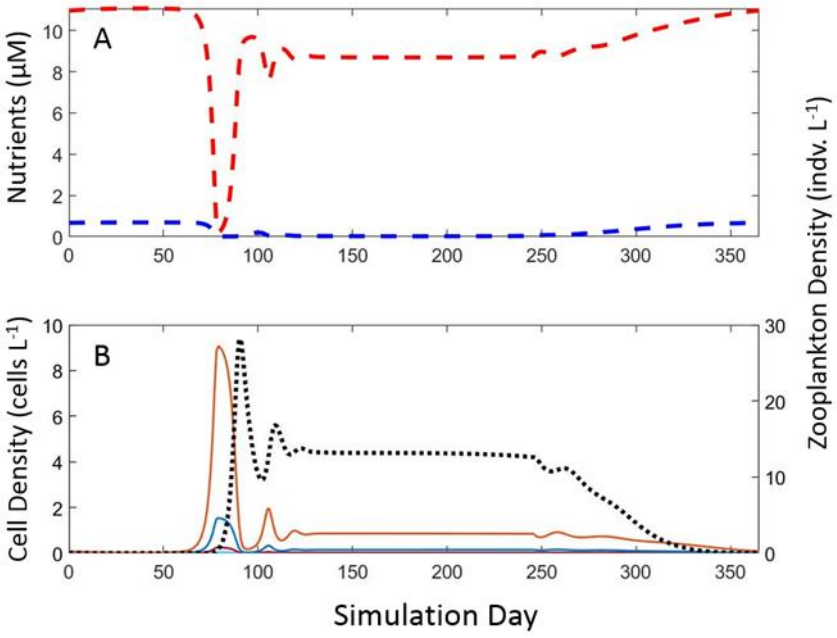


**Figure AD-1. Sensitivity analysis result for simulation where the minimum of the edibility range was shifted +50%. Phytoplankton species density shown with colored lines and zooplankton population density shown with dotted line.**

This was due to the ability of more edible species to proliferate under reduced grazing pressure (Figure V-10). The decreased parameter also caused a massive increase (575%) in phytoplankton species richness of both the fall and spring assemblages (Figure V-10). Similarly, species evenness and Shannon diversity at peak phytoplankton biomass also increased. Intuitively a decrease in the maximum grazing rate led to a decrease (-52.8%) in peak zooplankton biomass (Figure V-10).

Shifting the hydraulic flushing coefficient had more than a 100% effect on 5 of the 6 reported response variables. Increasing this parameter by 50% had a positive effect on fall phytoplankton edibility (97.08%) and spring nutrient concentrations (759.25%) and a negative effect on both spring and fall species richness (-50%) and diversity (-71.80, -82.61), and fall species evenness (-65.23) (Figure V-11, A&C). Increased flushing caused slow growing, k-selected species to be less abundant among the phytoplankton assemblage leading to decreased richness, diversity, and evenness. Additionally, nutrient concentrations likely remained high for longer in the spring while the low density wintertime assemblage struggled against hydraulic displacement to gain a foothold. Decreasing the parameter by 50% led to large increases in both the fall and spring assemblage's richness (100%), as well as an increase in spring evenness (103.71%) and diversity (205.57%) (Figure V-11, D). This outcome was likely due to the ability of more species to realize specific growth rates greater than the flushing rate, and thereby persist in the system. Further, decreasing this parameter caused a decrease in fall nutrient level (-56.32%), likely due to the increased species richness and ability of the more diverse assemblage to successfully sequester nutrients (Figure V-11, B).

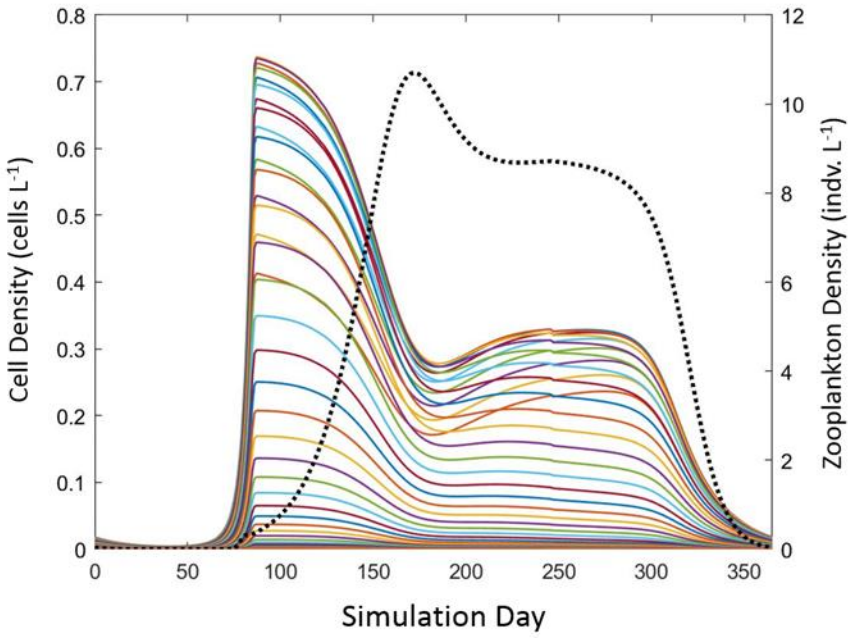


**Figure AD-2. Sensitivity analysis result for simulation where the minimum of the maximum zooplankton grazing rate was shifted +50%. Phytoplankton species density shown with colored lines and zooplankton population density shown with dotted line.**

Parameters that also effected a greater than 50% change in a response variable included the zooplankton specific mortality rate, the half-saturation for light limited growth, and the seasonal thermocline set day. Increasing the zooplankton specific mortality rate allowed an increase in edibility of the fall assemblage (96.35%), again likely due to the ability of more edible species to proliferate under reduced grazing pressure. When the half-saturation for light limited growth was increased the spring and fall nutrient concentrations also increased (58.78%, 56.94%). When the parameter was reduced, so too was the fall nutrient concentration (-59.82). These relationships likely occurred due to the interrelated nature of phytoplankton nutrient sequestration and light

limited growth. Reducing the seasonal thermocline set day caused a decrease in fall nutrient concentrations (-50.83%) (Figure V-12). This change is less intuitive but is related to increased late fall phytoplankton biomass resulting from changed dynamics due to an earlier onset of stratification and increased irradiance in the mixed layer. Also the actual change in nutrient concentration is quite small (a decrease from 0.0086 to 0.0042 μM-P).

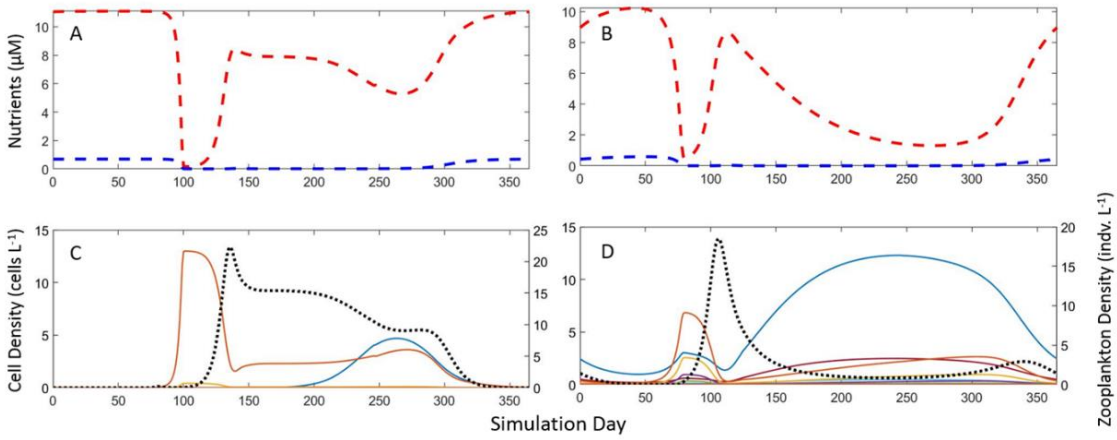


**Figure AD-3. Sensitivity analysis results for simulations where the minimum of the hydraulic flushing rate was shifted +50% (A&C) or -50% (B&D). Phytoplankton species density shown with colored lines and zooplankton population density shown with dotted line (C &D). Nutrient concentrations are shown in panels A&B where nitrogen is represented by the red dotted line and phosphorous by the blue dotted line.**

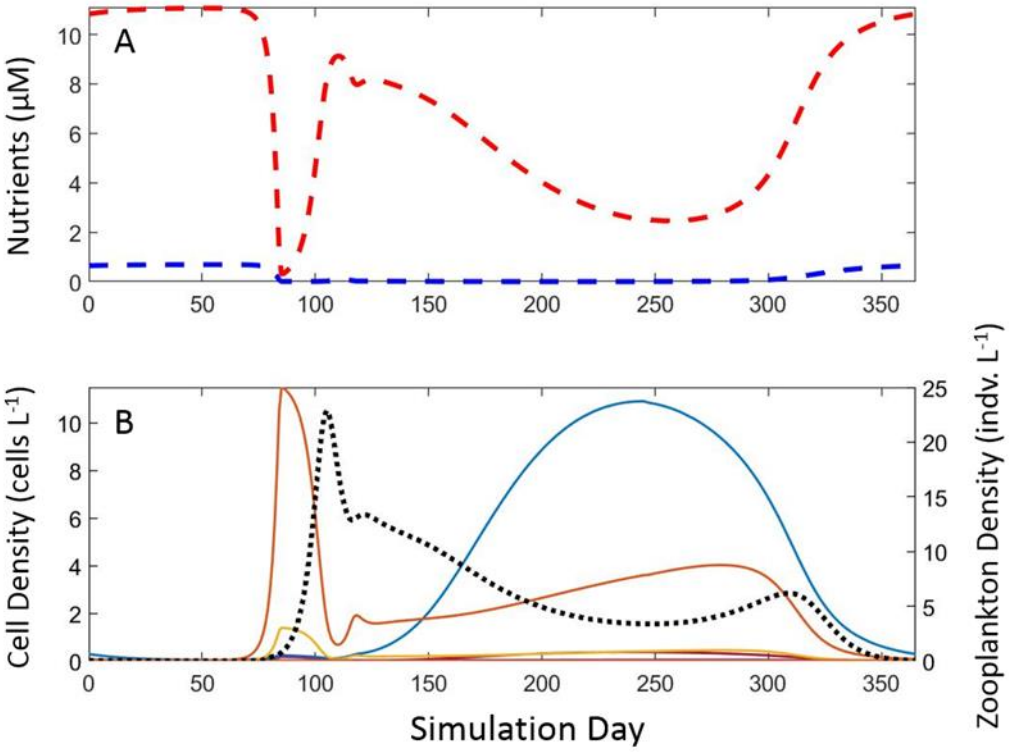


**Figure AD-4. Sensitivity analysis results for simulations where the seasonal thermocline set date was shifted -50%. Phytoplankton species density shown with colored lines and zooplankton population density shown with dotted line (B). Nutrient concentrations are shown in panel A where nitrogen is represented by the red dotted line and phosphorous by the blue dotted line.**

# APPENDIX E

## MODEL CODE FOR CHAPTER 4



```
% The following is a master program for a chemostat model with variable
% nutrient and species capabilities. The progam uses the following
% function files: PEG_func.m and daylightfunc.m
% Programming by Sierra Cagle

global  f  mark cycles
global  NoSp  K  C  r  E
global  E_PtoM  f_max  K_f  f_hold
global  Gz  K_G  C_Gz  M_G  Gz_hold  Hatch
global  NoN  NP
global  tD
global  T_opt  w   u_T  u_T_max  a  b  c  c1
global  pi  Chl  H  Kw  Kc  L mIo lat cloud
global  fall_mix  spring_strat min_d  max1_d  max2_d


%-------------------------------------------------------------------------
% PHYTOPLANKTON PARAMETER VALUES
%-------------------------------------------------------------------------

NoSp   = 100;          % Number of species
Chl    = 0.000125;     % Cellular content of Chla (mg Chla 10x6cell-1)
r_min  = 0.3;          % Max. growth rate- lower limit of assignment range (d-1)
r_max  = 3;            % Max. growth rate- upper limit of assignment range (d-1)
E_min  = .1;           % Edibility- lower limit of assignment range (unitless)
E_max  = 1;            % Edibility- upper limit of assignment range (unitless)
K_min  = 0.25;         % Half-sat. coef. for nutrient limited growth-
                       %  lower limit of assignment range (uM)
K_max  = 1;            % Half-sat. coef. for nutrient limited growth-
                       %  upper limit of assignment range (uM)

%%% Assign r, E, and K values to species based on min and max
set_up = NoSp*2;
r      = linspace(r_min,r_max,set_up);
E      = (((E_max-E_min)/(r_max-r_min)).*r)-(r_min.*((E_max-E_min)/(r_max-r_min))) ↙
+E_min;
K_N1   = (((K_max-K_min)/(r_max-r_min)).*r)-(r_min.*((K_max-K_min)/(r_max-r_min))) ↙
+K_min;
K_N2   = K_N1./16;
K      = [K_N1;K_N2];
C      = [1;1/16].*ones(2,NoSp);            % Fixed cellular content of N and P (umol ↙
10x6cell-1)

%%% Remove intermediate species
r(51:150)   = [];
E(51:150)   = [];
K(:,51:150) = [];

%-------------------------------------------------------------------------
% MIXOTROPH PARAMETER VALUES
```

```
%--------------------------------------------------------------------------

%%% Edibility of phytoplankton for Mixotroph (E>0.7 for mixotroph ingestion)
E_PtoM = zeros(1,length(E));
for i=1:length(E)
    if E(i)>0.7
        E_PtoM(i)=1;
    else
        E_PtoM(i)=0;
    end
end

r(1)    = 0.3;        % Mixotroph max. growth rate on inorganic nutrients  (d-1)
E(1)    = 0.9;        % Mixotroph edibility to zooplankton (unitless)
f_max   = 0.8;        % Maximum rate of phagotrophic ingestion (x10^6 ↙
cells/10^6cells*day)
K_f     = 0.01;       % Half saturation coeficient for phagotrophic ingestion ↙
(x10^6cells/L)
f_hold = 0.1;         % Ingestion threshold for phagotrophy (10^6cells/L)

%--------------------------------------------------------------------------
% ZOOPLANKTON PARAMETER VALUES
%--------------------------------------------------------------------------

Gz       = 0.192;           % Max grazing rate (x10^6 cells ind-1 d-1) .192
Gz_hold  = 0.1;             % Grazing threshold (x10^6 cells L-1)
K_G      = 3.79;            % Half-sat. coef. for grazing (x10^6 cells L-1)
C_Gz_N   = 0.0349;          % Zooplankton internal N quota  (umolN/ind)
C_Gz_P   = 0.0155;          % Zooplankton internal P quota  (umolP/ind)
C_Gz     = [C_Gz_N;C_Gz_P];
M_G      = 0.1;             % Zoopl mortality rate (day-1)
Hatch    = 0.0675;          % Hatching resting stage eggs (indv L-1)

%--------------------------------------------------------------------------
% NUTRIENT PARAMETER VALUES
%--------------------------------------------------------------------------

NoN     = 2;            % Number of nutrients
P       = 0.694;        % Maximum concentration of P (uM)
N       = P*16;         % Maximum concentration of N, =P*16 (µM)
NP      = [N,P];

%--------------------------------------------------------------------------
% FLOW PARAMETER VALUES
%--------------------------------------------------------------------------

tD          = 0.05;      % Dilution rate (d-1)

%--------------------------------------------------------------------------
% TEMPERATURE PARAMETER VALUES
```

```
%--------------------------------------------------------------------------

max_t    = 24.8;                    % Lower limit of water temp. range (degrees C)
min_t    = 1.74;                    % Upper limit of water temp. range (degrees C)
T_opt    = max_t;                   % Optimal growth temp. for all species
t_range  = max_t-min_t;
w        = t_range;                 % Temp. niche width for all species
pi       = 3.1416;
a        = 0.59;                    % Constant (speciefied by the Epply eq.)
b        = 0.0633;                  % Constant (speciefied by the Epply eq.)
day      = (linspace(0,1,365))';    % Day of year as a point between 0-1
c        = t_range/2;               % Temp. eq. coef.- determines amplitude
c1       = min_t;                   % Temp. eq. coef.- shifts curve up

%%% Determine temp. of each day of the year given the above parameters (degrees C)
T = (c.*cos(((2.*pi.*day)+pi)./1)+c)+c1;

%%% Determine the growth rate given temp. (Epply-Norberg Eq.) for each day
%%%  of the year and then find the maximum of those rates (d-1)
u_T = (1-((T-T_opt)./w).^2).*(a*exp(b*T));
u_T_max = max(u_T);

%--------------------------------------------------------------------------
% LIGHT PARAMETER VALUES
%--------------------------------------------------------------------------

spring_strat  =122;              % Day the seasonal thermocline is set-
                                 %  effects light by decreased mixing depth
fall_mix      =245;              % Day holamixis occurs- effects light by
                                 %  increasing mixing depth
min_d         =0;                % Water surface- top of mixed layer (m)
max1_d        =8;                % Depth of the thermocline (m)
max2_d        =25;               % Lake depth (m)
Kw            =0.146;            % Light attenuation by pure water, CDOM and Trypton ↙
(m-1)
Kc            =0.024;            % Light attenuation by Chla (m2/mgChla)
cloud         =0;                % Mean percent cloud cover for one day (decimal)
lat           =43;               % Latitude of Lake Mendota (degrees)
L             =lat*pi/180;       % Latitude (radians)
mIo           =4.871E+6;         % Yearly mean solar constant (Joules/m2/hr)
mIo           =mIo*8.3932e+10;   % Convert units (quanta/cm2/s)
H             =2.27E+17;         % Half sat. coef. for light limited growth ↙
(quanta/cm2/s)

%--------------------------------------------------------------------------
% INITIAL CONDITIONS
%--------------------------------------------------------------------------

Ain = ones(1,NoSp)*.1;     % Initial algal density (x10^6 cells L-1)
Rin = NP;                  % Initial nutrient concentration for all nutrients (µM)
```

```
Gin = 1;                    % Initial zooplankton density (indv L-1)

%-------------------------------------------------------------------------
% DEFINE LENGTH OF MODEL RUN
%-------------------------------------------------------------------------

f      = 365;           % Fluctuation period (days)
cycles = 50;            % Number of fluctuation cycles (years)

%-------------------------------------------------------------------------
% DO THE MODEL RUN
%-------------------------------------------------------------------------

t0        = 0.1;                % Time start
tfinal    = f*cycles;           % Time finish (days)
tspan     = [t0:1:tfinal];

mark      = t0;

zin       = [Ain, Rin, Gin, 0];
[t,z]     = ode45('PEG_func',tspan,zin);
```

```
% This is a function called by the master program.  It contains the
% differential equations used in the chemostat model.
% Programing by Sierra Cagle

%-------------------------------------------------------------------------

function zdot = PEG_func(t,z)


global  f  mark
global  NoSp  K  C  r  E
global  E_PtoM  f_max  K_f  f_hold
global  Gz  K_G  C_Gz  M_G  Gz_hold  Hatch
global  NoN  NP
global  tD
global  T_opt  w  u_T_max  a  b  c  c1
global  pi  Chl  H  Kw  Kc
global  fall_mix  spring_strat min_d  max1_d  max2_d


%-------------------------------------------------------------------------
% SPLIT UP INCOMING INFORMATION
%-------------------------------------------------------------------------

A   = z([1:NoSp])';             % Alga
G   = z(NoSp+NoN+1);            % Grazer
R   = z(NoSp+1:NoSp+NoN);       % Resources

%-------------------------------------------------------------------------
% NUMERICAL TRICK (prevent resources from going negative)
%-------------------------------------------------------------------------

for i=1:NoN
    if R(i) < 0
        R(i) = 0;
    end
end

%-------------------------------------------------------------------------
% DETERMINE JULIAN DAY
%-------------------------------------------------------------------------

decimal_day  = (t/f)-floor(t/f);         % day of year = point between 0-1
julian_day   = decimal_day*365;

%-------------------------------------------------------------------------
% TEMPERATURE MODERATION (on max autotroph growth)
%-------------------------------------------------------------------------

T = (c.*cos(((2.*pi.*decimal_day)+pi)./1)+c)+c1;    % Temp. of current day (degrees C)
```

```
%%% Determine the growth rate given temp. (Epply-Norberg Eq.) (d-1)
u_T = (1-((T-T_opt)./w).^2).*(a*exp(b*T));

T_moderator= u_T./u_T_max;                          % (unitless)

%-------------------------------------------------------------------------
% IRRADIENCE MODERATION (on max autotroph growth)
%-------------------------------------------------------------------------

intIo = Daylight_func(t);     % Integrated irradience at the earth's surface
                              %  for a specific Julian day (quanta cm-2 s-1)
A_tot   = sum(A);             % Totaled cell density (cells L-1)
A_tot1  = A_tot*1e3;          % Convert units (cells m-3)
Chl_tot = Chl*A_tot1;         % Total chl a for all cells in the system (mgChla m-3)
Kt      = Kw+(Kc*Chl_tot);    % Total light attenuation (m-1)

%%% Set the mixing depth based on julian day of year (m)
if julian_day < spring_strat
    mixing_depth=max2_d;
      elseif julian_day > fall_mix
              mixing_depth=max2_d;
else
    mixing_depth=max1_d;
end

%%% Calculate integrated irradience over the mixing depth using the
%%%  MATLAB integral function (quanta cm-2 s-1)
fun = @(x) intIo*exp(-Kt*x);
intI_depth = integral(fun,min_d,mixing_depth)/mixing_depth;

I_moderator =intI_depth/(intI_depth+H);          % (unitless)

%-------------------------------------------------------------------------
% NUTRIENT MODERATION (on max autotroph growth)
%-------------------------------------------------------------------------

for i=1:NoN
  MtermN(i,:)  = R(i)./(K(i,:)+R(i));        % Monod function
end

N_moderator=min(MtermN);                     % Use 'Law of Minimum' (unitless)

%-------------------------------------------------------------------------
% AUTOTROPH SPECIFIC GROWTH RATE
%-------------------------------------------------------------------------

u  = r.*T_moderator.*I_moderator.*N_moderator;       % (d-1)

%-------------------------------------------------------------------------
```

```
% MIXOTROPH GROWTH RATE
%------------------------------------------------------------------------

% Nutrients from phagotrophy are called S
for i=1:length(E_PtoM)
 if E_PtoM(i)>0
    E_PtoM_density(i)=1;
 end
end
E_species     = E_PtoM_density.*A;
E_species_tot = sum(E_species);
f_potential   = f_max*((E_species_tot-f_hold)/(K_f+E_species_tot));
f_spec        = E_PtoM.*f_potential.*(E_species./E_species_tot);
f_spec_total  = sum(f_spec);

u_M_f         = f_spec_total;
u_M_R         = u(1);

if u_M_R*A(1) >  max(A(2:NoSp))
    u_M       = u_M_f*T_moderator.*I_moderator;
    indicate  = 0;
else
    u_M       = max(u_M_R,u_M_f)*T_moderator.*I_moderator;
    indicate  = 1;
end

u(1) = u_M;

if u_M_R > u_M_f  &&  indicate==1
    condition  = [0,0];
    condition2 = 0;
else
     condition  = (C(1:2,1).*u_M_R.*A(1))';
     condition2 = 1;
end

%------------------------------------------------------------------------
% ZOOPLANKTON GROWTH RATE
%------------------------------------------------------------------------

A_prop    = A/A_tot;                        % Proportion of the autotroph
                                            %  population each species makes up
Gz_potent = Gz*((A_tot-Gz_hold)/(K_G+A_tot));   % Potential grazing rate
                                                %  (10x6cells indv-1 day-1)
Gz_spec   = E.*Gz_potent.*A_prop;           % Species specific grazing rate
                                            %  (10x6cells indv-1 day-1)
Ingest(1,1) = sum(Gz_spec.*C(1,:));         % rate of N ingestion
                                            %  (umol indv-1 day-1)
Ingest(2,1) = sum(Gz_spec.*C(2,:));         % rate of P ingestion
                                            %  (umol indv-1 day-1)
```

```
u_Z_NP      = Ingest./C_Gz;                % rate of N&P converted to zoopl.
                                           %  biomass (d-1)
u_Z         = min(u_Z_NP);                 % Use 'Law of Minimum' (d-1)

%%% Determine grazer egestion of nutrients ingested that are in excess of
%%%  zooplankton body composition (umol L-1 day-1)
if u_Z_NP(1) > u_Z_NP(2)
    Cycle_back(1) = G*(Ingest(1) - (Ingest(2)*(C_Gz(1)/C_Gz(2))));
    Cycle_back(2) = 0;
else
    Cycle_back(1) = 0;
    Cycle_back(2) = G*(Ingest(2) - (Ingest(1)*(C_Gz(2)/C_Gz(1))));

end

%-------------------------------------------------------------------------
% ZOOPLANKTON RESTING-STAGE
%-------------------------------------------------------------------------

Temp = floor(T);                    % Removes decimal from current temp.

%%% Introduce "hatched" individuals to the zooplankton population when
%%%  water temperature is 10C in spring.
if Temp==10 && julian_day<=200
    G_rest=Hatch;
else
    G_rest=0;
end

%-------------------------------------------------------------------------
% DIFFERENTIAL EQUATIONS
%-------------------------------------------------------------------------

% Autotroph & Mixotroph
z1dot = A.*(u-tD)-(G*Gz_spec)-(A(1)*f_spec.*condition2);

% Nutrients
z2dot = tD.*(NP - R')-(sum((C.*u.*A),2))'+condition+Cycle_back;

% Zooplankton
z3dot = G*(u_Z-M_G-tD)+G_rest;

z4dot = sin(10*t);     % Numerical trick - slow down the integration, important
                       %  when period between pulses is long and the Monod
                       %  equation is being used
%-------------------------------------------------------------------------
% COUNTER (for impatient modelers)
%-------------------------------------------------------------------------

if t>mark               % This provides feedback to the monitor so impatient
```

```
  format compact        %  modelers (like me) can check on the progress of the
  t                     %  simulation
  mark=mark+10;
end

%-------------------------------------------------------------------------
% OUTPUT
%-------------------------------------------------------------------------

zdot=[z1dot,z2dot,z3dot,z4dot]';
```

```
% The following is a function called lightdayfunc. It consists of light
% module that will estimate the integrated irradiance at the surface of
% the Earth over one day given time of year, latitude, and percent cloud
% cover. Latitude, percent cloud, water depth, and turbidity can be varied
% from the master progam.The program breaks down towards the poles.
% Formlulations and conversions from:
% Brock, T.D., 1981.  Ecological Modelling. 14:1-19.

function intIo=Daylight_func(t)

global  pi L mIo lat cloud

% Determine Julian Day in a given year
N_decimal=(t/365)-(floor(t/365));
N=N_decimal*365;

% Vary solar constant with Earth's eccentrical orbit
R1=1./((1+0.033*cos(2*pi*N/365)).^0.5);      % Dist correct Earth orbit
Io=mIo./(R1.^2);                % Time varying solar constant
                                %  on a day scale

%  Calculate declination (north is positive)
D1=23.45*sin(2*pi*(284+N)/365);             % Declination (degrees)
D1=D1*pi/180;                   % Declination (radians)

%  Calculate day length
W1=acos(-1*tan(L)*tan(D1));         % Hour-angle (radians)
L1=2*W1/(15*pi/180);                % Day length (hours)

%  Calculate integrated light over one day (top of atmosphere)
term1=W1*sin(L).*sin(D1);
term2=sin(W1)*cos(L).*cos(D1);
intIo=(24/pi)*Io.*(term1+term2);        % Integrated light over one day

%  Calculate integrated light (Earth surface)
intIo=intIo*3/8;                    % PAR at top of atmosphere
intIo=intIo-0.7*cloud*intIo;        % Loss due to cloud transmission
```